2012-06-28

Mdm2-p53 Signaling in Tissue Homeostasis and the DNA Damage Response: A Dissertation

Hugh S. Gannon
University of Massachusetts Medical School

MDM2-P53 SIGNALING IN TISSUE HOMEOSTASIS AND THE DNA DAMAGE RESPONSE

A Dissertation Presented

By

Hugh S. Gannon Jr.

Submitted to the Faculty of the
University of Massachusetts Graduate School of Biomedical Sciences, Worcester
in partial fulfillment of the requirements for the degree of

DOCTOR OF PHILOSOPHY

June 28, 2012

PROGRAM IN CELL BIOLOGY

Mdm2-p53 Signaling in Tissue Homeostasis and the DNA Damage Response

A Dissertation Presented

By

Hugh S. Gannon Jr.

Approved as to style and content by:

Hong Zhang, Ph.D., Chair of Committee

Roger Davis, Ph.D., Member of Committee

Michelle Kelliher, Ph.D., Member of Committee

Brian Lewis, Ph.D., Member of Committee

Philip Hinds, Ph.D., Member of Committee

Stephen N. Jones, Ph.D., Thesis Advisor

Anthony Carruthers, Ph.D.
Dean of the Graduate School of Biomedical Sciences

Cell Biology

June 28, 2012

TABLE OF CONTENTS

COPYRIGHT NOTICE

Parts of this dissertation have been presented in the following publications:

Gannon, H.S., and Jones, S.N. Genetic analysis of MDM-p53 signaling in development, cell growth, and tumorigenesis. *Genes and Cancer*. *In press.*

Gannon, H.S., Woda, B.A., and Jones, S.N. (2012). ATM phosphorylation of Mdm2 Ser394 regulates the amplitude and duration of the DNA damage response in mice. *Cancer Cell*. 21:668-679.

Gannon, H.S., Donehower, L.A., Lyle, S., and Jones, S.N. (2011). Mdm2-p53 signaling regulates epidermal stem cell senescence and premature aging phenotypes in mouse skin. *Developmental Biology.* 353:1-9.

Additional Relevant Publications:

Coles, A. H., **Gannon, H.**, Cerny, A., Kurt-Jones, E., and Jones, S. N. (2010). Inhibitor of growth-4 promotes IκB promoter activation to suppress NF-κB signaling and innate immunity. *Proc Natl Acad Sci U S A.* 107: 11423-11428.

Mason, E. F., Zhao, Y., Goraksha-Hicks, P., Coloff, J. L., **Gannon, H.**, Jones, S. N., and Rathmell, J. C. (2010). Aerobic glycolysis suppresses p53 activity to provide selective protection from apoptosis upon loss of growth signals or inhibition of BCR-Abl. *Cancer Research.* 70: 8066-8076.

Sluss, H. K., **Gannon, H.**, Coles, A. H., Shen, Q., Eischen, C. M., and Jones, S. N. (2010). Phosphorylation of p53 serine 18 upregulates apoptosis to suppress Myc-induced tumorigenesis. *Molecular Cancer Research.* 8: 216-222.

DEDICATION

This dissertation is dedicated to my wife Kristina.

You have been and always will be my inspiration and constant.

ACKNOWLEDGEMENTS

I am extremely grateful to the many people that have contributed to my development as a graduate student. I would like to particularly thank my thesis mentor, Dr. Stephen Jones, whose teaching and direction helped me not only to learn numerous experimental techniques, but, more importantly, taught me how to think as a scientist. Additionally, I would like to thank the members of the Jones lab, past and present, and the members of my TRAC for their answers to my questions and helpful input on the problems I faced along the way. Finally, I would like to thank my family and friends for all their love and support throughout my life.

SUMMARY

The p53 transcription factor responds to various cellular stressors by regulating the expression of numerous target genes involved in cellular processes such as cell cycle arrest, apoptosis, and senescence. As these downstream pathways are harmful to the growth and development of normal cells when prolonged or deregulated, p53 activity needs to be under tight regulatory control. The Mdm2 oncoprotein is the chief negative regulator of p53, and many mouse models have demonstrated that absence of *Mdm2* expression leads to constitutive p53 activation in a variety of cell types. While unregulated p53 can be deleterious to cells, functional p53 is essential for tumor suppression; as many human cancers harbor *p53* mutations and *p53* knockout mice rapidly develop spontaneous tumors. Therefore, the mechanisms that control p53 regulation by Mdm2 are critical to ensure p53 activity in the appropriate cellular context.

Many genetically engineered mouse models have been created to analyze p53 and Mdm2 functions and these studies have yielded valuable insights into their physiological roles. This dissertation will describe the generation and characterization of novel mutant Mdm2 mouse models and their use to interrogate the roles of p53-Mdm2 signaling in tissue homeostasis and cell stress responses. Deletion of *Mdm2* in epidermal progenitor cells of the skin and hair follicles resulted in progressive hair loss and decreased skin integrity, phenotypes that are characteristic of premature aging. Furthermore, p53 protein levels, p53 target gene expression, and cellular senescence were all upregulated in the

skins of these mice, and epidermal stem cell numbers and function were diminished. These results indicate that Mdm2 is necessary to limit p53 activity in adult tissues to ensure normal stem cell function.

Additional mouse models used to determine the role of Mdm2 phosphorylation will also be presented. DNA damage triggers an extensive cellular response, including activation of the ATM kinase. ATM activity is necessary for p53 protein stabilization and, therefore, p53 activation, but *in vivo* evidence suggests that phosphorylation of p53 itself had little effect on p53 stability. ATM was previously shown to phosphorylate MDM2 at serine residue 395 (394 in mice), and we generated knock-in mutant mouse models to study the role of this posttranslational modification *in vivo*. Absence of this phosphorylation site led to greatly diminished p53 stability and function in response to γ-irradiation and increased spontaneous tumorigenesis in mice. Conversely, a phospho-mimic model demonstrated prolonged p53 activation in cells treated with γ-irradiation, which revealed that phosphorylation of this Mdm2 residue controls the duration of the DNA damage response. Therefore, these mouse models have uncovered new roles for the p53-Mdm2 regulatory axis *in vivo* and will be useful reagents in future studies of posttranslational modifications in oncogene and DNA damage-induced tumorigenesis.

LIST OF TABLES

CHAPTER I

CHAPTER III

LIST OF FIGURES

CHAPTER I

CHAPTER II

CHAPTER III

CHAPTER IV

CHAPTER I:

INTRODUCTION

1.1 Foreword

The p53 tumor suppressor protein and MDM oncoproteins (Mdm2 and MdmX) constitute a signaling axis that controls the response of cells to a wide variety of genetic or metabolic stresses. The p53 transcription factor alters the expression of numerous genes whose products affect proliferation, senescence, cellular metabolism, apoptosis, and DNA repair (Vousden and Lu, 2002; Vousden and Ryan 2009; Sengupta and Harris, 2005). By activating these various effector pathways, p53 prevents the transmission of mutations to subsequent generations of cells, thereby suppressing tumorigenesis at the organismal level. Chief among the negative regulators of p53 are the MDM oncoproteins Mdm2 and MdmX. These MDM proteins complex with the p53 transcription factor and inhibit p53-transactivation of various p53-target genes, including *Mdm2* and *MdmX* (Figure 1.1). By inhibiting p53 activity in the cell, these MDM proteins facilitate the growth of normal cells required for embryonic development and adult tissue maintenance. Many mouse models bearing genetic alterations in *Mdm2* and *MdmX* have been generated to probe the role of the Mdm2-p53 signaling axis in development, in tissue homeostasis, in aging, and (especially) in cancer. Analysis of these mouse models has provided strong genetic evidence that support preceding *in vitro* studies of MDM protein functions while disproving others.

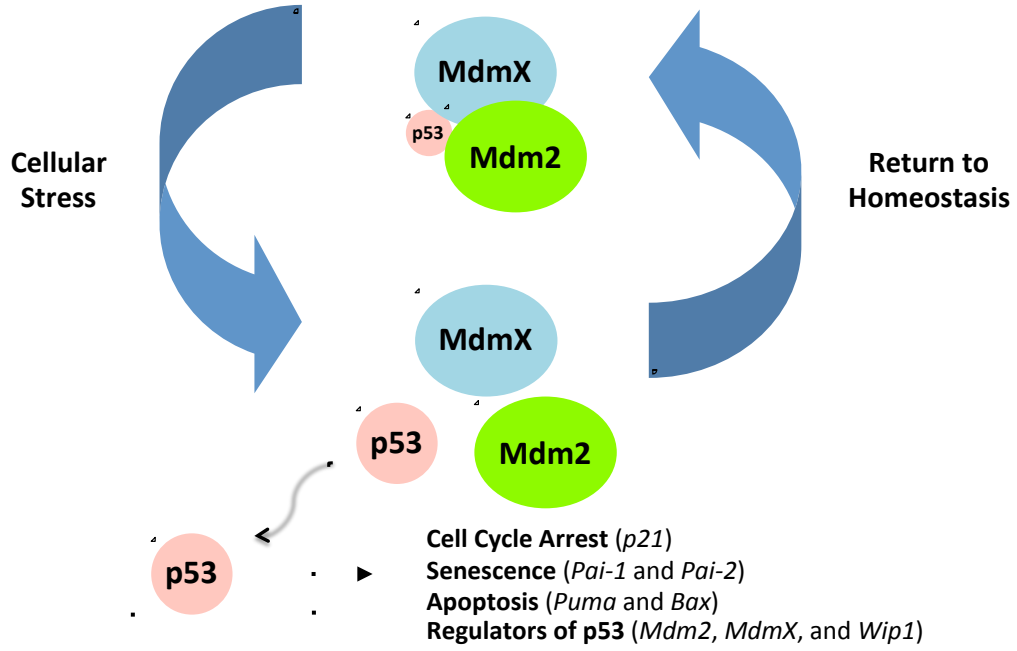

Figure 1.1: The p53-Mdm2-MdmX signaling pathway.

1.2 The p53 Transcription Factor

The p53 protein was initially discovered to be overexpressed and complexed with the large T antigen in a variety of simian virus 40 (SV40)-transformed mammalian cell lines (Chang *et al.*, 1979; Kress *et al.*, 1979; Lane and Crawford, 1979; Linzer and Levine, 1979; Melero *et al.*, 1979). Further experimentation showed that introduction of p53 cDNA cooperated with Ha-ras to transform rat embryonic fibroblasts (Eliyahu *et al.*, 1984; Parada *et al.*, 1984). These initial results suggested that p53 was an oncogene, as increased p53 correlated with increased transformation potential in cells. However, it was later determined that these original p53 cDNA constructs contained p53 inactivating mutations. It was subsequently found that wild-type (WT) p53 cDNA was unable to cooperate to transform cells and p53 expression was frequently lost in mutagenesis-induced tumor mouse models (Eliyahu *et al.*, 1989; Finlay *et al.*, 1989; Mowat *et al.*,

1985; Munroe *et al.*, 1988), which ultimately led to succeeding studies that described p53 as a tumor suppressor.

The p53 protein was shown to bind DNA in a site-specific manner (Kern *et al.*, 1991; Funk *et al.*, 1992; El-Deiry *et al.*, 1992), and further analyses revealed that p53 is a transcription factor that activates the expression of numerous target genes involved in various cell signaling pathways including cell cycle arrest, senescence, apoptosis, DNA repair, and cellular metabolism. One of the first p53-inducible targets to be discovered, the cyclin dependent kinase inhibitor p21, was found to be necessary for p53-dependent cell cycle arrest (El-Deiry *et al.*, 1993; Brugarolas *et al.*, 1995). The p21 protein has also been shown to be a key mediator of the cellular senescence response, an irreversible cell cycle arrest that is dependent on p53 functions (Harvey and Levine, 1991; Fang et al., 1999; Wang et al., 1999; Chang et al., 2000). The transcriptional activity of p53 is also necessary to induce the expression of multiple genes involved in apoptosis. These include, but are not limited to, the pro-apoptotic Bcl-2 family members *Bax* (Miyashita and Reed, 1995), *Noxa* (Oda *et al.*, 2000), and *Puma* (Nakano and Vousden, 2001; Yu *et al.*, 2001). The protein products of these genes trigger the pro-apoptotic caspase cascade after permeabilization of the mitochondrial membrane releases cytochrome c into the cytosol (Bossy-Wetzel and Green, 1999). Novel p53-dependent target genes and signaling pathways are constantly arising in the literature, and the relative contribution of each signaling pathway to the tumor suppressive function of p53 is still under debate (Li *et al.*, 2012).

1.3 The Role of p53 in Tumor Suppression

The importance of p53 in tumor suppression is further evidenced by the fact that over 50% of all human cancers have a mutated *p53* gene (Levine, 1997; Soussi and Beroud, 2001). Likewise, cancers that harbor wild type p53 often have a compromised p53-dependent response due to mutations in positive regulators or gene amplification of negative regulators of p53, demonstrating that p53 function is critical for tumor suppression (Levine, 1997). Genetic disruption of *p53* in mice enabled the necessity of p53 tumor suppression to be truly be assessed at the physiological level.

Because early *in vitro* studies suggested that p53 was a critical regulator of the cell cycle (Baker *et al.*, 1990; Diller *et al.*, 1990; Stürzbecher *et al.*, 1990; Bischoff *et al.*, 1990), *p53* knockout mice were anticipated to have severe defects in embryonic development and cellular growth. Surprisingly, p53-null mice proved to be viable and physically indistinguishable from wild-type littermates at an early age (Donehower *et al.*, 1992). However, these mice rapidly developed spontaneous tumors, confirming a critical role for p53 in tumor suppression. These tumors were mostly lymphomas (chiefly T-cell in origin), with some incidence of sarcomas and other tumor types. Subsequent analysis of primary fibroblasts derived from this model revealed that *p53* reduction or deletion could upregulate cell proliferation and inhibit the growth arrest of cells exposed to DNA damaging agents and other growth arrest signals, revealing a role for p53 in the DNA damage response (Harvey *et al.*, 1993).

Other groups developed additional *p53* knockout mouse models that also formed spontaneous tumors with a relatively similar spectrum (Jacks *et al.*, 1994; Armstrong *et al.*, 1995). These subsequent studies observed that a subset of p53-null mice die *in utero* due to exencephaly (Armstrong *et al.*, 1995), and that thymocyte apoptosis normally induced by exposure to ionizing radiation was greatly compromised by *p53* deficiency, underscoring a critical role for p53 in regulating cell death in response to DNA damage (Lowe *et al.*, 1993). These $p53^{-/-}$ mice were also more susceptible to tumorigenesis induced by ionizing radiation (Kemp *et al.*, 1994). Interestingly, the tumorigenic phenotype of $p53^{+/-}$ mice differed from $p53^{-/-}$ mice, with heterozygous mice displaying neoplasia at a later age and forming mostly sarcomas, with a lessor percentage of lymphomas and other tumor types. As anticipated from earlier studies of familial cancer syndromes, loss of heterozygosity (LOH) for the wild-type p53 allele could be detected in tumors isolated from $p53^{+/-}$ mice (Jacks *et al.*, 1994). However, subsequent work determined that only half of the tumors isolated from p53-heterozygous mice undergo LOH, suggesting that perturbation of other members of the p53 signaling axis might account for functional loss of p53 in these tumors or that a simple reduction in p53 function is sufficient to increase the susceptibility of the cell to tumorigenesis (Venkatachalam *et al.*, 1998). Collectively, these initial studies of p53-null and p53-heterozygous mice demonstrated the importance of p53 in governing the DNA damage response and in suppressing tumorigenesis, validating the use of mouse modeling as a powerful tool to study both tumor suppressor genes and the p53 signaling pathway particularly *in vivo*.

Numerous labs have continued to utilize p53-deficient and *p53* knock-in mouse models to successfully uncover multiple roles for p53 in the regulation of cell growth and tumorigenesis. These p53 models have greatly assisted in our understanding of the tumorigenic effects of p53 loss of function and gain of function mutations, and have highlighted roles for p53 in other biological settings, including reproduction, development, and aging. Many of these *in vivo* p53 functions are discussed in several recent reviews of p53 mouse model phenotypes (Donehower, 2009; Lozano, 2009; Donehower and Lozano, 2009; Toledo and Wahl, 2006).

1.4 Mdm Proteins Tightly Regulate p53 *In Vivo*

Since p53 activity limits the capacity of cells to grow and function, p53 protein levels and functions must be kept under tight check in both non-damaged cells and in cells that have repaired their damaged genomes. Mdm2 was one of the earliest cellular negative regulators of p53 to be discovered and studied in depth (Momand *et al.*, 1992; Oliner *et al.*, 1993; Chen *et al.*, 1995). Mdm2 was identified and cloned as one of several genes present on a double minute chromosome that was isolated from a spontaneously transformed 3T3 cell line (Fakharzadeh *et al.*, 1993). Subsequent transfection studies revealed that Mdm2 interacts with p53, sterically hindering the amino-terminal activation domain of the p53 protein and sequestering p53 away from target gene promoters *in vitro* (Momand *et al.*, 1992; Oliner *et al.*, 1993; Chen *et al.*, 1995; Freedman and Levine, 1998; Geyer *et al.*, 2000). The Mdm2-p53 interaction also blocks the ability of p53 to bind transcriptional cofactors, thereby directly inhibiting its function as a transcription factor (Iwakuma *et al.*, 2003). This negative regulation ensures that cellular functions are not

inappropriately perturbed by p53-dependent cell cycle arrest or apoptosis under normal conditions. Additionally, the *Mdm2* gene is a target of the p53 transcription factor, forming a tight negative regulatory loop that quickly returns p53 protein and activity to basal levels (Juven *et al.*, 1993; Wu *et al.*, 1993).

Interest in the oncogenic potential of Mdm2 was greatly increased when the *Mdm2* gene was found amplified in a significant fraction of human sarcomas (Oliner *et al.*, 1992) and human tumors of the lung, breast, bone, and soft tissues (Momand *et al.*, 1998). It is thought that Mdm2 constitutively inhibits wild-type p53 in these tumors, as elevated *Mdm2* expression and concurrent *p53* mutations are rarely observed. To study the role of Mdm2 *in vivo*, two separate Mdm2 knockout mouse models were generated (Jones *et al.*, 1995; Montes de Oca Luna *et al.*, 1995). Unlike p53-null mice, which undergo relatively normal development, Mdm2-null mice die post-implantation at E5.5-6.5 of early development. The embryos appeared much smaller than wild-type littermates and displayed a highly disorganized architecture. These developmental defects were due to unregulated p53 activity in the embryo, as concomitant knockout of *p53* completely rescued the early developmental lethality of Mdm2-null mice (Jones *et al.*, 1995; Montes de Oca Luna *et al.*, 1995). These results clearly documented a critical role for Mdm2-dependent regulation of p53 during development.

Mice deleted for both *Mdm2* and *p53* are viable, and form spontaneous tumors with a similar tissue spectrum as p53-null mice (Jones *et al.*, 1996). As the phenotype of Mdm2/p53 double-null mice and primary cells is indistinguishable from p53-null mice

(Jones *et al.*, 1996), it would appear that the chief role of Mdm2 in cell growth is to act as a negative regulator of p53 activity. Analysis of Mdm2 and p53 functions using transfection studies in human cells and murine fibroblasts generated from Mdm2/p53 double-null embryos subsequently determined that Mdm2-p53 binding promoted the destabilization of p53 (Haupt *et al.*, 1997; Kubbutat *et al.*, 1997), providing an additional potential mechanism for Mdm2-mediated inhibition of p53 function. Subsequent *in vitro* work determined that the Mdm2 protein contains a carboxy-terminal Really Interesting New Gene (RING) domain with E3-ubiquitin ligase activity. Furthermore, Mdm2 was found to add ubiquitin moieties to p53, leading to p53 nuclear export and degradation via the 26S proteasome (Honda *et al.*, 1997; Haupt *et al.*, 1997; Kubbutat *et al.*, 1997; Fang *et al.*, 2000; Li *et al.*, 2003).

The negative regulation of p53 by Mdm2 needs to be transiently inhibited in order for p53 protein levels to rise and p53 downstream pathways to be activated in response to stress. The mechanism that allows p53 to escape Mdm2 is not known for all cellular stresses, but one well-studied regulator of Mdm2 in the response to oncogene activation in mice is the tumor suppressor $p19^{ARF}$ ($p14^{ARF}$ in humans). Upon activation, the $p19^{ARF}$ protein directly interacts with Mdm2, resulting in Mdm2 relocalization to the nucleolus (Bates *et al.*, 1998; Kamijo *et al.*, 1998; Pomerantz *et al.*, 1998; Stott *et al.*, 1998; Zhang *et al.*, 1998; Honda and Yasuda, 1999; Midgley *et al.*, 2000; Ito *et al.*, 2001; Weber *et al.*, 1999). This permits p53 protein stabilization and increased p53 function to limit the transformative effects of abnormal activation of cellular oncogenes (Sherr and Weber, 2000).

Additional mouse models, such as the Mdm2-hypomorph (*Mdm2*^{puro}), were generated to further explore the role of Mdm2 regulation of p53 in adult tissues (Mendrysa *et al.*, 2003). A majority of heterozygous mice bearing an Mdm2-hypomorphic allele and an Mdm2-null allele (*Mdm2*$^{puro/\Delta 7\text{-}9}$) were viable, indicating that the Mdm2 hypomorph protein partially retained wild-type Mdm2-dependent regulation of p53 during development. However, the Mdm2-compromised, adult mice had decreased body weights and defects in hematopoiesis. In agreement with a p53-dependent phenotype, the mice also displayed increased endogenous p53 target gene expression and spontaneous apoptosis. Furthermore, Mdm2$^{puro/\Delta 7\text{-}9}$ mice exhibited increased sensitivity to p53-dependent responses resulting in greatly decreased survival after whole-body irradiation. This increased IR-induced lethality was shown to be solely dependent on p53, as Mdm2$^{puro/\Delta 7\text{-}9}$, p53-null mice were completely radio-resistant.

MdmX, a close protein family member of Mdm2, was also shown to be a critical regulator of p53 *in vivo*. MdmX and Mdm2 share 34% amino acid identity (Figure 1.2) with each containing homologous p53-binding, acidic, zinc finger, and RING finger domains (Shvarts *et al.*, 1996). Like *Mdm2*, the *MdmX* gene is amplified and/or overexpressed in a number of different tumor types, including breast cancer, brain, soft tissue tumors, and retinoblastoma (Riemenschneider *et al.*, 1999; Riemenschneider *et al.*, 2003; Danovi *et al.*, 2004; Bartel *et al.*, 2005; Laurie *et al.*, 2006). However, *in vitro* studies have determined that MdmX does not mediate p53 protein degradation, suggesting that MdmX directly inhibits p53 activity solely through steric inhibition of p53 transcriptional activity (Jackson and Berberich 2000; Stad *et al.*, 2000).

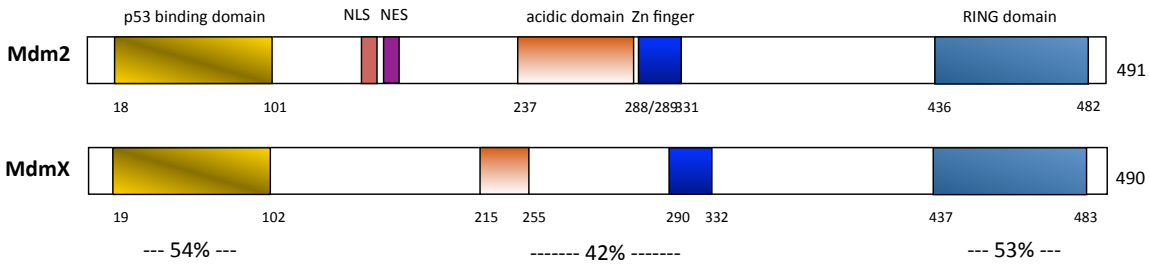

Figure 1.2: The domains of the Mdm2 and MdmX oncoproteins. The percent identity of the individual domains shared by the two proteins are shown. NLS: nuclear localization signal; NES: nuclear export signal; Zn finger: Zinc finger.

Several groups have generated MdmX-null alleles in mice (Parant *et al.*, 2001; Migliorini *et al.*, 2002; Finch *et al.*, 2002). In the initial study, MdmX-null mice displayed an embryonic lethality at E8.5-9.5 (Parant *et al.*, 2001), although subsequent MdmX-null models displayed lethality at E10.5-11.5 of gestation (Migliorini *et al.*, 2002; Finch *et al.*, 2002). As with the Mdm2-null models, these MdmX-null mouse models can be rescued by co-deletion of p53. Differences in the time of lethality between the two MdmX-null models may be due to subtle differences in the genetic backgrounds of the mice, or may arise due to slight differences in the MdmX-targeted alleles themselves.

The difference in the time of lethality between Mdm2-null mice (E5.5-6) and MdmX-null mice (E8.5-11) indicates developmental differences in the requirements for Mdm2 and MdmX-mediated inhibition of p53 during development. Furthermore, MdmX-null lethality in mice appears to be caused by a lack of cellular proliferation rather than by an increase in apoptosis (as seen in Mdm2-null embryos), and subsequent work has revealed that co-deletion of *p21* can delay the embryonic lethality of MdmX-null mice to E13.5-15.5 (Steinman *et al.*, 2004). While there is significant overlap in

Mdm2 and MdmX protein structure and homology, it is clear from these knockout mouse models that the roles and requirements of their negative regulation of p53 are notably different.

1.5 *Mdm2* and *MdmX* conditional knockout mice

While the results generated from the Mdm2 and MdmX knockout studies demonstrated the critical roles for each in regulating p53 during gestation, the embryonic lethal phenotypes of these models preclude further analysis of MDM functions in latter stages of development or in adult tissues. To further explore the roles of Mdm2 and MdmX *in vivo*, Mdm2 and MdmX conditional knockout mouse models have been generated (Steinman and Jones, 2002; Grier *et al.*, 2002; Grier *et al.*, 2006). These models allow temporal and/or spatial-restricted ablation of MDM proteins in mice, circumventing the early embryonic lethality in the constitutive MDM-null models. Using loxP-based conditional models and various Cre-driver mice, Mdm2 and MdmX expression has been subsequently ablated in many different tissue types. A listing of these published studies and their results are summarized in Table 1.1.

Tissue	Mdm2/MdmX Mouse Model	Cre-Transgene	Lethality	Phenotype	p53-dependent response	Ref
Bone	$Mdm2^{\Delta Ex11-12}$	Col3.6-Cre	Yes, before E19.5	Severely impaired osteoblast differentiation and bone formation	Increased p53 activity, but not protein levels, cellular proliferation and differentiation defects	Lengner *et al.*, 2006
Intestine	$Mdm2^{\Delta Ex5-6}$	Villin-Cre	No	Severe intestinal defects with eventual recovery due to selection against $Mdm2^{-/-}$ cells	Increased p53 protein levels, apoptosis	Valentin-Vega *et al.*, 2008
Cardio-myocytes	$Mdm2^{\Delta Ex5-6}$	αMyHC-Cre	Yes, before E13.5	Severe developmental defects in the heart with reduced cardiac cellularity	Increased p53 protein levels, apoptosis	Grier *et al.*, 2006
	$MdmX^{\Delta Ex2}$	αMyHC-Cre	Yes, after 1 year	Normal cardiac development and morphology, reason for premature death unknown	N/A	Grier *et al.*, 2006
CNS	$Mdm2^{\Delta Ex5-6}$	Nestin-Cre	Neonatal	Hydranencephaly, severe brain structure abnormalities	Increased p53 protein levels and activity, apoptosis	Xiong *et al.*, 2006
	$MdmX^{\Delta Ex2}$	Nestin-Cre	Neonatal	Proencephaly, less severe phenotype compared to Mdm2 knockout	Increased p53 protein levels and activity, apoptosis and cell cycle arrest	Xiong *et al.*, 2006
	$Mdm2^{\Delta Ex5-6}$ and $MdmX^{\Delta Ex2}$	Nestin-Cre	Neonatal	Synergistic effects more severe than either single knockout phenotype	Increased p53 activity, apoptosis and cell cycle arrest	Xiong *et al.*, 2006
RBC	$Mdm2^{\Delta Ex5-6}$	ER-GFP-Cre	Yes, E13	Severe defects in primary fetal erythropoiesis	Increased p53 protein levels, apoptosis	Maetens *et al.*, 2007
	$MdmX^{\Delta Ex2}$	ER-GFP-Cre	Partial between E12.5 and 21 days after birth	Fetal anemia	Increased p21 and Ptprv expression, cell proliferation defects	Maetens *et al.*, 2007
Smooth Muscle	$Mdm2^{\Delta Ex5-6}$	Tamoxifen-cre	12 days after deletion	Severe lesions in smooth muscle walls	Increased p53 protein levels and activity, caspase-3 independent apoptosis	Boesten *et al.*, 2006
	$MdmX^{\Delta Ex2}$	Tamoxifen-cre	No	No effect on smooth muscle walls	N/A	Boesten *et al.*, 2006

Table 1.1: Published Mdm2 and MdmX tissue-specific knockout studies to date.

Analysis of these models has revealed major differences in the requirements of MDM proteins in the development of different tissue types. For example, both Mdm2 and MdmX are critical for development of the central nervous system (CNS) in mice (Xiong *et al.*, 2006). However, absence of both Mdm2 and MdmX in the CNS resulted in a more severe phenotype than either single knockout, suggesting non-overlapping effects in this tissue. Conversely, deletion of Mdm2 in cardiomyocytes lead to embryonic lethality, whereas deletion of MdmX in these cells resulted in no obvious developmental defects (Grier *et al.*, 2006). The observations drawn from these models also suggest that Mdm2 and MdmX inhibit different p53-dependent responses in a tissue-specific manner. For example, Mdm2 clearly regulates p53-dependent apoptosis in adult intestine, cardiomyocytes, red blood cells, and embryonic epithelium (Valentin-Vega *et al.*, 2008; Grier *et al.*, 2006; Maetens *et al.*, 2007; Chavez-Reyes *et al.*, 2003). However, in osteoblasts, deletion of Mdm2 results in upregulated p21 expression and a p53-dependent cell growth arrest, with no increase in apoptosis (Lengner *et al.*, 2006). Thus, the mechanism by which Mdm2 or MdmX regulates cell growth in a given tissue, whether by promoting cell proliferation or inhibiting apoptosis, is highly dependent upon the precise role of p53 in the biology of that specific tissue.

1.6 *Mdm2* and *MdmX* transgenic mice

Mice bearing increased levels of *Mdm2* or *MdmX* expression have also been generated to further explore MDM-p53 signaling and to model MDM gene amplification events frequently observed in human tumors. Given that p53-null mice are viable, the *Mdm2* transgenic models have been surprisingly difficult to generate. This may be partly

due to the unusual toxicity frequently seen in primary cells induced to overexpress *Mdm2* (Brown *et al.*, 1998). However, several overexpressing MDM models have been successfully produced and studied. The first was an Mdm2-overexpressing mouse model that was generated by introducing a cosmid containing the murine *Mdm2* gene (including transcriptional start sites, introns, and 3' sequences) into mouse embryonic stem (ES) cells (Jones *et al.*, 1998). Clones were selected that had multiple copies of *Mdm2* integrated into a single site in the genome. These cells were used to generate chimeric mice, which were then bred to generate a line of Mdm2-transgenic mice that have a three to five fold increase in *Mdm2* expression levels in various tissues. Interestingly, ES cell lines exhibiting greater than 5-fold increase in *Mdm2* expression proved to be incapable of generating even chimeric mice, suggesting that large increases in Mdm2 are incompatible with normal embryonic cell biology. This is likely due to p53-independent effects, as p53-null ES cells are indistinguishable from wild-type ES cells and p53-null mice develop normally.

As was seen in human cancers, overexpression of Mdm2 in mice led to spontaneous tumorigenesis (Jones *et al.*, 1998). This result indicated that overexpression of Mdm2 was a major contributor to tumorigenesis and not just a "passenger" event in human cancers. Furthermore, the mice presented with a broad spectrum of spontaneous tumors similar to those seen in p53-null mice, and p53 activity and protein levels were diminished in tissues and cells derived from these mice. Sequence analysis confirmed that the *Mdm2* transgene was wild-type, revealing that *Mdm2* did not require additional "activating" mutations to promote tumorigenesis when overexpressed. Surprisingly,

Mdm2-transgenic, p53-null mice displayed a somewhat different tumor spectrum than p53-null mice, suggesting the existence of a p53-independent role for Mdm2 in tumorigenesis when overexpressed, at least in cells with inactivated p53. The relative contributions of p53-dependent signaling and p53-independent mechanisms in the neoplastic transformation of cells that overexpress Mdm2 are important topics for future studies.

Subsequent crosses of Mdm2-transgenic mice with $MdmX^{+/-}$ mice determined that overexpression of Mdm2 can fully rescue the embryonic lethality of the MdmX-null model (Steinman *et al.*, 2005). As it was previously established that deletion of p53 rescues the embryonic lethality of MdmX-null mice (Parant *et al.*, 2001; Migliorini *et al.*, 2002; Finch *et al.*, 2002), the ability of the Mdm2 transgene to inhibit p53 activity in mice likely underlies the recovery of the Mdm2-transgenic, MdmX-null mice. These results also demonstrated that MdmX is not absolutely required for Mdm2 to properly inhibit p53 function.

Efforts to understand the role of *MdmX* amplification in tumorigenesis have produced mixed results. One study generated a conditional *MdmX* transgene ($MdmX^{Tg}$) driven by the chicken *β–actin* promoter and CMV immediate-early enhancer (Xiong *et al.*, 2010). This conditional allele allowed temporal control over widespread *MdmX* overexpression to avoid the problems encountered in the Mdm2-transgenic model. However, it was determined that *MdmX* overexpression in this model did not lead to embryonic defects, and a subsequent constitutive MdmX-transgenic model ($MdmX^{Tg15}$)

was generated. Both the *MdmX*^{Tg} and *MdmX*^{Tg15} mice displayed increased tumorigenesis with a predominance of sarcomas, mirroring the tumor latency and spectrum of the Mdm2-transgenic model. Because *MdmX* overexpression is caused by chromosome amplification, this study also served to verify that *MdmX* is an oncogene and not a "passenger" to other "driver" oncogene(s) on the same chromosome (Xiong *et al.*, 2010).

Interestingly, the results of a separate ROSA26-driven, Myc-tagged MdmX-transgenic model (*MdmX*^{T}) revealed a very different phenotype (De Clercq *et al.*, 2010). Inheritance of one *MdmX* transgene (*MdmX*$^{T/+}$) resulted in elevated MdmX levels in the hemizygous mice, but did not increase spontaneous, DNA damage-induced, or *Eμ-Myc*-induced tumorigenesis. This may be due to MdmX levels needing to be above a certain threshold to affect tumorigenesis. However, mice homozygous for the transgene (*MdmX*$^{T/T}$) die early in embryonic development and present with severe vascular defects. Unlike the typical lethality seen in other mouse models with varying Mdm2 and/or MdmX levels, the lethality in the *MdmX*$^{T/T}$ mice was completely p53-independent. This may be due to the high levels of MdmX or to aspects of the transgene unrelated to MdmX itself. A side-by-side comparison of the MdmX levels in the two MdmX-transgenic models might explain the vast differences in the phenotypes observed in these two studies.

1.7 *Mdm2* and *MdmX* knock-in mice: exploring RING domain function

Mouse models have also been used to study the roles of specific Mdm2 and MdmX protein domains. These models were developed as valuable tools to not only

confirm or refute the physiological relevance of the initial experimental results *in vitro*, but to determine whether specific domains should be favored as therapeutic targets to effectively manipulate p53 signaling. As stated above, Mdm2 negatively regulates p53 via two mechanisms: direct protein binding and E3-ligase-dependent ubiquitination. To differentiate the importance of these two distinct functions, a mouse model with a specific knock-in mutation in the RING domain of Mdm2 (C462A) was generated (Itahana *et al.*, 2007). Co-immunoprecipitation experiments indicate that this mutation specifically abolished the E3-ligase activity of Mdm2 without altering the p53 binding function. Surprisingly, these mice die very early in embryonic development at E7.5 in a p53-dependent manner. While this proved problematic for further experimentation, the lethality in these mice demonstrated that binding of Mdm2-p53 is not sufficient to inhibit p53 activity during development. It remains to be seen if Mdm2 E3 ligase activity is required for Mdm2-dependent inhibition of p53 activity at later times in development or in adult mice. Although most of the phenotypes described in the various Mdm2-conditional studies listed in Table 1.1 can be attributed to excess p53 activity in the cell, not all tissues ablated for Mdm2 in these studies displayed increased p53 protein levels (Lengner *et al.*, 2006), and it is possible that a ligase-dead Mdm2 might still functionally inhibit p53 in certain tissues or in adult mice.

Although MdmX and Mdm2 both contain a carboxy-terminal RING domain, MdmX does not appear to share the intrinsic E3 ligase activity that Mdm2 possesses for p53. Rather, MdmX has been proposed to block p53 activity by binding and inhibiting the transactivation domain of p53 and/or by forming a heterodimer with Mdm2 and

promoting p53-ubiquitination indirectly by enhancing the E3 ligase activity of Mdm2 (Shvarts *et al.*, 1996; Stad *et al.*, 2000; Badciong and Haas, 2002; Linares *et al.*, 2003). Two mouse models with MdmX RING domain mutations have been generated to further explore the function of this protein domain. One model is a conditional MdmX RING domain knockout in which the endogenous *MdmX* exon 11 was replaced with a modified exon 11 that is missing sequences encoding 49 amino acids from the RING domain (Pant *et al.*, 2011). Mice homozygous for the RING deletion allele ($MdmX^{\Delta RING/\Delta RING}$) did not develop past E9.5 due to aberrant p53 activation, so these mice were crossed to a conditional hypomorphic p53 model that restored wild-type p53 levels in the presence of Cre-recombinase. MEFs generated from $MdmX^{\Delta RING/\Delta RING}$ embryos showed that the MdmX RING domain was dispensable for the ubiquitination and degradation of Mdm2 and p53, suggesting that the lethality in $MdmX^{\Delta RING/\Delta RING}$ mice may be due to a lack of p53 transcriptional inhibition. It is interesting to note that ablation of the MdmX RING domain in adult tissues had no noticeable impact on tissue function, suggesting a singular role for the MdmX RING domain in embryonic development.

Interestingly, data from a concurrent study in which a single amino acid substitution was made in the endogenous murine MdmX RING domain (C462A) confirmed some of the results from the ΔRING model while refuting others (Huang *et al.*, 2011). Mouse embryos that were homozygous for the RING domain mutation ($MdmX^{C462A/C462A}$) were not recovered past E9.5 due to p53-dependent apoptosis and cell proliferation arrest, exactly replicating the embryonic lethality of the $MdmX^{\Delta RING/\Delta RING}$ model. Likewise, the $MdmX^{C462A/C462A}$ embryos displayed increased p53 target gene

expression that likely contributed to the embryonic lethal phenotype. However, analysis of Mdm2 in MEFs generated from *MdmX*$^{C462A/C462A}$/p53-null mice indicated that an intact MdmX RING domain was required for full MdmX-Mdm2 binding and Mdm2 ubiquitination, contrary to what was seen in MEFs from the *MdmX*$^{\Delta RING/\Delta RING}$ model. While it is clear that the MdmX RING domain is critical in limiting p53 activity during development, the precise role of the MdmX RING in p53 inhibition is still open to debate. New MdmX models may be required, including those mutated for p53 recognition but retaining the RING domain. Such mice might be useful in resolving the precise contribution of the MDMX RING domain to the inhibition of p53 function.

1.8 *Mdm2* and *MdmX* knock-in mice: exploring cellular stress responses

The above studies clearly illustrate the important roles of MDM proteins in inhibiting p53 activity during development and in normal tissue growth. However, in order for p53 to become fully activated in response to various forms of cellular stress, MDM inhibition of p53 must be temporarily attenuated to facilitate p53 protein stabilization and subsequent target gene activation. This rapid, transient activation of p53 was long-thought to rely on post-translational modifications of numerous proteins within the p53 pathway. These modifications might be induced by various kinases or acetyl transferases activated in a stress-specific manner, and would facilitate the rapid and specific response of cells to different types of stress.

Activation of the p53 transcription factor during the DNA damage response has been the focus of numerous *in vitro* and *in vivo* studies, and many molecular models

integrating DNA damage signaling with p53 stabilization and activation have been proposed. Multiple DNA damage responsive proteins recognize DNA breaks, caused by ionizing radiation (IR) or cytotoxic drugs, and mediate downstream pathways such as DNA repair and apoptosis. The ataxia telangiectasia mutated (ATM) kinase is a major effector of the DNA damage response that phosphorylates a wide variety of protein targets. It has been previously shown that p53 protein stabilization is dependent on functional ATM signaling, and p53 encodes several residues in or adjacent to the Mdm2-interaction domain that are known to be direct and indirect targets of ATM phosphorylation (Jack *et al.*, 2002; Gurley and Kemp, 2007; Chao *et al*., 2000; MacPherson *et al.*, 2004; Wu *et al*., 2002). Several p53 knock-in mouse models have revealed that ATM phosphorylation of p53 is necessary for the full transcriptional activity of p53 after DNA damage, particularly those genes involved in apoptosis. However, these modifications had only modest effects on p53 protein stability and p53-mediated tumor suppression (Sluss *et al.*, 2004; Chao *et al.*, 2003; Chao *et al.*, 2006; Toledo and Wahl, 2006).

Because activated ATM also phosphorylates Mdm2 and MdmX *in vitro*, it was proposed that ATM modification of MDM proteins might potentially regulate IR-induced p53 stabilization. MdmX was proposed to be a target for DNA damage-induced phosphorylation by multiple kinases, including ATM (serine residue 402 in mice) and Chk2 (serine residues 341 and 367 in mice). All three of these serine residues were mutated to alanine in a triple knock-in mouse model ($MdmX^{3SA}$) to study the effect of DNA damage-induced phosphorylation of MdmX on p53 function (Wang *et al.*, 2009).

MdmX$^{3SA/3SA}$ mice had impaired p53 stabilization and decreased p53 activity in response to IR. Most *MdmX*$^{3SA/3SA}$ mice were radio-resistant to normally lethal doses of IR, and these phosphorylation events were necessary for robust suppression of lymphomas induced by an *Eμ-Myc* transgene. However, spontaneous tumorigenesis was not observed in *MdmX*$^{3SA/3SA}$ knock-in mice. Differences in the phenotypes of the Mdm2-null and MdmX-null mice suggest that there may be differences in the ability of Mdm2 and MdmX to regulate p53 activities following DNA damage. Therefore, the contributions of other Mdm2 and MdmX post-translational modifications to p53 regulation and p53 tumor suppression following DNA damage warrant examination.

1.9 Aims of this Dissertation

This dissertation will address some of the major questions that remain in the Mdm2-p53 field. Chapter 2 will illustrate the role of Mdm2 in limiting p53 activity in a specific tissue type in adult mice. As described above, many tissue-specific *Mdm2* knockout mouse models have been generated, but few survive long enough to observe the functional consequence of unregulated p53 in adult tissues. Ablation of *Mdm2* in the epidermis allows the long-term study of Mdm2-p53 signaling in adult cells and permits stem cell functional assays to be studied while causing minimal harm to the animals. Chapters 3 and 4 will describe the *in vivo* role of a specific phosphorylation site on Mdm2. *In vitro* studies have demonstrated that activated ATM phosphorylates MDM2 serine residue 395, and the timing of this modification is concurrent with increased p53 protein stability. Generation of mouse models bearing knock-in mutations at this specific residue enables the necessity of this posttranslational modification to be assessed at the

physiological level. These studies have contributed to the p53-Mdm2 field and open new scientific avenues that can be addressed in the future.

CHAPTER II:

MDM2-P53 SIGNALING REGULATES EPIDERMAL STEM CELL SENESCENCE AND PREMATURE AGING PHENOTYPES IN MOUSE SKIN

Foreword

The p53 transcription factor is activated by various types of cellular stress and induces the expression of genes that control cell growth and inhibit tumor formation. Analysis of mice that express mutant forms of p53 suggest that inappropriate p53 activation can alter tissue homeostasis and life span, connecting p53 tumor suppressor functions with accelerated aging. However, other mouse models that display increased levels of wild-type p53 in various tissues fail to corroborate a link between p53 and aging phenotypes, possibly due to the retention of signaling pathways that negatively regulate p53 activity in these models. In this study, we have generated mice lacking Mdm2 in the epidermis. Deletion of *Mdm2*, the chief negative regulator of p53, induced an aging phenotype in the skin of mice, including thinning of the epidermis, reduced wound healing, and a progressive loss of hair. These phenotypes correlate with an increase in p53-mediated senescence and a gradual loss of epidermal stem cell numbers and functions. The results of this study reveal that activation of endogenous p53 by ablation of *Mdm2* can induce accelerated aging phenotypes in mice.

Introduction

Analysis of several p53 mouse models has suggested that p53 must be negatively regulated in adult mice in order to facilitate homeostatic regulation of normal tissues and to prevent accelerated organismal aging. We have previously generated a mouse model that has one of the endogenous p53 alleles replaced with a mutant p53 allele (*m*) that encodes an amino-truncated p53 protein (Tyner *et al.*, 2002). This mutant p53 protein lacks transcription factor activity but does enhance the activity of the wild-type p53

protein. In keeping with an enhanced p53 phenotype, we found that $p53^{+/m}$ mice display a significantly reduced cancer incidence relative to wild-type mice. However, $p53^{+/m}$ mice have greatly reduced longevity due to early aging phenotypes including osteoporosis, reduced organ mass, a thinning of the dermis, and deficiencies in hair re-growth and wound healing (Tyner *et al.*, 2002). It was proposed that the increase in p53 activity in the $p53^{+/m}$ mice led to reduced stem cell proliferation in the affected tissues, which resulted in loss of tissue cellularity and early aging phenotypes (Tyner *et al.*, 2002). More recently, the Scrable lab generated transgenic mice expressing a short, naturally occurring, p53 splice isoform lacking sequences encoding the amino terminal portion of the p53 protein. The variant p53 protein (p44) encoded by this transgene induced p53 hyperactivity and a reduced cancer incidence in these transgenic mice. The *p44* mice displayed an increase in aging-associated insulin growth factor signaling and accelerated aging phenotypes, which parallels the results of the $p53^{+/m}$ model and supports a positive relationship between p53 activity and aging (Maier *et al.*, 2004).

In contrast to these findings, other mouse models that contain increased amounts of p53 activity fail to present with accelerated aging phenotypes. The "super-p53" transgenic mice harbor an extra copy of wild-type *p53* and display upregulated p53 activities and increased cancer resistance, yet these mice have normal life span and normal skeletal structure, hair growth, and skin thickness (Garcia-Cao *et al.*, 2002). Likewise, mice bearing reduced levels of Mdm2 activity due to the presence of a hypomorphic Mdm2 allele ($Mdm2^{puro}$) were found to have increased levels of p53

activity and increased resistance to tumor formation, but did not possess any of the features characteristic of accelerated aging (Mendrysa *et al.*, 2006).

One possible explanation for the differences in the aging phenotypes in these various mouse models is that the p53 proteins encoded by the m allele and the *p44* transgene lack the amino-terminal portion of p53 containing the p53-Mdm2 interaction domain. Therefore, these variant p53 proteins would not be subject to Mdm2 regulation, whereas Mdm2 would negatively regulate the wild-type, full-length p53 proteins encoded in the super p53 transgenic mice. And although there is reduced Mdm2 function and increased p53 activity in the Mdm2-hypomorphic model, the endogenous wild-type p53 proteins encoded in these mice are still subject to Mdm2 binding and regulation, albeit at a reduced level. While other p53-interacting proteins may be affected, it is possible that the ability of Mdm2 to fully regulate p53 may underlie the presence or absence of any accelerated aging phenotypes in these various mouse models.

An alternate explanation for the differences in aging phenotypes in these models is that the amino-truncated forms of p53 encoded by the m allele or the *p44* transgene might be inducing an early aging phenotype by altering the activity of p63, a p53 family member that has been recently demonstrated to regulate senescence in fibroblasts and epithelial cells in a p53-independent manner and to induce premature aging phenotypes in the skin of mice (Guo *et al.*, 2009; Flores and Blasco, 2009). Therefore, the role of p53 in regulating accelerated aging in mice remains a matter of much debate (Poyurovsky and Prives, 2006; Vijg and Hasty, 2005; Gentry and Venkatachalam, 2005).

In this study, we have utilized an *Mdm2* conditional knockout mouse model to determine whether epidermal-specific loss of Mdm2-p53 signaling in newborn mice can induce a premature aging phenotype in the skin. Such an approach allows us to avoid the embryonic lethality associated with ubiquitous or tissue-specific inactivation of Mdm2 during development (Jones *et al.*, 1995; Montes de Oca Luna *et al.*, 1995; Itahana *et al.*, 2007; Lengner *et al.*, 2006; Xiong *et al.*, 2006). Furthermore, Mdm2 does not regulate the stability and transcriptional activity of the p63 protein (Wang *et al.*, 2001; Little and Jochemsen *et al.*, 2001). Therefore, ablation of *Mdm2* permits a specific assessment of the effects of the endogenous p53 protein in organismal aging.

Our results reveal that deletion of *Mdm2* in mouse epidermis leads to increased p53 protein levels, but not p63 protein levels, and increased expression of p53 target genes that are specifically involved in regulating cellular senescence. These *Mdm2*-ablated mice display hallmarks of accelerated aging in their skin, including a thinning of the epidermal layer, reduced integrity of the skin, and widespread and progressive hair loss. Analysis of the epidermis in these mice indicates increased cellular senescence in the follicular bulge region and a reduction in skin epidermal stem cell numbers and functions, as determined by FACS analysis, wound healing, and hair growth assays. These findings document a role for Mdm2-p53 signaling in the maintenance of the epidermal stem cell compartment, and demonstrate that increased activity of endogenous p53 can induce early aging phenotypes in mouse skin.

Results

To study the role of Mdm2 in regulating p53-mediated effects on premature aging phenotypes, *Mdm2* conditional knockout mice ($Mdm2^{c/c}$) were mated with transgenic mice bearing the *Cre recombinase* (*Cre*) transgene under the transcriptional control of *Keratin 5* promoter sequences (*K5-Cre*) (Steinman and Jones, 2002; Zhou et al., 2002). Since the *K5* promoter is active in early postnatal development in epidermal progenitor cells of the skin and hair follicles, induction of *Cre* expression should excise exons 11 and 12 in the conditional Mdm2 allele, resulting in loss of functional Mdm2 in the epidermis (Figure 2.1).

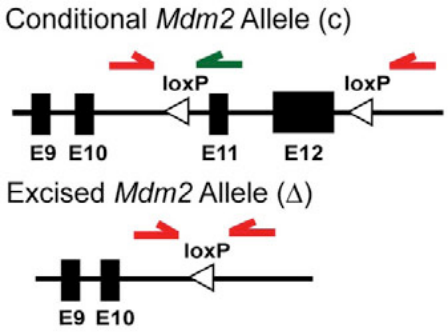

Figure 2.1: The $Mdm2^{c/c}$ and $Mdm2^{\Delta/\Delta}$ alleles. Exons 11 and 12 of the conditional Mdm2 allele (c) are flanked by loxP sites (*top*). Cre recombinase deletes these floxed exons, generating an Mdm2 knockout allele (Δ, *bottom*). Colored arrows represent PCR primers used to identify the conditional *Mdm2* allele and to detect genomic rearrangement.

To confirm robust Cre recombinase function in the epidermis of *K5-Cre* mice, Rosa26 Flox-Stop-β-Geo reporter (*R26R*) mice were crossed with *K5-Cre* mice and the pattern of *β–galactosidase* (*β–gal*) gene activity was examined in these compound

heterozygous mice. β–galactosidase activity was detected in the interfollicular epidermis and hair follicles of 4-week old *K5-Cre*, *R26R* mice, indicating robust Cre recombinase mediated excision of floxed alleles specifically in epidermal cells (Figure 2.2). To document excision of the floxed exons in the *Mdm2* conditional knockout mice, genomic DNA was isolated from tissues of $Mdm2^{c/c}$ and $Mdm2^{c/c}$, *K5-Cre* mice ($Mdm2^{\Delta/\Delta}$), and PCR was performed to determine the status of the Mdm2 alleles. Loss of functional Mdm2 alleles was observed in the skin of $Mdm2^{\Delta/\Delta}$ mice, but not in various control tissues such as spleen (Figure 2.3). To confirm that Cre-excision of the floxed *Mdm2* exons in the epidermis resulted in loss of Mdm2 function, we examined p53 levels in the epidermis of $Mdm2^{\Delta/\Delta}$ mice at 5 months of age. Western blot analysis revealed that endogenous p53 protein levels are slightly increased (3-4 fold by densitometry) in the skin of $Mdm2^{\Delta/\Delta}$ mice (Figure 2.4).

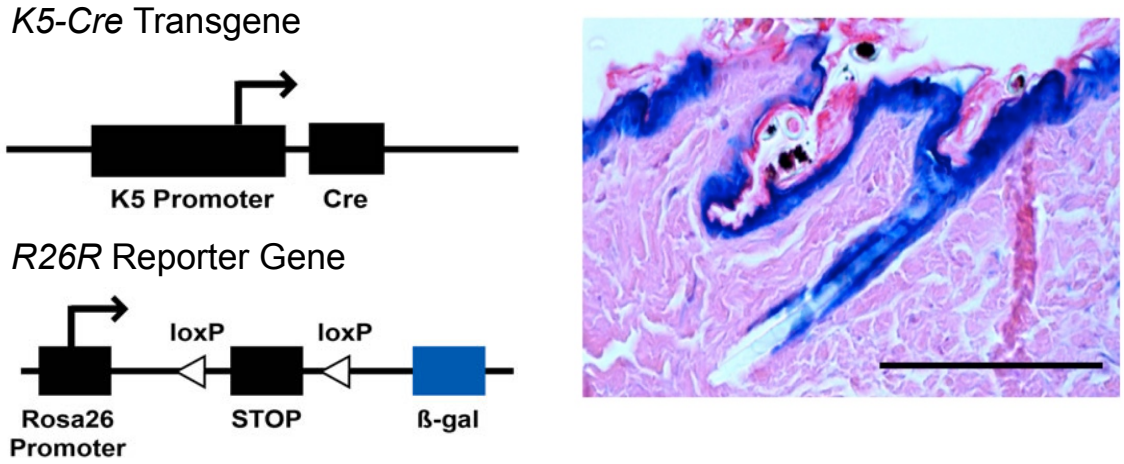

Figure 2.2: LacZ staining in Rosa26 Flox-Stop β-Geo reporter mice expressing the *K5-Cre* transgene. Scale bar represents 100 μm.

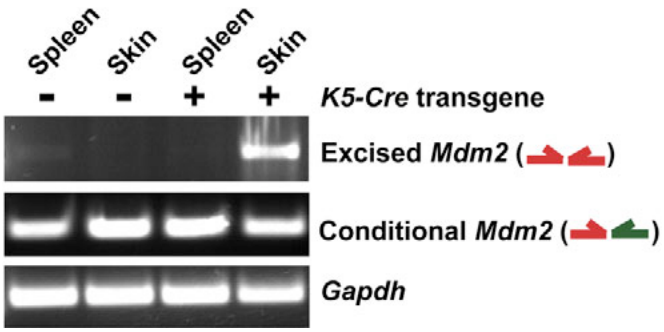

Figure 2.3: PCR indicates excision in the skin of *Mdm2*$^{\Delta/\Delta}$ mice. Genomic PCR indicates excision of the Mdm2 allele specifically in the skin of *Mdm2*$^{c/c}$ mice that also inherited the K5-Cre transgene. Colored arrows correspond to the primers in Figure 2.1. *Gapdh* was used as a loading control.

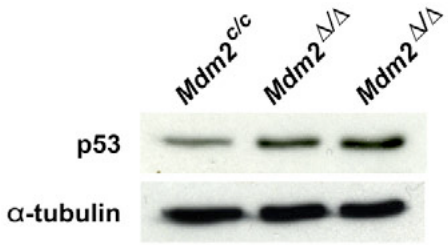

Figure 2.4: Western blot of p53 protein levels in skin from 5-month-old mice. α-Tubulin was used as a loading control.

Loss of Mdm2 function has been associated with an increase in p53-mediated cell growth arrest or apoptosis in a number of mouse models, resulting in aberrant tissue function (Jones *et al.*, 1995; Montes de Oca Luna *et al.*, 1995; Itahana *et al.*, 2007; Mendrysa *et al.*, 2006; Lengner *et al.*, 2006; Xiong *et al.*, 2006; Grier *et al.*, 2006). Surprisingly, *Mdm2*$^{\Delta/\Delta}$ mice younger than 10 months of age display no overt phenotype, despite the loss of Mdm2 function and increased p53 stabilization in the epidermis (Figures 2.5 and 2.6).

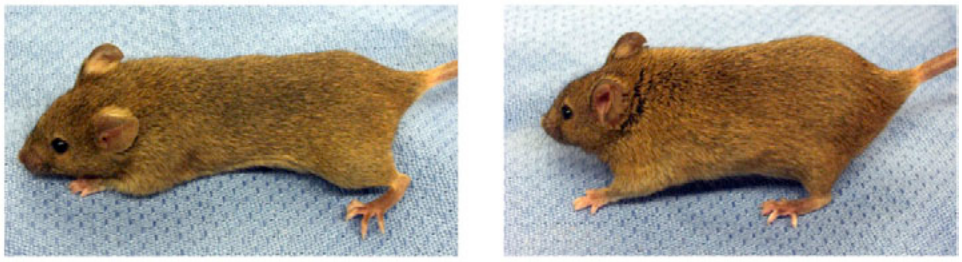

Figure 2.5: Younger *Mdm2*$^{c/c}$ (*left*) and *Mdm2*$^{\Delta/\Delta}$ mice (*right*) reveals no overt phenotypic difference.

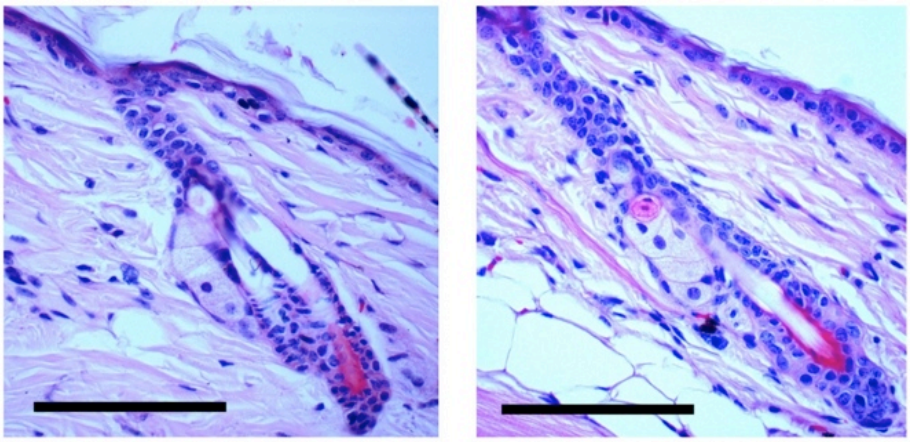

Figure 2.6: H&E staining of representative hair follicles from young *Mdm2*$^{c/c}$ (*left*) and *Mdm2*$^{\Delta/\Delta}$ mice (*right*). Scale bars represent 100 μm.

However, all *Mdm2*$^{\Delta/\Delta}$ mice displayed progressive hair loss and decreased skin elasticity as they continued to age (Figure 2.7). Analysis of hematoxylin & eosin (H&E) -stained sections of skin from older (14-15 month old) *Mdm2*$^{\Delta/\Delta}$ mice revealed fewer hair follicles per millimeter (fl/mm) of dorsal skin in *Mdm2*$^{\Delta/\Delta}$ mice (0.70 fl/mm) than in

control *Mdm2*$^{c/c}$ mice (1.4 fl/mm) (p=0.003). In addition, 27.1% of *Mdm2*$^{\Delta/\Delta}$ follicles display an abnormal phenotype compared to 7.0% of the follicles in age-matched *Mdm2*$^{c/c}$ controls (p=0.004). These abnormal *Mdm2*$^{\Delta/\Delta}$ follicles were dilated, debris-laden, devoid of a hair shaft, cellularly atrophic, and morphologically disorganized (Figure 2.8).

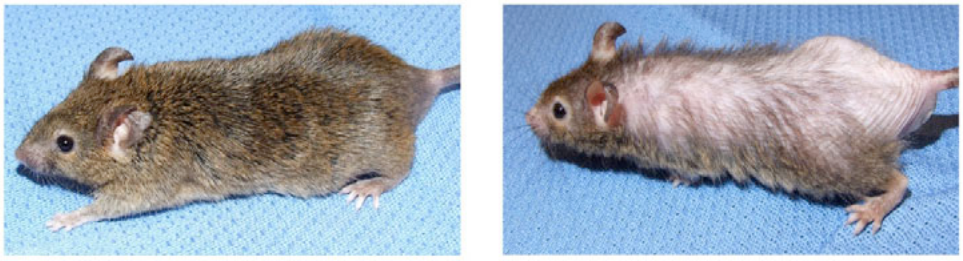

Figure 2.7: Phenotype of older *Mdm2*$^{\Delta/\Delta}$ mice (*right*). These include increased hair loss in aged mice deleted for *Mdm2* compared to older *Mdm2*$^{c/c}$ mice (*left*).

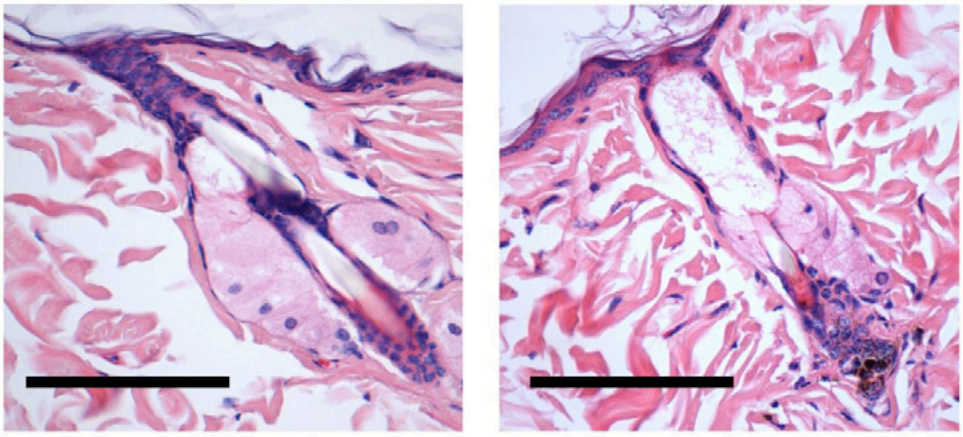

Figure 2.8: H&E staining of representative hair follicles from older *Mdm2*$^{c/c}$ (*left*) and *Mdm2*$^{\Delta/\Delta}$ mice (*right*). Scale bars represent 100 μm.

In addition to defects in hair maintenance, approximately 10% of all *Mdm2*$^{\Delta/\Delta}$ mice developed severe open skin wounds between 18-24 months of age. As these affected mice were housed individually, the skin lesions were likely caused by self-grooming. Similar wounding was not observed in age-matched, *Mdm2*$^{c/c}$ control mice or in older *K5-Cre* transgenic mice. To further examine the epidermal defects in these mice, skin biopsies were taken from *Mdm2*$^{\Delta/\Delta}$ mice and *Mdm2*$^{c/c}$ control mice at 16 months of age. There was an obvious decrease in the thickness of the interfollicular epidermis in older *Mdm2*$^{\Delta/\Delta}$ mouse relative to age-matched controls, accounting for the diminished integrity of the epidermal layer in older *Mdm2*$^{\Delta/\Delta}$ mice (Figure 2.9). These phenotypes are not present in young *Mdm2*$^{\Delta/\Delta}$ mice (Figure 2.6), suggesting a gradual degeneration of epidermal skin and hair follicle morphology in *Mdm2*$^{\Delta/\Delta}$ mice over time.

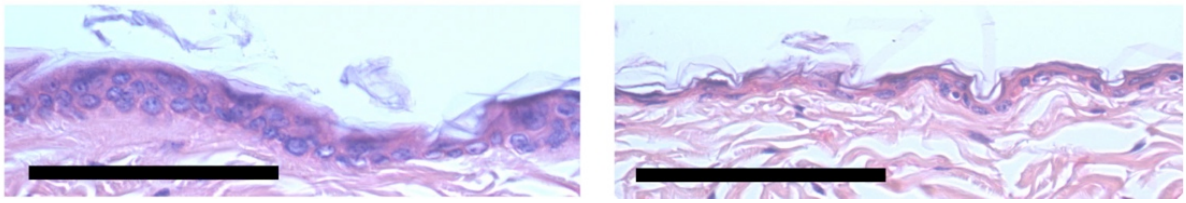

Figure 2.9: H&E staining of interfollicular epidermis from older *Mdm2*$^{c/c}$ (*left*) and *Mdm2*$^{\Delta/\Delta}$ mice (*right*). Scale bars represent 100 μm.

To examine epidermal p53 levels in older mice, we performed western blot analysis using skin protein lysates isolated from 20- to 23-month old *Mdm2*$^{\Delta/\Delta}$ and

Mdm2$^{c/c}$ mice, as well as lysates isolated from γ–irradiated (3Gy) control mice (Figure 2.10). The amount of p53 present in older *Mdm2*$^{\Delta/\Delta}$ skin was far greater than the level of p53 detected in age-matched control *Mdm2*$^{c/c}$ skin, and was comparable to p53 levels observed in irradiated *Mdm2*$^{c/c}$ controls.

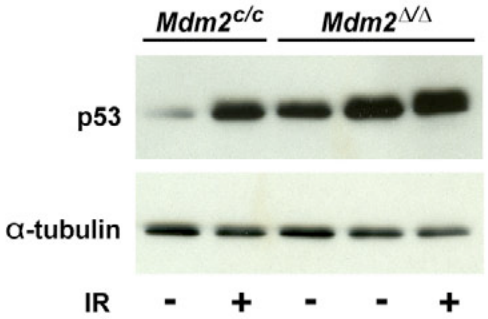

Figure 2.10: Western blot of p53 protein levels in skin from untreated and γ-irradiated (3Gy, 15 hours) 20- to 23-month-old mice. α-Tubulin was used as a loading control.

To determine if the highly elevated p53 levels in older *Mdm2*$^{\Delta/\Delta}$ mice correlated with increased p53 activity, we examined the expression levels of select p53 target genes in the skin of 5-month old mice and 16-month old mice by quantitative real-time PCR (qRT-PCR) (Figure 2.11). Little or no elevation of the expression levels of p53 target genes was observed in the younger mouse skin (*left panel*). In contrast, the large increase in p53 protein levels in the older mouse skin correlated with an increase in p53 target gene activation (*right panel*). However, only a subset of p53 target genes displayed increased expression in older *Mdm2*$^{\Delta/\Delta}$ skin samples. Interestingly, these upregulated

p53 targets included genes associated with cell cycle arrest and senescence (*p21*, *Pai-1* and *Pai-2*) but not apoptosis (*Puma* and *Noxa*).

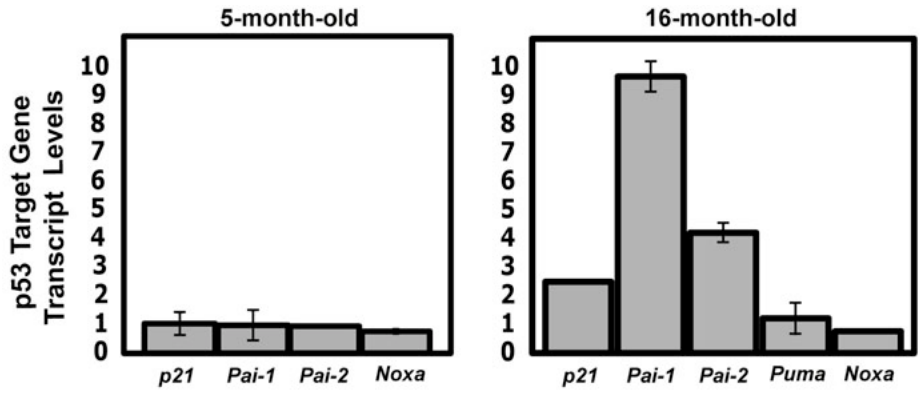

Figure 2.11: Relative mRNA levels of p53 target genes in untreated skin from young (*left*) and older (*right*) mice determined by qRT-PCR. Values represent the fold difference in $Mdm2^{\Delta/\Delta}$ mice compared to $Mdm2^{c/c}$ mice (n=3 per genotype). All levels were normalized to *Gapdh*. Standard deviation indicated by error bars.

To confirm that ablation of Mdm2 and upregulation of p53 activity in the skin of $Mdm2^{\Delta/\Delta}$ mice did not induce apoptosis in this tissue, we performed terminal deoxynucleotidyl transferase dUTP nick end labeling (TUNEL) staining on skin sections of 14-16 month old $Mdm2^{\Delta/\Delta}$ and $Mdm2^{c/c}$ mice (Figure 2.12). TUNEL staining was readily detected at the base of those follicles undergoing remodeling (catagen-phase). This staining was anticipated, because normal hair remodeling is ongoing even in older mice and appears to be regulated primarily by Bcl2 and not by p53 (Stenn and Paus, 2001). However, TUNEL positive cells were not observed in either the follicular or interfollicular epidermis of older $Mdm2^{c/c}$ or $Mdm2^{\Delta/\Delta}$ mice indicating that increased p53

activity in the skin of *Mdm2*$^{\Delta/\Delta}$ mice did not correlate with an increased number of apoptotic cells (note the lack of any cellular staining in the figures). These negative results correlate with the lack of increased apoptotic gene expression seen in the skin of *Mdm2*$^{\Delta/\Delta}$ mice, confirming that the loss of hair and thinning of the epidermis seen in the *Mdm2*$^{\Delta/\Delta}$ mice is unlikely to be due to p53-mediated apoptosis in the skin.

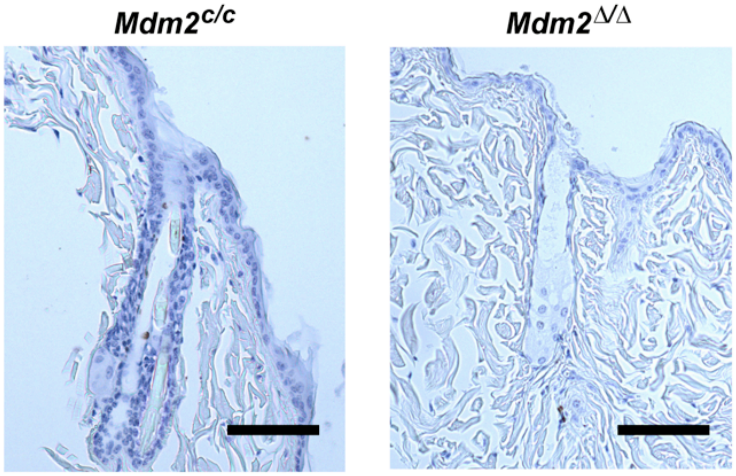

Figure 2.12: TUNEL staining of skins from aged *Mdm2*$^{c/c}$ and *Mdm2*$^{\Delta/\Delta}$ mice. Scale bars represent 100 μm.

Increased cellular senescence has been linked to aging phenotypes in other mouse models (Rodier et al., 2007). Since upregulation of p53 activity in *Mdm2*$^{\Delta/\Delta}$ mice resulted in the activation of p53 target genes primarily involved in cell senescence, we examined the epidermis of older *Mdm2*$^{\Delta/\Delta}$ mice for senescent cells. Skin sections of 16-month old *Mdm2*$^{\Delta/\Delta}$ mice and *Mdm2*$^{c/c}$ mice were fixed and stained for senescence-

associated-β–galactosidase (SA-β-Gal) activity. SA-β-Gal activity was undetectable in the follicular epithelium of *Mdm2*$^{c/c}$ control mice, whereas 21% (±3.6%) of the hair follicles in *Mdm2*$^{\Delta/\Delta}$ mice stained positive for SA-β-Gal activity (Figure 2.13). Interestingly, SA-β-Gal staining was particularly acute in the follicular bulge, the region of the follicle containing the epidermal stem cell compartment (Tumbar et al., 2004).

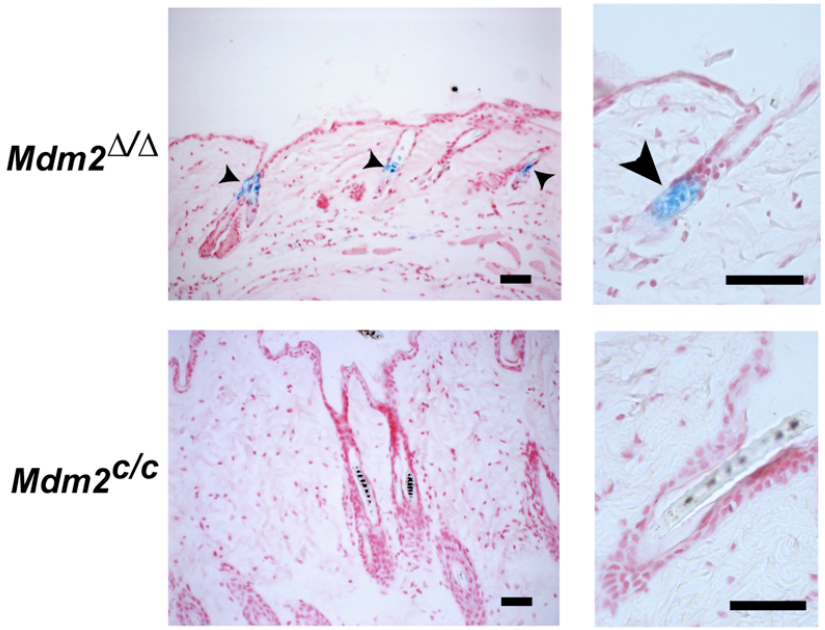

Figure 2.13: Senescence-associated-β-galactosidase activity detected in skin of aged *Mdm2*$^{\Delta/\Delta}$ mice (*top*) but not in *Mdm2*$^{c/c}$ mice (*bottom*). Sections were counterstained with Nuclear Fast Red. Scale bars represent 50 μm. Arrowheads denote SA-β-gal stain.

To confirm senescence of epidermal cells in *Mdm2*$^{\Delta/\Delta}$ mice, we examined expression of the *p16*^{INK4A} tumor suppressor, a gene whose expression is not governed by p53 and that has been previously reported to be increased in senescent and aging skin

cells of older mice and humans (Jenkins, 2002; Ressler et al., 2006; Campisi, 2005). A significant increase in $p16^{INK4A}$ expression was detected by qRT-PCR in the skin of older $Mdm2^{\Delta/\Delta}$ mice, relative to expression levels in age-matched $Mdm2^{c/c}$ skin (Figure 2.14), confirming that loss of Mdm2-p53 signaling induces an established molecular marker of senescence and accelerated aging in the epidermis.

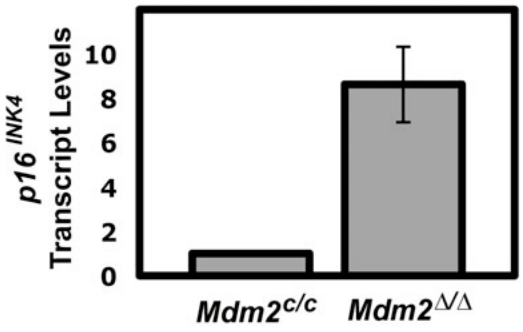

Figure 2.14: Relative $p16^{INK4A}$ mRNA levels in skin from older mice determined by qRT-PCR (n=3 per genotype). Levels were normalized to *Gapdh*. Standard deviation indicated by error bars.

SA-β-Gal staining of the follicular bulge region and upregulation of $p16^{INK4A}$ expression indicates premature cell senescence in the epidermal stem cell compartment of $Mdm2^{\Delta/\Delta}$ mice. To confirm that the defect in $Mdm2^{\Delta/\Delta}$ mice is due to the reduced numbers of epidermal stem cells, we examined $Mdm2^{\Delta/\Delta}$ follicular bulge cells for cytokeratin 15 (K15) and LIM homeobox protein 2 (Lhx2) staining, specific markers of bulge stem cells in mice (Liu et al., 2003; Rhee et al., 2006). Staining of skin cross sections of older $Mdm2^{\Delta/\Delta}$ and control $Mdm2^{c/c}$ mice revealed a decrease in K15-positive

and Lhx2-positive cells in *Mdm2*$^{\Delta/\Delta}$ mice (Figure 2.15). Typical follicles in *Mdm2*$^{\Delta/\Delta}$ mice have very faint K15 and Lhx2 staining compared to age-matched control follicles, and staining is absent in the all of the abnormal follicles examined in *Mdm2*$^{\Delta/\Delta}$ mice.

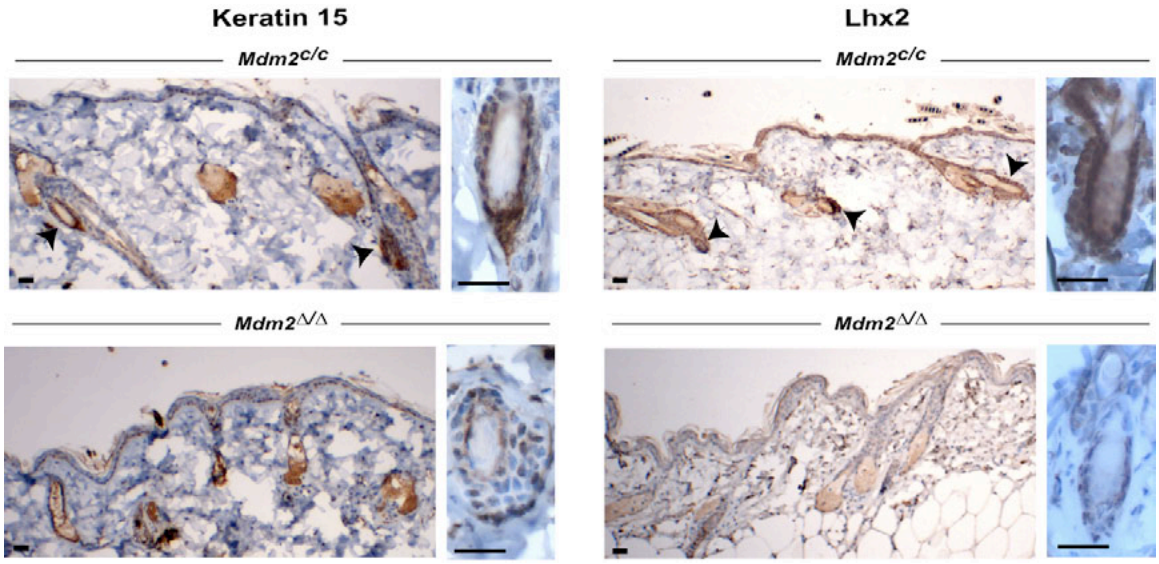

Figure 2.15: Follicular cytokeratin 15 (*left*) and Lhx2 (*right*) staining in older *Mdm2*$^{c/c}$ and *Mdm2*$^{\Delta/\Delta}$ mice. Arrowheads denote specific staining. Scale bars represent 25 μm.

To confirm a reduction in numbers of epidermal stem cells in mice ablated for *Mdm2*, we performed FACS analysis of epidermal cells harvested from age-matched *Mdm2*$^{\Delta/\Delta}$ and control *Mdm2*$^{c/c}$ mice and documented the numbers of cells expressing high levels of both CD34 and a6-integrin, well-established epidermal stem cells markers (Nowak and Fuchs, 2009). In agreement with our K15 and Lhx2 staining results, fewer CD34/a6-intgrin double-positive cells are present in the skin of *Mdm2*$^{\Delta/\Delta}$ mice compared

to the numbers of double positive cells in *Mdm2*$^{c/c}$ control mice (Figure 2.16). Interestingly, while fewer epidermal stem cells are seen in the skin of *Mdm2*$^{\Delta/\Delta}$ mice at 3 months and 9 months of age (before the skin phenotype is observed in these mice), a much larger decrease in epidermal stem cell numbers is seen in 14-month old *Mdm2*$^{\Delta/\Delta}$ mice (Figure 2.16), when the phenotype of the *Mdm2*$^{\Delta/\Delta}$ mice is readily apparent (see Figure 2.7 and 2.8).

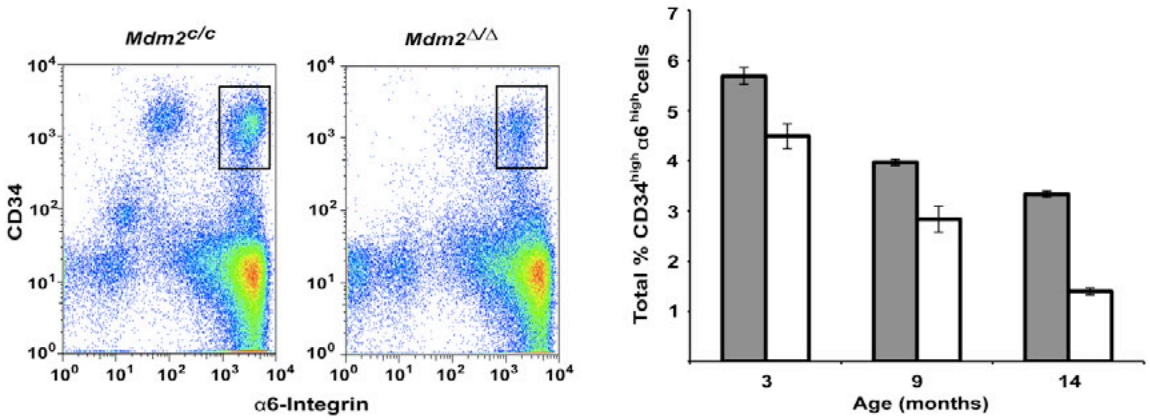

Figure 2.16: Quantification of bulge stem cells by FACS. Representative FACS plots for 9-month-old *Mdm2*$^{c/c}$ and *Mdm2*$^{\Delta/\Delta}$ mice (*left*). Bulge stem cells (CD34^{high}/α6-Integrin^{high}) are shown in black boxes. The total percentages of CD34^{high}/α6-Integrin^{high} cells determined by FACS analysis in *Mdm2*$^{c/c}$ (grey bars) and *Mdm2*$^{\Delta/\Delta}$ (white bars) mice are plotted at right (n=3 per genotype). Standard deviation indicated by error bars.

Loss of tissue regenerative potential and disrupted organ homeostasis are hallmarks of normal aging in mice and are often exacerbated in mouse models of accelerated aging (Rodier et al., 2007; Campisi, 2005). In skin, follicular bulge stem cells produce transiently amplifying epidermal progenitor cells that migrate to wounded

areas of the interfollicular epidermis and coordinate the wound healing response (Tumbar et al., 2004; Taylor et al., 2000). To confirm that epidermal stem cell function is compromised in older $Mdm2^{\Delta/\Delta}$ mice, we compared the decrease in diameter of an introduced 3mm^2 dorsal wound in $Mdm2^{\Delta/\Delta}$ mice and $Mdm2^{c/c}$ control mice. Wounds in younger (2 to 4-month old) $Mdm2^{\Delta/\Delta}$ and $Mdm2^{c/c}$ mice healed at a similar rate (Figure 2.17), with an average 65% wound closure in mice of both genotypes at 8 days. Wounds in older (14 to 16-month old) $Mdm2^{c/c}$ control mice closed at a rate similar to that seen in the younger mice. In contrast, wounds in the older $Mdm2^{\Delta/\Delta}$ mice closed at a much slower rate, consistent with a decrease in epidermal stem cell function. After 8 days, the wound sites in control $Mdm2^{c/c}$ mice were fully healed, whereas the wound sites in age-matched $Mdm2^{\Delta/\Delta}$ mice remained mostly open (Figure 2.17).

Epidermal stem cells are also required to promote the anagen-telogen-catagen hair cycle (Tumbar et al., 2004; Morris and Potten, 1999), and the rate of hair regrowth after shaving of mice is another direct measure of follicular stem cell function. To further confirm loss of epidermal stem cell-mediated functions in older $Mdm2^{\Delta/\Delta}$ mice, we shaved the hair from a 4cm^2 dorsal area on $Mdm2^{\Delta/\Delta}$ mice and $Mdm2^{c/c}$ control mice and measured hair re-growth over time (Figure 2.18). Parallel to the wound healing results, hair growth in older (14-16 month old) $Mdm2^{\Delta/\Delta}$ mice is significantly delayed relative to

control mice in the 3-week interval after shaving (Figure 2.18). In addition, older *Mdm2*$^{\Delta/\Delta}$ mice display reduced hair growth even 80 days post-shaving (Figure 2.18).

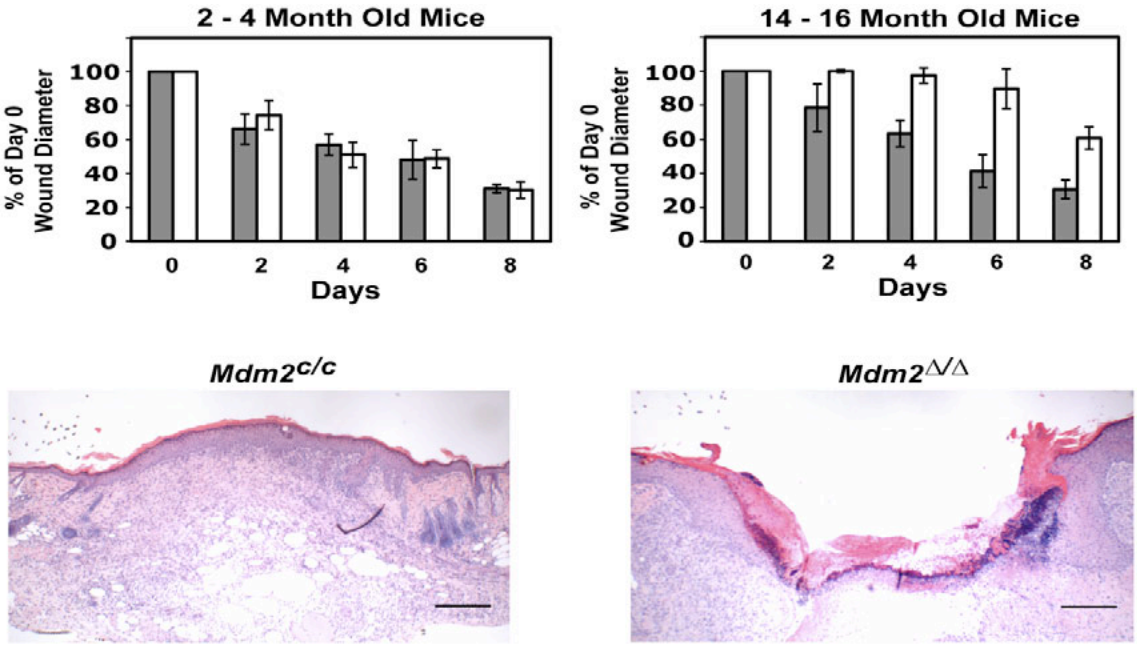

Figure 2.17: Wound healing assay of 2- to 4-month old and 14- to 16-month old *Mdm2*$^{c/c}$ (grey bars) and *Mdm2*$^{\Delta/\Delta}$ mice (white bars). The decrease in diameter of a dorsal punch biopsy wound was measured over time (n=3 per genotype). Standard deviation indicated by error bars. H&E staining of wounds (*bottom*) from a *Mdm2*$^{c/c}$ mouse and a *Mdm2*$^{\Delta/\Delta}$ mouse at day 8 of the wound healing assay. Scale bars represent 250 μm.

Discussion

The *Mdm2*$^{\Delta/\Delta}$ mice present a premature aging phenotype in the epidermis that is highly similar to the accelerated aging phenotype that we observed previously in the skin

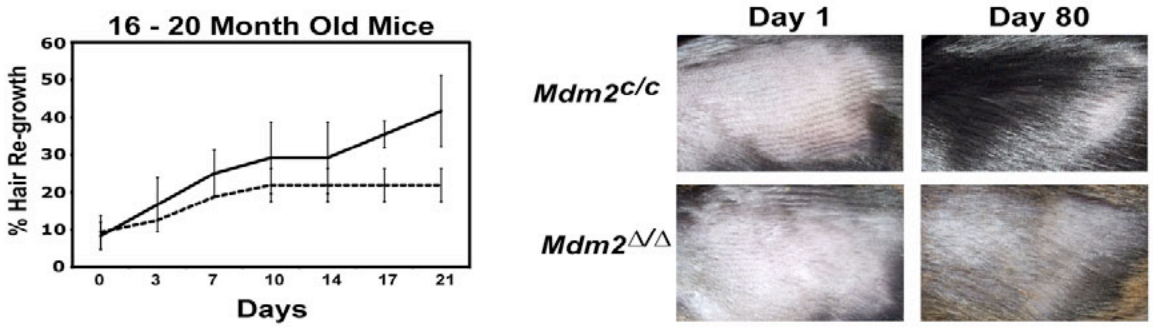

Figure 2.18: Hair re-growth in 16- to 20-month-old mice. The percentage hair growth for $Mdm2^{c/c}$ mice (solid line) and $Mdm2^{\Delta/\Delta}$ mice (dotted line) was plotted over time (n=3 per genotype). Standard deviation indicated by error bars. Pictures of an aged $Mdm2^{c/c}$ mouse and $Mdm2^{\Delta/\Delta}$ mouse at day 1 and day 80 post-shaving (*right*).

of $p53^{+/m}$ mice, including a thinning of the epidermal layer, reduced wound healing, and a reduced capacity to re-grow hair. As deletion of *Mdm2* results in an increase in endogenous p53 levels, but no detectable change in p63 protein levels (Figure 2.19), and upregulation of select p53 target gene expression in the epidermis of $Mdm2^{\Delta/\Delta}$ mice, our results corroborate that an increase in p53 activity in $p53^{+/m}$ mice is responsible for the accelerated aging phenotypes observed previously in this model and in certain other p53 models (Tyner et al., 2002; Maier et al., 2004). However, not all mouse models bearing increased levels of p53 display premature aging, and retention of some degree of Mdm2-p53 signaling in these models may well account for the lack of accelerated aging-like phenotypes in these mice (Garcia-Cao et al., 2002; Mendrysa et al., 2006).

It is interesting to note that ablation of *Mdm2* and upregulation of p53 in the epidermis did not result in p53 activation of pro-apoptotic genes and immediate cell death as seen in other settings (Lengner et al., 2006; Xiong et al., 2006; Martins et al., 2006).

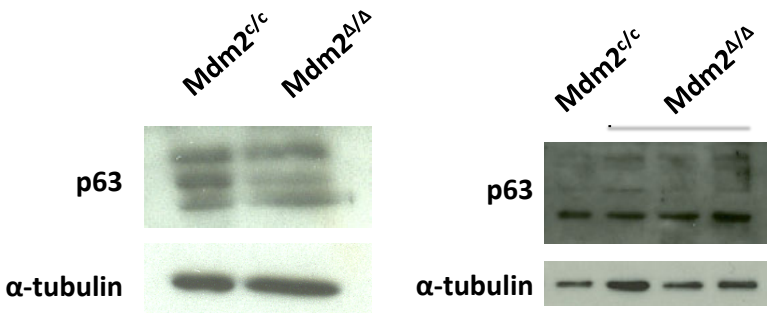

Figure 2.19: Western blot of p63 protein levels in skin from older mice. The multiple isoforms of p63 resulted in multiple bands on the western blot. α-Tubulin was used as a loading control.

This may be due to epigenetic networks of histone modifications that have recently been found to exist in epidermal stem cells (Mulder *et al.*, 2012). Disruption of Mdm2-p53 signaling induced SA-β-Gal staining of the follicular bulge region, indicating cellular senescence within the epidermal stem cell compartment in $Mdm2^{\Delta/\Delta}$ mice. Thus, the ability of Mdm2 to properly regulate p53-mediated senescence in this tissue determines the presence or absence of p53-associated aging phenotypes. Activation of p53-mediated cell senescence in epidermal stem cells and altered wound healing has also been observed in mice bearing shortened telomeres (Flores and Blasco, 2009), supporting a role for p53 activation in regulating epidermal stem cell function. However, as hair loss and reduced skin integrity was not reported in these mice, the differences in the level of p53 activation or the timing of p53-induced senescence in the epidermis may also underlie the presence or absence of aging-like phenotypes in the skin.

The results of our study reveal that loss of Mdm2, the concomitant upregulation of p53, and the subsequent induction of p53-mediated senescence induces an accelerated aging (but not progeria-like) phenotype in the skin. Although increased p53 levels can be detected in the skin of younger $Mdm2^{\Delta/\Delta}$ mice (Figure 2.4), these mice do not display upregulated levels of p53-target genes in their skin (Figure 2.11), and the $Mdm2^{\Delta/\Delta}$ mice appear unaffected up to 10 months (Figures 2.5 and 2.6). However, after 10 months of age hair loss and epidermal thinning becomes readily apparent in these mice. As stem cells in the epidermal bulge region are generated during late embryogenesis in the mouse (Stenn and Paus, 2001), the postnatal ablation of *Mdm2* induced by Cre recombinase in our model may be governing epidermal stem cell renewal and not the functional differentiation of pre-existing epidermal stem cells and their subsequent progenitors. In keeping with this possibility, it has been established previously that follicle bulge cells are slow cycling, with an average of 14 months in the mouse (Morris and Potten, 1999). Thus, the pre-established epidermal stem cell compartment in $Mdm2^{\Delta/\Delta}$ mice likely retains cells that are still capable of differentiating into committed progenitor cells that form the follicular and inter-follicular epidermis, but have lost the capacity to self-renew the epidermal stem cell compartment, leading to exhaustion of the stem cell population with age.

An alternate possibility of the late developing phenotype seen in the $Mdm2^{\Delta/\Delta}$ mice is that the epidermal stem cell niche is being affected by the loss of Mdm2 and is indirectly impacting epidermal stem cell function. Most of the experiments presented

studied a mixed population of epidermal and dermal cells from whole skin extracts. Further isolation of the various cells of the epidermis would uncover many characteristics of the epidermal stem cells from *Mdm2*$^{\Delta/\Delta}$ mice such as direct genomic rearrangement of the *Mdm2* locus and whether these cells are undergoing senescence via known markers and expression changes in *p21*, *Pai-1*, and *Pai-2*. These studies could decipher between these two hypotheses regarding why the phenotypes do not present before 10 months and may reveal additional possibilities.

Furthermore, the precise role of p53-induced senescence in regulating epidermal stem cell self-renewal or the epidermal stem cell niche will be a matter for further investigation. The role of Mdm2 loss leading to increased *p16*^{INK4A} expression is also an interesting avenue for discovery to determine whether senescence in one cell (due to p53) could have paracrine effects on surrounding cells (due to increased *p16*^{INK4A}) to perpetuate the senescence response within the stem cell niche. Additional Mdm2 (and perhaps MdmX) deletion models in different cell types may further elucidate this role.

Our findings reveal that activation of p53 due to loss of Mdm2 in the skin of *Mdm2* conditional knockout mice induces p53-mediated senescence within the epidermal stem cell compartment and a reduction in epidermal stem cell percentage, overall numbers, and functions in older mice. In addition, Mdm2-mediated inhibition of p53 activity in epithelial cells of the skin is essential for maintenance of skin integrity and hair as mice age. Thus, Mdm2-p53 signaling governs certain rapid-aging phenotypes in

skin. The ability of Mdm2 to properly downregulate p53 in other p53 mouse models may therefore account for the presence or absence of aging-like phenotypes in these models.

Materials and Methods

Mice and Genotyping

The generation of both the *Mdm2* conditional knockout mice (Steinman and Jones, 2002) and the *K5-Cre* transgenic mice (Zhou et al., 2002) has been described previously. Rosa26 Flox-Stop-β-Geo reporter mice (Stock#: 003310) were obtained from Jackson Laboratories. All experimental and littermate control mice used in this study were on a mixed 129Sv X C57Bl/6 background. Genomic PCR was used to identify inheritance of the *K5-Cre* transgene (primers 5'-CGGTCGATGCAACGAGTGAT-3' and 5'-CCACCGTCAGTACGTGAGAT-3'), to identify inheritance of the conditional Mdm2 allele (primers 5'-GGTCTTCCCATTTATGTATGT-3' and 5'-AAGAGTCTGTATCGCTTTCT-3'), and to verify *Mdm2* allelic excision (primers 5'-GGTCTTCCCATTTATGTATGT-3' and 5'-TCCACCTCTTTCTTCTTCCTG-3'). Animals were maintained and used in accordance with federal guidelines and those established by the Institutional Animal Care and Use Committee at the University of Massachusetts Medical School.

Western Blotting and Reagents

Protein lysates were collected using a modified protocol described previously (Balasubramanian et al., 1998). A $10mm^2$ dorsal section of skin tissue was homogenized in 1 ml NP-40 lysis buffer [50 mM Tris-HCl, pH 7.5; 150 mM NaCl; 0.5% NP-40; 20%

Glycerol; 1X protease inhibitor cocktail (Roche); 1X phosphatase inhibitor cocktail (Roche)]. Samples were placed on ice for 15 minutes, vortexed, and centrifuged at 13000 rpm for 20 minutes. Supernatants were collected, and 50 μg of each sample loaded onto a 10% SDS-polyacrylamide gel. Antibodies against p53 (1:500 of both Ab-1 and Ab-3 from Calbiochem), p63 (1:500 H-137, sc-8343 from Santa Cruz), and α-tubulin (1:4000 T5168 from Sigma) were diluted in 5% non-fat milk.

Gene Expression Analysis

Total mRNA from skin tissue was isolated according to the Trizol Reagent (Invitrogen) protocol, and cDNA was generated using the SuperScript II First Strand Synthesis Kit (Invitrogen). The following primers were used in real time PCR reactions to determine relative gene expression:

p21: 5'-TGAGGAGGAGCATGAATGGAGACA-3' and

5'-AACAGGTCGGACATCACCAGGATT-3',

Pai-1: 5'-GCTGCACCCTTTGAGAAAGA-3' and

5'-GCCAGGGTTGCACTAAACAT-3',

Pai-2: 5'-GGGCTTTATCCTTTCCGTGT-3' and

5'-GTGTGTCTTTGCTGATCCAC-3',

Puma: 5'-CCTGGAGGGTCATGTACAATCT-3' and

5'-TGCTACATGGTGCAGAAAAAGT-3',

Noxa: 5'-CCACCTGAGTTCGCAGCTCAA-3' and

5'-GTTGAGCACACTCGTCCTTCAA-3',

$p16^{INK4A}$: 5'-ATCTGGAGCAGCATGGAGTC-3' and

5’-TCGAATCTGCACCGTAGTTG-3’,

Gapdh: 5’-TGGCAAAGTGGAGATTGTTGCC-3’ and

5’-AAGATGGTGATGGGCTTCCCG-3’.

Histology

Skin tissue was fixed in 10% formalin overnight. Skin sections (5μm) were stained with hematoxylin and eosin (H&E), anti-cytokeratin 15 (K15) antibody from Neomarkers (Freemont, CA), or anti-Lhx2 from Santa Cruz (sc-19342) as performed by the UMMS DERC Morphology Core. TUNEL staining of tissue sections to detect apoptotic cells was performed using the *In Situ* Cell Death Detection Kit, POD (Roche, 11684817910).

Senescence-Associated-β-Galactosidase Staining

Fresh skin tissue was washed twice with PBS, followed by briefly fixing in 2% formaldehyde/0.2% glutaraldehyde for 5 minutes. The tissue was rinsed twice in PBS and then completely submerged in staining solution [all diluted in 40 mM citrate/sodium phosphate buffer (pH 6): 5 mM potassium ferricyanide; 5 mM potassium ferrocyanide; 2 mM $MgCl_2$; 150 mM NaCl; 1mg/ml X-gal] for 4 hours in the dark at 37 °C. After two washes with PBS, the tissue was fixed overnight in 10% formalin and paraffin embedded. Sections were counterstained with either H&E or Nuclear Fast Red.

Isolation of Bulge Stem Cells

Epidermal bulge stem cells were isolated according to a previous protocol (Nowak and Fuchs, 2009). Whole skin was treated with 0.25% trypsin overnight, which allowed

complete segregation of the epidermis from the dermis. The resulting epidermal cell suspensions were washed with media, resuspended in staining buffer (2% fetal bovine serum in sterile PBS), and stained with the following antibodies: phycoerythrin-conjugated rat anti-human CD49f [integrin α6 chain] (clone GoH3) from BD Pharmingen; biotin-conjugated rat anti-mouse CD34 (clone RAM34) from eBioscience; strepavidin-allophycocyanin conjugate from BD Pharmingen). Cells were stained with 7-aminoactinomycin D (7-AAD, Cat. No. 00-6993-50) from eBioscience to determine cell viability. FACS was performed by the UMASS Medical School Flow Cytometry Core Facility.

Wound Healing Assay

The wound healing procedure was modified from a previously described protocol (Tyner et al., 2002). The dorsal surface of anesthetized mice (0.023 cc/gram body weight, 1.2% Avertin) was completely shaved with an electric razor and disinfected with Betadine (Cardinal Health) and 75% ethanol. A 3mm punch biopsy was used to introduce a single wound on the dorsum of each mouse. The wounds were imaged each day and the diameter of each wound was measured. Healing was defined as the decrease in wound diameter over time, and was expressed as the percentage of the day 0 wound diameter.

Hair Growth Assay

The procedure for this assay was modified from a previously described protocol (Tyner et al., 2002). A $2cm^2$ dorsal section of skin on age-matched mice was shaved with an electric razor at day 0. A $0.5cm^2$ square grid was used to measure hair re-growth, which

was defined as the percentage of the total number of squares that are covered with over 50% new hair. Measurements were taken every 3-4 days.

CHAPTER III:

ATM PHOSPHORYLATION OF MDM2 SER394 REGULATES THE AMPLITUDE AND DURATION OF THE DNA DAMAGE RESPONSE IN MICE

Foreword

DNA damage induced by ionizing radiation (IR) activates the ATM kinase, which subsequently stabilizes and activates the p53 tumor suppressor protein. Although phosphorylation of p53 by ATM was found previously to modulate p53 levels and transcriptional activities *in vivo*, it does not appear to be a major regulator of p53 stability. We have utilized mice bearing altered Mdm2 alleles to demonstrate that ATM phosphorylation of Mdm2 serine 394 is required for robust p53 stabilization and activation after DNA damage. In addition, we demonstrate that dephosphorylation of Mdm2 Ser394 regulates attenuation of the p53-mediated response to DNA damage. Therefore, the phosphorylation status of Mdm2 Ser394 governs p53 protein levels and functions in cells undergoing DNA damage.

Introduction

The p53 tumor suppressor has been called the "guardian of the genome" due to its ability to prevent genotoxic insults from inducing heritable alterations in damaged cells (Lane, 1992). In response to cellular stresses such as DNA double-strand breaks, hypoxia, and inappropriate oncogene activation, the p53 transcription factor is stabilized within the cell and induces the expression of various p53 target genes involved in cell cycle arrest, apoptosis, and senescence (Vousden and Lu, 2002). These p53-dependent effector pathways regulate the proliferation and propagation of damaged cells to limit cellular transformation and tumorigenesis, and mice deleted for p53 rapidly develop thymic lymphomas, sarcomas and other tumor types (Donehower *et al*., 1992). Additionally, over 50% of all human tumors harbor *p53* mutations (Soussi and Beroud,

2001; Hollstein *et al.*, 1991). These findings clearly demonstrate the necessity of functional p53 signaling in suppressing tumorigenesis.

DNA damage induced by ionizing radiation is a well-established initiator of p53 activity. Wild-type (WT) mice that are treated with whole body IR undergo p53-dependent apoptosis in both radiosensitive tissues such as thymus, spleen, and small intestine, and in hematopoietic cells (Gudkov and Komarova, 2003). Mice exposed to 8 Grays (Gy) or more of IR will die within 3 weeks due to depletion of the hematopoietic compartment, a condition known as hematopoietic syndrome (Komarova *et al.*, 2004). In contrast, p53-null mice are more tolerant of acute radiation, as their hematopoietic cells are less prone to IR-induced apoptosis. However, p53-deficient mice display an increased rate of tumorigenesis following IR treatment (Kemp *et al.*, 1994).

Activation of p53 in response to DNA damage necessitates a transient attenuation of Mdm2-dependent p53 inhibition. Post-translational modifications of the p53 protein by DNA damage-inducible kinases, specifically ATM, were initially thought to inhibit the interaction of p53 and Mdm2 (Shieh *et al.*, 1997). Atm-null mice do not survive past 6 months of age due to the increase in T-cell lymphomagenesis, demonstrating a key role for ATM in tumor suppression (Barlow *et al.*, 1996; Elson *et al.*, 1996; Xu and Baltimore, 1996; Herzog *et al.*, 1998). Experiments utilizing the cells of these Atm-null mice demonstrated the necessity of ATM signaling in p53 stabilization in mouse embryonic fibroblasts (MEFs) and murine thymus following IR (Jack *et al.*, 2002; Gurley and Kemp, 2007). ATM directly and indirectly (via Chk2) phosphorylates p53 on Ser18

and Ser23 in irradiated mice (Ser15 and Ser20 on human p53) (Chao *et al*., 2000; Wu *et al*., 2002). These serine residues are located within or adjacent to the Mdm2 binding domain of p53, and initial *in vitro* studies demonstrated that phosphorylation of p53 decreased the p53-Mdm2 interaction in transfection and overexpression experiments (Shieh *et al.*, 1997). Several groups, including our own, subsequently generated mouse models bearing modified p53 alleles to examine the role of these post-translational modifications in p53 regulation and function *in vivo* (Chao *et al.*, 2003; Sluss *et al.*, 2004; Chao *et al.*, 2006). These studies revealed that phosphorylation of these ATM-target serines on p53 modulated the transcriptional activity of p53, but had only a moderate effect on DNA damage-induced stabilization of the p53 protein.

In addition to modifying p53, transfection-based assays have revealed that ATM can directly phosphorylate serine 395 of human MDM2 (Khosravi *et al.*, 1999; Maya *et al.*, 2001). This suggested for the first time that p53 stabilization after DNA damage could be due to posttranslational modifications on Mdm2. One study utilized an MDM2 expression construct with the serine residue 395 codon replaced by sequences encoding aspartic acid (S395D), thus mimicking a constitutively phosphorylated serine residue. The MDM2 S395D protein exhibited a decreased capacity to induce p53 degradation and nuclear export, suggesting that phosphorylation of MDM2 Ser395 altered p53 activation following DNA damage (Maya *et al.*, 2001). Further *in vitro* work suggested that ATM phosphorylation of multiple amino acid residues on MDM2, including Ser395, inhibited both MDM2 RING domain oligomerization and E3 ligase activity (Cheng *et al.*, 2009; Cheng *et al.*, 2011). Interestingly, recent work has indicated that ATM phosphorylation

of MDM2 switches MDM2 from a negative to a positive regulator of p53, as phosphorylation of MDM2 Ser395 increased the interaction between Mdm2 protein and p53 mRNA and led to increased p53 translation (Gajjar *et al.*, 2012). These transfection-based studies suggest that the ATM-dependent induction of the p53 protein is mediated by ATM phosphorylation of MDM2.

In keeping with a role for MDM2 Ser395 phosphorylation in the p53 DNA damage response, we have previously shown that the wild type p53-induced phosphatase 1 (Wip1) oncoprotein can dephosphorylate MDM2 Ser395 *in vitro* (Lu *et al.*, 2007). Multiple *in vitro* studies have shown that Wip1 dephosphorylates, and thus inactivates, proteins that are activated by ATM including Chk1, p53 (Lu1 *et al.*, 2005), Chk2 (Olivia-Trastoy *et al.*, 2007), and even ATM itself (Shreeram *et al.*, 2006a). Therefore, Wip1 has been proposed to reset DNA damage signaling to pre-stress levels following resolution of the DNA damage response (Lu *et al.*, 2008). Overexpression of Wip1 has been shown to inhibit the normal IR-induced p53 response *in vitro* (Lu *et al*., 2007), and Wip1-null mice and MEFs have growth kinetics, cell cycle defects, p53 target gene expression, and delayed tumorigenesis indicative of a prolonged p53 response (Choi *et al.*, 2002; Nannenga *et al.*, 2006). As its name suggests, the *Wip1* gene is a transcriptional target of p53, so that, like Mdm2, p53 activation quickly induces its own negative regulators to ensure tight control (Fiscella *et al.*, 1997). Although the coincidental timing of MDM2 Ser395 phosphorylation and dephosphorylation suggests that this modification may coordinate the p53-dependent response to DNA damage, the *in vivo* functional

significance of MDM2 phosphorylation in Mdm2-p53 regulation, p53 activation, and in tumorigenesis remains unknown.

To determine the role of MDM2 Ser395 phosphorylation in p53 regulation under physiological settings, we have generated two knock-in mouse models bearing Mdm2 Ser394 substitutions (the orthologous human Ser395 residue in the mouse). Our results generated from these two models reveal that Mdm2 Ser394 phosphorylation is necessary for DNA damage-induced p53 stabilization in hematopoietic tissues and primary cells and is a critical regulator of p53-mediated apoptosis, growth arrest, and tumor suppression. Additionally, Mdm2 Ser394 phosphorylation impacts the duration of the p53 response to DNA damage.

Results

To investigate the role of Mdm2 Ser394 phosphorylation under physiological conditions, we generated a mouse model in which this serine residue is substituted with an alanine residue (A394). This model produces a mutant Mdm2 protein with a conserved native structure that cannot be phosphorylated at position 394. Site-directed mutagenesis was performed to introduce missense mutations within the 394 codon of *Mdm2* exon 12 (Figure 3.1), and a gene-replacement vector was constructed to replace the endogenous *Mdm2* exon 12 sequences with a mutated exon 12 (Figure 3.2). The introduced mutations also inserted a novel *BcgI* restriction digest site at codon 394, which allows direct detection of the mutated sequence by a PCR strategy. Gene targeting experiments in PC3 (129SV) embryonic stem (ES) cells (O'Gorman *et al.*, 1997) yielded

properly-targeted ES cell clones, as confirmed by Southern and PCR analyses (Figure 3.3). Blastocyst injection experiments produced several high-degree male chimeras that passed the A394 allele through their germ line while simultaneously deleting the floxed neomycin cassette due to expression of the *protamine-Cre* transgene (present in the PC3 ES cells). The resultant F_1 and F_2 generation mice were identified by Southern blot of genomic DNA and the presence of the A394 mutation in these mice was confirmed by utilizing the PCR-*BcgI* digest strategy (Figure 3.4). This corroborated the Southern genotyping results and demonstrated retention of the mutation in both heterozygous ($Mdm2^{A/+}$) and homozygous ($Mdm2^{A/A}$) mice, but not in wild-type ($Mdm2^{+/+}$) mice. All genotyping techniques were reaffirmed by direct genomic sequencing of the exon 12 region in F_1 and F_2 mouse genomic DNA (Figure 3.4).

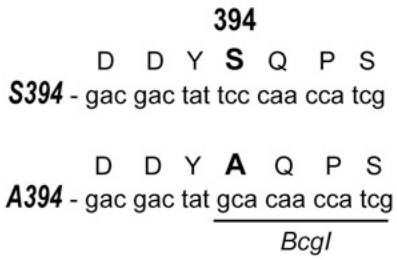

Figure 3.1: Sequence of the wild-type (S394) and mutant (A394) alleles at Mdm2 codon 394. The mutations in A394 also introduce a *BcgI* restriction digest site.

$Mdm2^{A/+}$ and $Mdm2^{A/A}$ mice are viable and were recovered from heterozygous intercrosses at Mendelian ratios (Table 3.1). Because $Mdm2^{-/-}$ mice are embryonic lethal (Jones *et al.*, 1995; Montes de Oca Luna *et al.*, 1995), total ablation of Mdm2 function during development must not be occurring in $Mdm2^{A/+}$ or $Mdm2^{A/A}$ mice. We also did

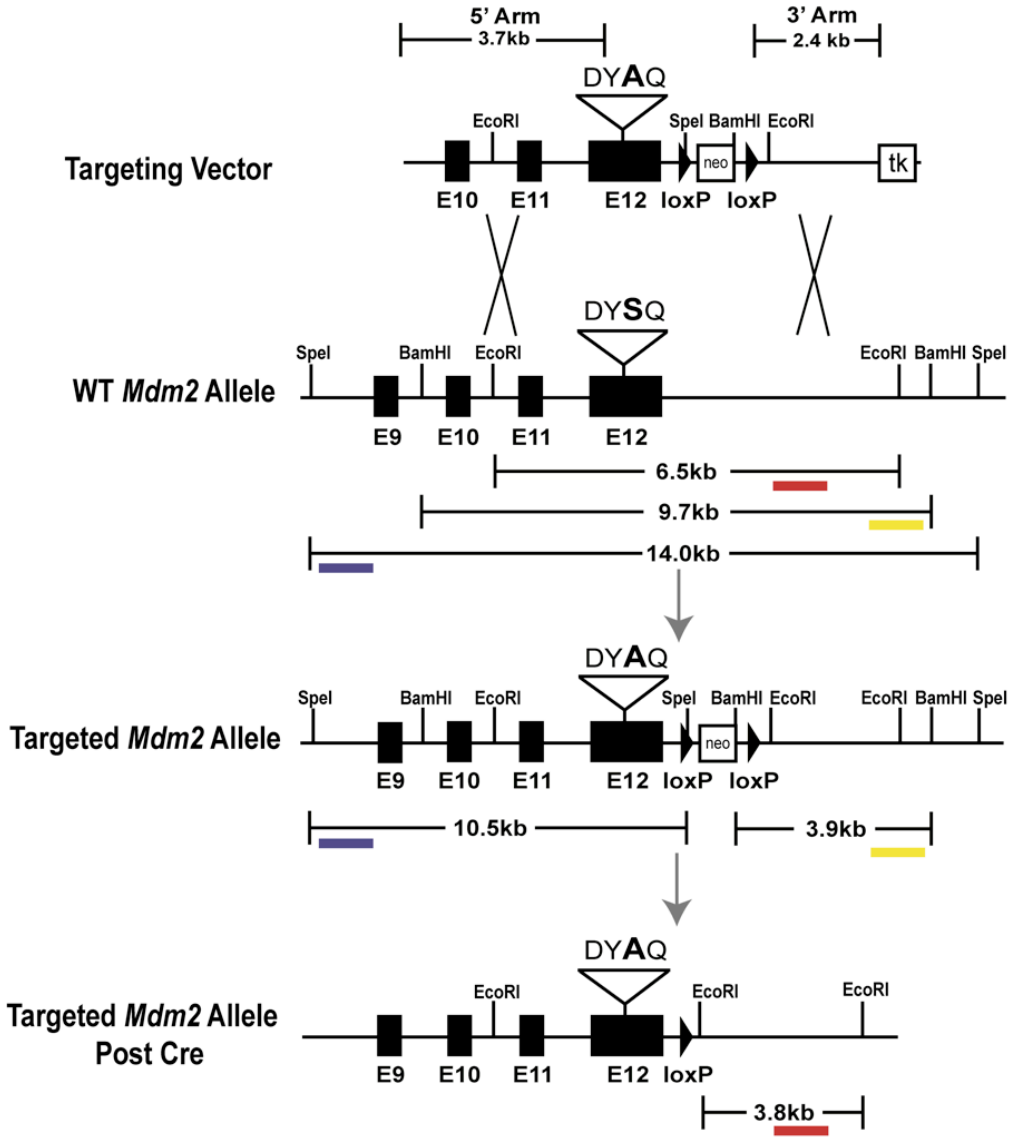

Figure 3.2: Diagram of the targeting strategy used to generate the A394 allele. The targeting vector contains a floxed neomycin cassette (neo) and a 3' thymidylate kinase cassette (tk) for positive and negative drug selection, respectively. The targeting vector was linearized and electroporated into PC3 ES cells, and proper homologous recombination was detected by Southern blot. We took advantage of *BamHI* and *SpeI* sites found within the neo cassette to probe on both the 5' (purple bar) and 3' (yellow bar) ends, respectively. PC3 cells have a protamine-cre recombinase transgene that excised the floxed neo cassette in chimeric male germ cells. We utilized a final Southern blot with an *EcoRI* digest and 3' probe (red bar).

not detect any differences between *Mdm2*$^{+/+}$ and *Mdm2*$^{A/A}$ mice in body weights at 8 weeks of age (*Mdm2*$^{+/+}$ 25.67±2.9 grams and *Mdm2*$^{A/A}$ 24.3±4.2 grams), in male-to-female sex distribution (*Mdm2*$^{+/+}$ 1:0.82 and *Mdm2*$^{A/A}$ 1:0.90), or in overall litter size (*Mdm2*$^{+/+}$ 8.5±1.8 and *Mdm2*$^{A/A}$ 8.7±1.9). Since mice with decreased p53 function have decreased fecundity (Levine *et al.*, 2011), our results suggest that basal p53 activity is not perturbed in *Mdm2*$^{A/A}$ mice.

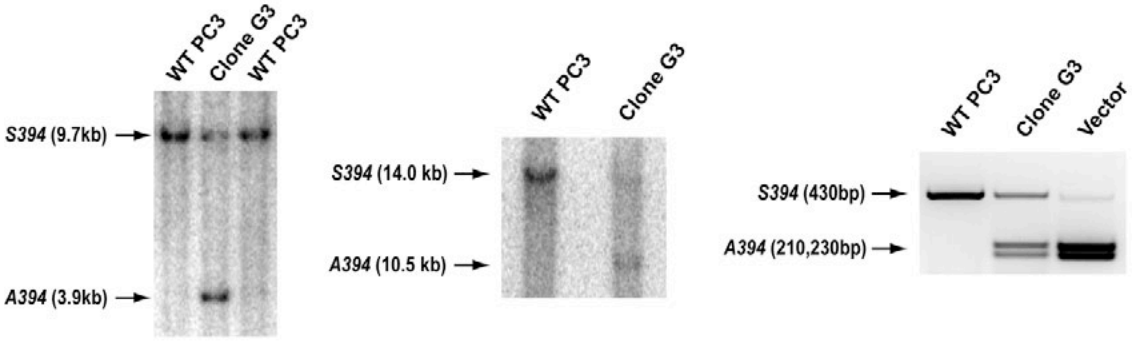

Figure 3.3: Southern blots and genomic PCR in A394 targeted ES cells. Initial Southern blot of ES cells (*left*). DNA samples were digested with *BamHI* and probed with a 3' external probe (yellow bar from Figure 3.2). The neo cassette within the A394 gene replacement vector inserted an exogenous *BamHI* site, resulting in the shorter band (3.9 kb) seen in the targeted ES cell clone in lane 2. Southern blot of ES cells (*center*). DNA samples were digested with *SpeI* and probed with a 5' external probe (purple bar from Figure 3.2). The neo cassette within the A394 gene replacement vector inserted an exogenous *SpeI* site, resulting in the shorter band (10.5 kb) seen in the targeted ES cell clone in lane 2. PCR-*BcgI* analysis of targeted ES cells (*right*). Primers flanking Mdm2 codon 394 were used to amplify DNA samples from WT PC3 cells (lane 1), the targeted ES cell clone (lane 2), and the A394 gene replacement vector (lane 3), followed by *BcgI* digestion.

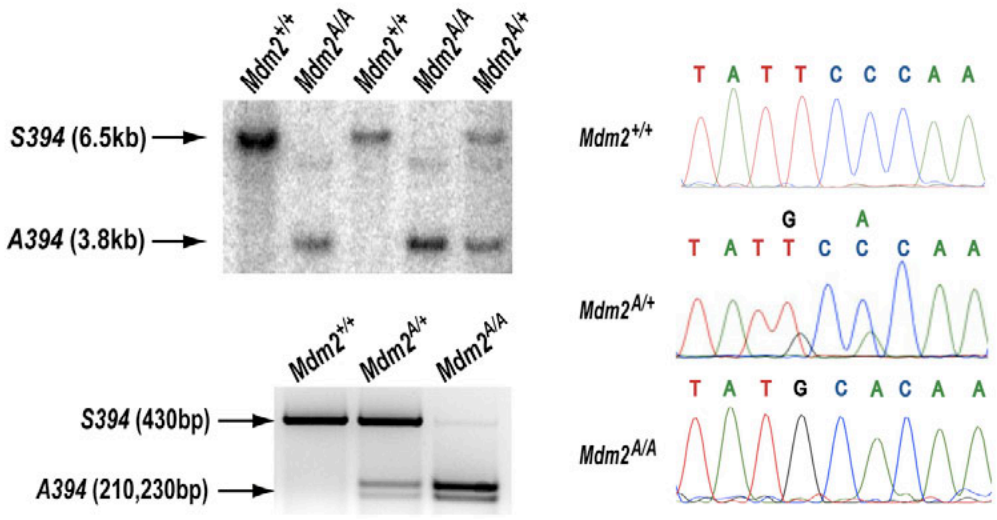

Figure 3.4: Southern blot, genomic PCR, and genotyping in A394 mice. Southern blot of F_2 generation mice (*top left*). DNA samples were digested with *EcoRI* and probed with a 3' internal probe (red bar from Figure 3.2). The A394 allele inserted an exogenous *EcoRI* site resulting in the shorter band (3.8 kb). PCR-*BcgI* analysis of F_2 generation mice (*bottom left*). Primers flanking Mdm2 codon 394 were used to amplify DNA samples from $Mdm2^{+/+}$, $Mdm2^{A/+}$, and $Mdm2^{A/A}$ F_2 generation mice, followed by *BcgI* digestion. Representative DNA sequencing chromatograms of the Mdm2 394 codon from $Mdm2^{+/+}$, $Mdm2^{A/+}$, and $Mdm2^{A/A}$ F_2 generation mice (*right*).

Genotype	Observed	Expected
$Mdm2^{+/+}$	29	26
$Mdm2^{A/+}$	53	52
$Mdm2^{A/A}$	22	26

Table 3.1: $Mdm2^{A/+}$ and $Mdm2^{A/A}$ viability. $Mdm2^{A/+}$ and $Mdm2^{A/A}$ mice are viable and were observed at Mendelian ratios after heterozygous intercrosses (p=0.322).

Because ATM phosphorylation of MDM2 Ser395 was previously observed in cell lines following IR treatment (Maya *et al.*, 2001), we assessed the sensitivity of $Mdm2^{A/A}$ mice to whole body γ-irradiation. We irradiated cohorts of $Mdm2^{+/+}$, $Mdm2^{A/A}$, and $p53^{-/-}$

mice with a threshold-lethal dose of IR (8Gy). As expected, 86% of *Mdm2*$^{+/+}$ mice died by 16 days post-IR (Figure 3.5). However, like *p53*$^{-/-}$ mice, *Mdm2*$^{A/A}$ mice were completely radioresistant, indicating that Mdm2 Ser394 phosphorylation regulates p53 activity *in vivo* following DNA damage. Likewise, reduced red and white blood cell counts indicative of hematopoietic syndrome were seen in *Mdm2*$^{+/+}$ mice at 7 days following 8Gy treatment, whereas the irradiated *Mdm2*$^{A/A}$ mice showed little change in these levels compared with untreated mice (Figure 3.6).

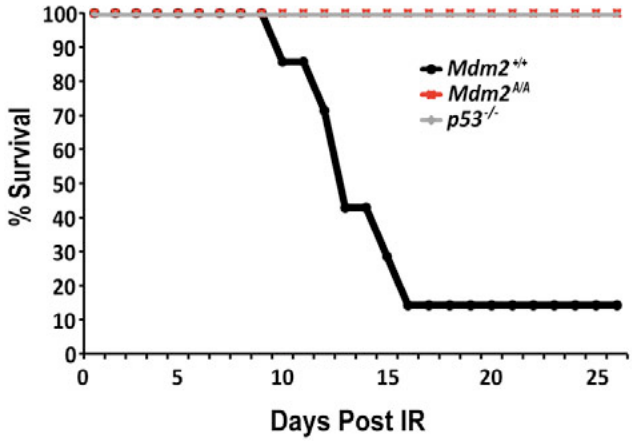

Figure 3.5: Survival in whole-body irradiated mouse cohorts. Cohorts of *Mdm2*$^{+/+}$ (n=14), *Mdm2*$^{A/A}$ (n=14), and *p53*$^{-/-}$ (n=8) mice were irradiated with 8Gy and survival was observed over 26 days.

Activation of p53 by IR damage in mice induces apoptosis in radiosensitive organs such as small intestine, spleen, and thymus (Gudkov and Komarova, 2003). To evaluate p53 apoptotic function in these tissues, we treated *Mdm2*$^{+/+}$, *Mdm2*$^{A/A}$, and *p53*$^{-/-}$ mice with 2Gy IR and 6 hours later assayed apoptosis by terminal deoxynucleotidyl transferase dUTP nick end labeling (TUNEL) and cleaved caspase-3 immunohistochemistry (Figure 3.7). Very few apoptotic cells were detected in the small intestine, spleen, or the thymus

of *Mdm2*$^{A/A}$ mice following DNA damage, whereas apoptosis was readily apparent in all of these tissues in irradiated *Mdm2*$^{+/+}$ mice. These studies indicate markedly reduced p53-dependent apoptotic function in *Mdm2*$^{A/A}$ mice after IR treatment.

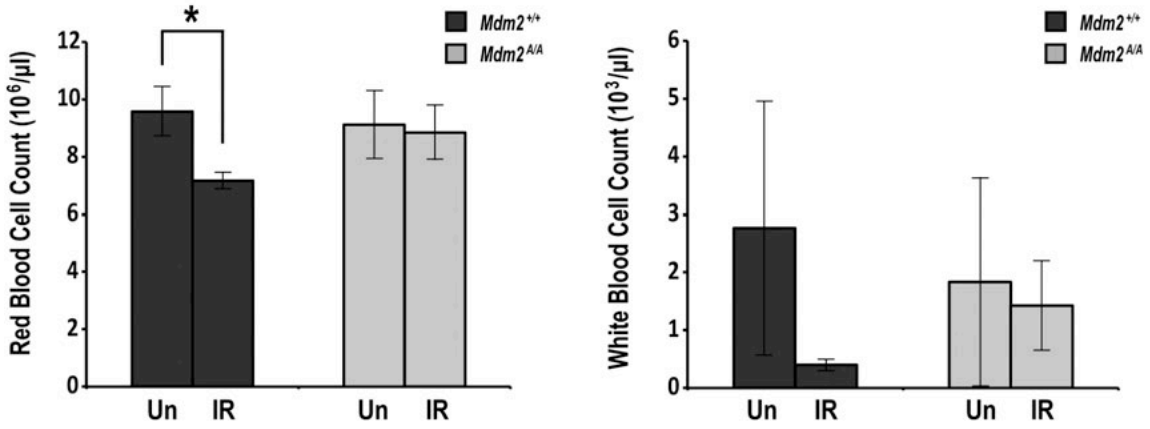

Figure 3.6: Complete blood counts in irradiated *Mdm2*$^{+/+}$ and *Mdm2*$^{A/A}$ mice. Complete blood cell counts were obtained 7 days following 8Gy treatment (n=3 per genotype). Standard deviation indicated by error bars. Asterisks indicate a significant difference (p=0.01).

To more accurately quantitate this IR-dependent effect, we utilized Annexin V and propidium iodide (PI) staining to assay apoptosis in *ex vivo* thymocytes by flow cytometry. *Mdm2*$^{+/+}$ thymocytes are sensitive to apoptosis due to p53-induced activation of pro-apoptotic *Puma* expression (Jeffers *et al.*, 2003). In agreement with the whole-body IR results, *Mdm2*$^{+/+}$ thymocytes treated with 2Gy IR displayed 3.1-fold more early apoptotic (Annexin V^{high} PI^{low}) cells at 12 hours compared to untreated *Mdm2*$^{+/+}$ cells, whereas *Mdm2*$^{A/A}$ thymocytes displayed only a modest 1.5-fold increase in apoptotic cells and *Mdm2*$^{A/A}$ thymocytes showed no induction of apoptosis after DNA damage (Figure 3.8).

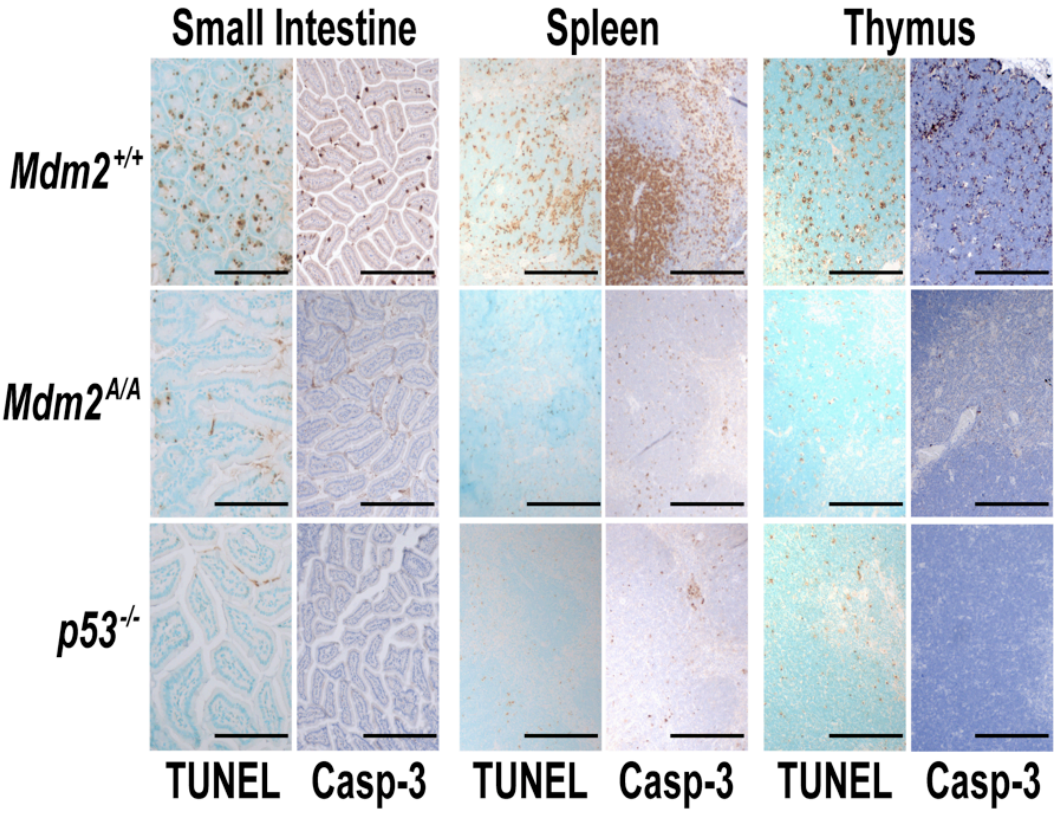

Figure 3.7: Apoptosis in radiosensitive tissues of IR-treated *Mdm2*$^{+/+}$ and *Mdm2*$^{A/A}$ mice. *Mdm2*$^{+/+}$, *Mdm2*$^{A/A}$, and *p53*$^{-/-}$ mice were irradiated with 2Gy and were sacrificed 6 hours later. Small intestine, spleen, and thymus were harvested and stained for TUNEL or anti-cleaved caspase-3 (Casp-3). Scale bars represent 250 μm.

To establish that the decreased apoptosis in DNA damaged *Mdm2*$^{A/A}$ thymocytes is due to altered p53 function, we treated *Mdm2*$^{+/+}$, *Mdm2*$^{A/A}$, and *p53*$^{-/-}$ thymocytes with Nutlin-3a, a small-molecule inhibitor of Mdm2-p53 binding (Vassilev *et al.*, 2004). *Mdm2*$^{+/+}$ and *Mdm2*$^{A/A}$ thymocytes co-treated with Nutlin-3a and IR each stabilized p53 after IR damage, and blocking the interaction of p53 with Mdm2 completely rescued the ability of p53 to induce apoptosis in *Mdm2*$^{A/A}$ thymocytes following DNA damage (Figure 3.9). To confirm that Nutlin-3a treatment restored IR-induced apoptosis in

Mdm2$^{A/A}$ cells by inhibiting Mdm2-p53 signaling, we performed FACS analysis on *Mdm2*$^{A/A}$ thymocytes that were genetically deleted for p53. As expected, the addition of Nutlin-3a failed to restore IR-induced apoptosis in *Mdm2*$^{A/A}$ cells lacking p53 (Figure 3.10).

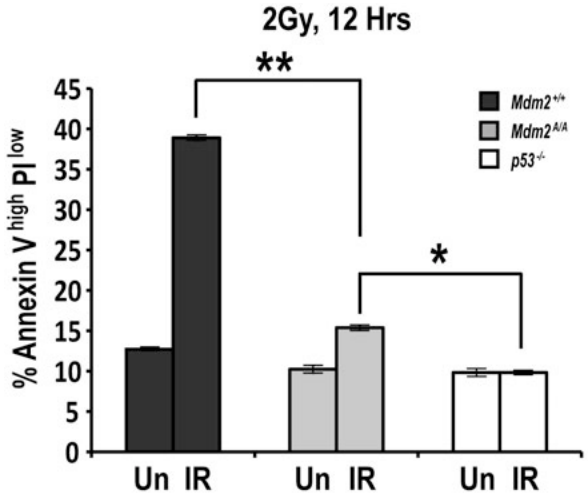

Figure 3.8: Quantification of apoptotic cells in primary *Mdm2*$^{+/+}$ and *Mdm2*$^{A/A}$ thymocytes. *Ex vivo* thymocytes were either left untreated or irradiated with 2Gy for 12 hours (n=3 per genotype). Standard deviation indicated by error bars. Asterisk (p=0.0001) and double asterisk (p=0.0001) indicate significant differences.

To verify that the effect of the Mdm2 A394 mutation on IR-apoptosis was truly ATM-dependent, we repeated the apoptosis assays using the ATM-specific inhibitor KU55933 (Hickson *et al.*, 2004). Inhibition of ATM reduced apoptosis in irradiated thymocytes to levels observed in untreated cells in all genotypes (Figure 3.11). Additionally, the ATM inhibitor blocked the robust ATM activation and p53 protein stabilization induced by IR damage (Figure 3.11).

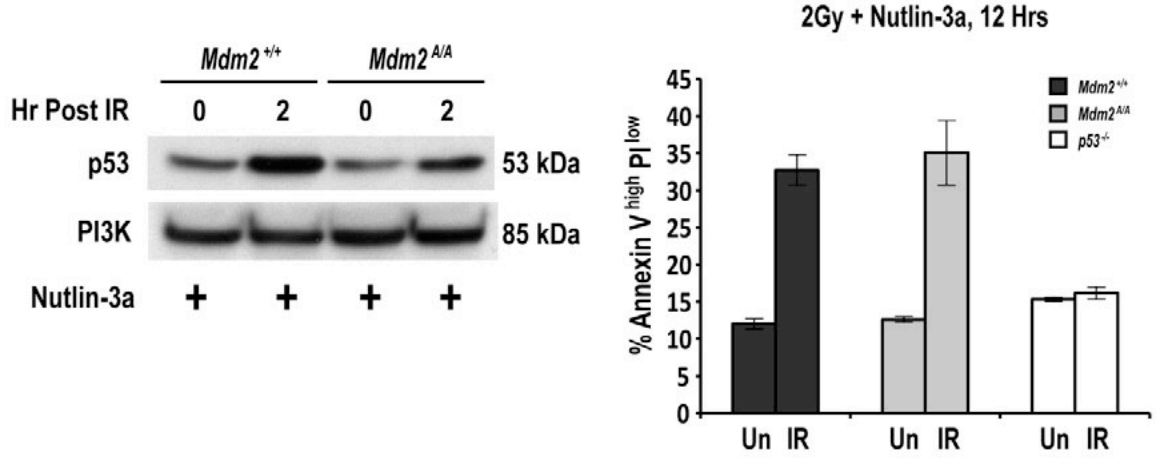

Figure 3.9: Nutlin-3a treatment affects p53 protein levels and apoptosis in *Mdm2*$^{+/+}$ and *Mdm2*$^{A/A}$ thymocytes. Western blot of thymocyte extracts (*left*). *Ex vivo* cells were either untreated or irradiated with 2Gy for 1 hour, and all cells were then incubated with 12 μM Nutlin-3a for 1 hour. Quantification of apoptotic cells by flow cytometry (*right*). *Ex vivo* thymocytes were either left completely untreated or irradiated with 2Gy for 12 hours and incubated with 12 μM Nutlin-3a 3 hours after IR (9 hours total) (n=3 per genotype). Standard deviation indicated by error bars.

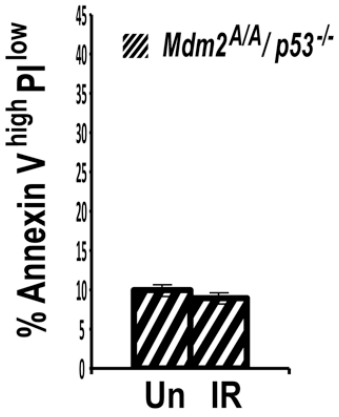

Figure 3.10: Nutlin-3a has no effect on irradiated *Mdm2*$^{A/A}$, *p53*$^{-/-}$ thymocyte apoptosis. *Ex vivo* thymocytes were either left completely untreated or irradiated with 2Gy for 12 hours and incubated with 12 μM Nutlin-3a 3 hours after IR (9 hours total) (n=3 per genotype). Standard deviation indicated by error bars.

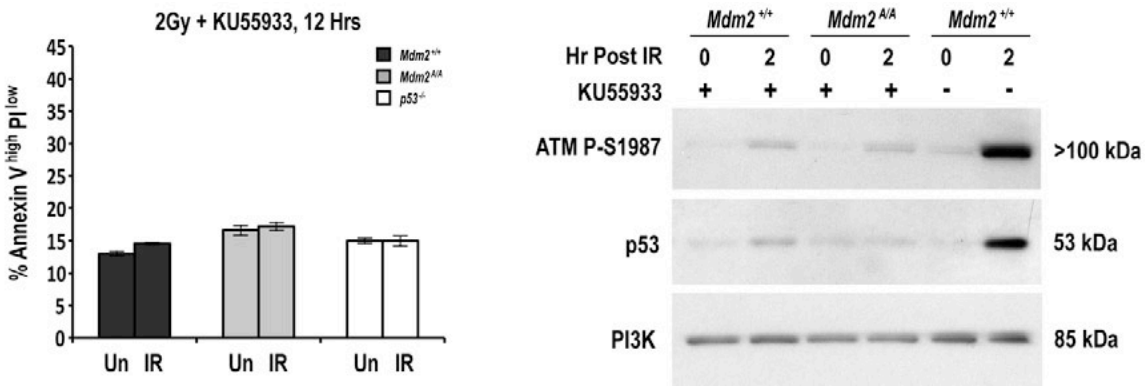

Figure 3.11: ATM activity is necessary for IR-induced apoptosis and p53 stabilization. Quantification of apoptotic cells by flow cytometry (*left*). *Ex vivo* thymocytes were preincubated with 10 μM KU55933 for 1 hour. Cells were then either left untreated or irradiated with 2Gy for 12 hours (n=3 per genotype). Standard deviation indicated by error bars. Western blot of thymocyte extracts (*right*). *Ex vivo* thymocytes were either left untreated or preincubated with 10 μM KU55933 for 1 hour. Cells were then either untreated or irradiated with 2Gy for 2 hours.

To further investigate the lack of IR-induced p53 function in *Mdm2*$^{A/A}$ mice, we compared the stabilization and activity of p53 in *Mdm2*$^{+/+}$ and *Mdm2*$^{A/A}$ radiosensitive tissues after DNA damage. We first harvested whole spleen protein extracts 4 hours after whole-body IR treatment. As expected, activation of the ATM kinase in *Mdm2*$^{+/+}$ mice by 4Gy IR was readily detected, as judged by the extent of auto-phosphorylated ATM Ser1987, the mouse orthologue of human ATM Ser1981 (Pellegrini *et al.*, 2006), and this tissue displayed robust IR-stabilization of p53 (Figure 3.12). However, *Mdm2*$^{A/A}$ mice lack any detectable stabilization of the p53 protein, despite comparable activation of ATM by IR. This lack of p53 protein upregulation in IR-treated *Mdm2*$^{A/A}$ spleen extracts corresponded with greatly decreased induction of the p53-target genes *Puma*, *p21*, *Bax,* and *Noxa*, as measured by quantitative real time PCR (Figure 3.13). However, IR-treated

Mdm2$^{A/A}$ spleens did show a low-level activation of p53, as expression of p53 target genes was slightly elevated relative to levels in IR-treated *p53*$^{-/-}$ spleens.

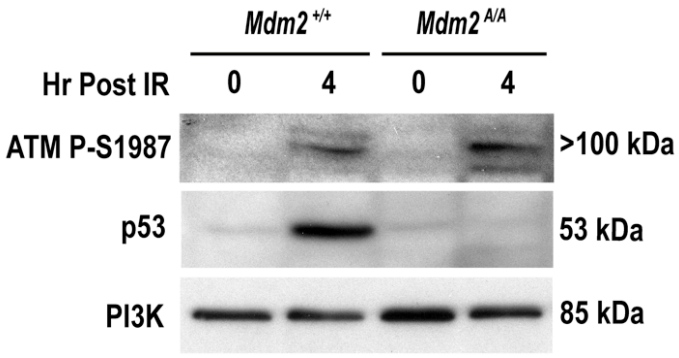

Figure 3.12: Western blot of *Mdm2*$^{+/+}$ and *Mdm2*$^{A/A}$ whole spleen extracts. Mice were either untreated or irradiated with 4Gy and spleens were harvested 4 hours later.

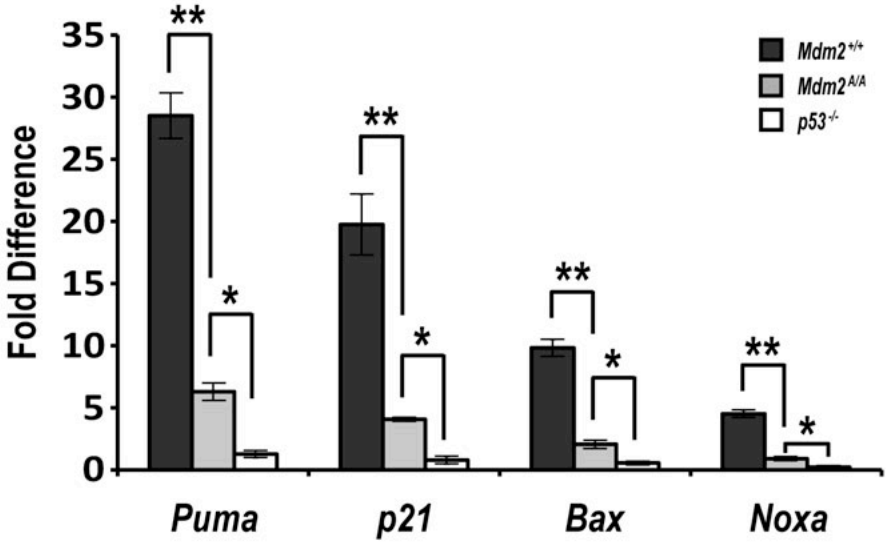

Figure 3.13: Relative expression of p53 target genes in *Mdm2*$^{+/+}$ and *Mdm2*$^{A/A}$ spleens determined by qRT-PCR. Mice were either untreated or irradiated with 4Gy and spleens were harvested 4 hours later (n=3 per genotype). Levels were normalized to untreated wild-type and are presented as the ratio of mRNA to *Gapdh* mRNA. Standard deviation indicated by error bars. Asterisks indicate a significant difference: double asterisk *Puma* p=0.002, *p21* p=0.01, *Bax* p=0.003, *Noxa* p=0.002; single asterisk *Puma* p=0.01, *p21* p=0.001, *Bax* p=0.01, *Noxa* p=0.008.

Similar results were seen at multiple time points in thymus extracts following whole-body IR treatment of mice (Figure 3.14). The level of p53 protein in *Mdm2*$^{+/+}$ thymus was upregulated by 6.4-fold (1 hour), 4.8-fold (2 hour), and 1.8-fold (4 hours) following 4Gy IR, whereas p53 levels in IR-treated *Mdm2*$^{A/A}$ thymus were upregulated by only 2.1-fold, 1.3-fold, and 1.2-fold at these respective time points. Again, these differences were seen despite similar activation of the ATM kinase (Figure 3.14).

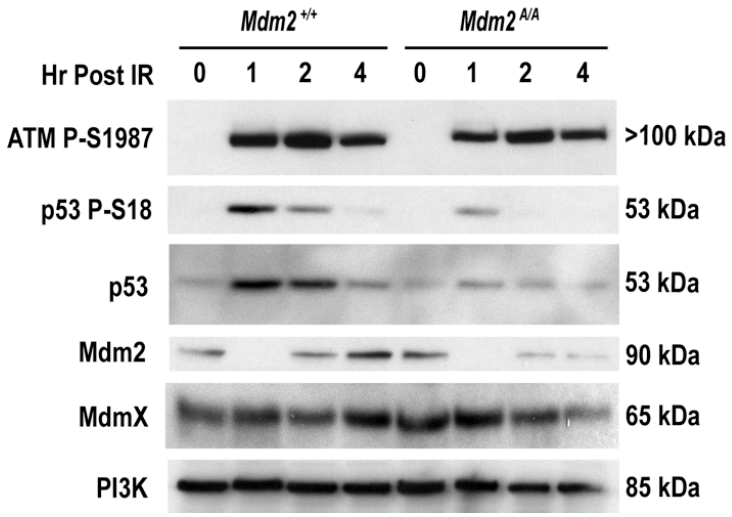

Figure 3.14: Western blot of *Mdm2*$^{+/+}$ and *Mdm2*$^{A/A}$ whole thymus extracts. Mice were either untreated or irradiated with 4Gy for the indicated times.

As observed in spleen, expression of the p53-target genes *Puma* and *p21* were significantly reduced in *Mdm2*$^{A/A}$ thymus at all time points after IR treatment (Figure 3.15). Since the p53 protein is phosphorylated by ATM on p53 Ser18 in the treated *Mdm2*$^{A/A}$ thymus (Figure 3.14), the reduced levels of p53 target gene expression in this tissue are likely due to decreased p53 protein stabilization in *Mdm2*$^{A/A}$ mice after IR, and not due to failure of ATM to induce proper post-translational modification of p53.

Analysis of multiple p53 target genes in irradiated *Mdm2*$^{+/+}$ and *Mdm2*$^{A/A}$ thymocytes using p53 signaling pathway PCR arrays confirmed reduced activation of multiple p53 target genes in treated *Mdm2*$^{A/A}$ cells (Table 3.2). These results reveal that Mdm2 Ser394 phosphorylation is required *in vivo* for p53 stabilization and robust p53 activation after DNA damage.

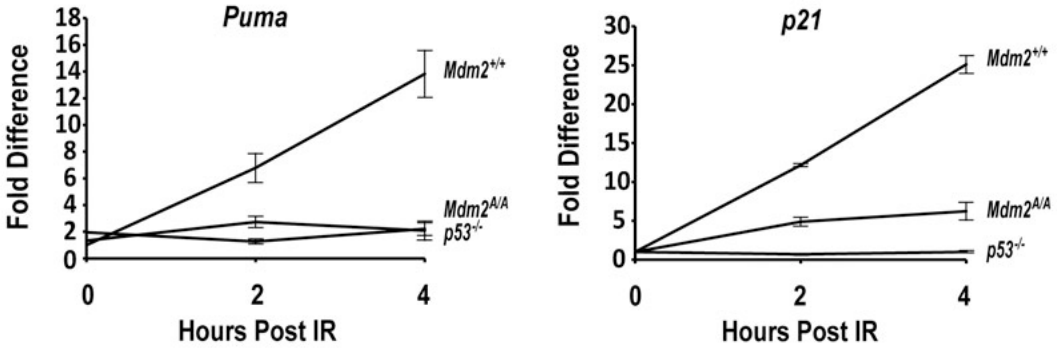

Figure 3.15: Relative expression of p53 target genes in *Mdm2*$^{+/+}$ and *Mdm2*$^{A/A}$ thymus. Mice were either untreated or irradiated with 4Gy and thymii were harvested 2 or 4 hours later (n=3 per genotype). Data are presented as the ratio of mRNA to *Gapdh* mRNA. Standard deviation indicated by error bars. Significant differences were seen between *Mdm2*$^{+/+}$ and *Mdm2*$^{A/A}$ *Puma* at 2 (p=0.035) and 4 (p=0.002) hours and between *Mdm2*$^{+/+}$ and *Mdm2*$^{A/A}$ *p21* at 2 (p=0.0001) and 4 (p=0.0001) hours.

Mdm2 destabilization in response to DNA damage has been shown previously (Stommel and Wahl, 2004), and we observed an initial decrease in Mdm2 protein in both *Mdm2*$^{+/+}$ and *Mdm2*$^{A/A}$ tissues. Interestingly, these Mdm2 levels recovered at 2 and 4 hours in both genotypes, with more Mdm2 protein being present in *Mdm2*$^{+/+}$ at these times compared to *Mdm2*$^{A/A}$ (Figure 3.15). Interestingly, the phosphorylation status of Mdm2 Ser394 had no effect on the levels of MdmX, an Mdm2-related p53 regulatory protein, in this tissue.

p53 Target Genes	*Mdm2*$^{+/+}$	*Mdm2*$^{A/A}$	*Mdm2*$^{A/A}$
Bax	14.3	2.6	1.1
Cyclin B2	1.1	0.5	0.7
GADD45	0.9	0.5	-0.3
Msh2	3.1	1.5	1.0
Noxa	1.3	-0.5	-0.2
Wip1	2.2	1.5	0.9
Sesn2	3.6	0.9	0.6

Table 3.2: *Mdm2*$^{+/+}$ and *Mdm2*$^{A/A}$ thymocyte target gene expression by PCR Array. Relative expression levels of p53 target genes in irradiated thymocyte extracts determined by qRT-PCR using Qiagen p53 Signaling Pathway PCR Arrays. Cells were either untreated or irradiated with 2Gy and were harvested 4 hours later. Data are presented as the fold increase in individual treated *Mdm2*$^{+/+}$ and *Mdm2*$^{A/A}$ animals normalized to untreated WT levels and as the ratio of mRNA to *Gapdh* mRNA.

We next wanted to determine why differences in p53 and Mdm2 levels are observed in irradiated *Mdm2*$^{+/+}$ versus *Mdm2*$^{A/A}$ cells. One possibility is that p53 and Mdm2 protein levels are initially lower in *Mdm2*$^{A/A}$ cells than in *Mdm2*$^{+/+}$ cells, leading to an overall reduced DNA damage response in *Mdm2*$^{A/A}$ mice. To test this, we carefully quantitated p53 and Mdm2 protein levels in untreated *Mdm2*$^{+/+}$ and *Mdm2*$^{A/A}$ whole thymus extracts and found no significant difference in the levels of either p53 or Mdm2 proteins at baseline (Figure 3.16). These data support the similar baseline levels of apoptosis and gene expression that we observed in *Mdm2*$^{+/+}$ and *Mdm2*$^{A/A}$ tissues in the absence of DNA damage (Figures 3.8, 3.9, 3.11, 3.13, and 3.15). Furthermore, careful quantitation confirmed that there is less p53 protein and Mdm2 protein in *Mdm2*$^{A/A}$ thymus than in *Mdm2*$^{+/+}$ thymus after IR (Figure 3.17). Since baseline Mdm2 levels were equivalent in *Mdm2*$^{A/A}$ and *Mdm2*$^{+/+}$ tissue, the reduced amount of Mdm2 and p53

in *Mdm2*$^{A/A}$ versus *Mdm2*$^{+/+}$ tissues reflects a specific difference in the response of *Mdm2*$^{A/A}$ cells to DNA damage.

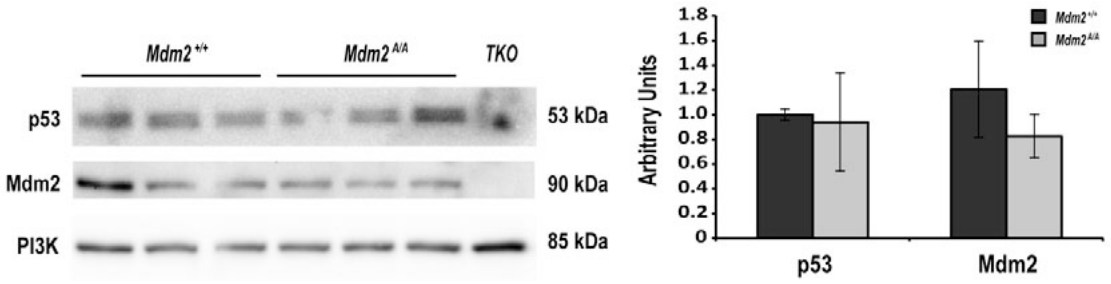

Figure 3.16: Basal levels of p53 and Mdm2 protein in *Mdm2*$^{+/+}$ and *Mdm2*$^{A/A}$ thymus. All mice were untreated (n=3 per genotype). Quantified levels of p53 and Mdm2 relative to PI3K were normalized to WT.

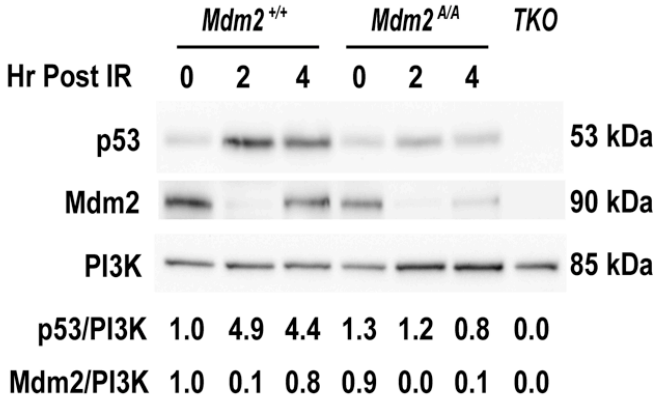

Figure 3.17: Quantified p53 and Mdm2 protein levels in irradiated *Mdm2*$^{+/+}$ and *Mdm2*$^{A/A}$ thymus. Mice were either untreated or irradiated with 4Gy for the indicated times. Quantified levels of p53 and Mdm2 relative to PI3K were normalized to untreated wild-type.

To further examine the effects of Mdm2 Ser394 phosphorylation on p53 and Mdm2 stability, we performed western blots using irradiated *Mdm2*$^{+/+}$ and *Mdm2*$^{A/A}$ *ex*

vivo thymocytes. Stabilization of p53 was detected in primary *Mdm2*$^{+/+}$ thymocytes at 1 to 2 hours post-IR, and p53 levels remained elevated in these cells 6 hours after IR damage (Figure 3.18). In contrast, p53 stabilization was not apparent in *Mdm2*$^{A/A}$ thymocytes at these early time points after DNA damage, even though ATM was clearly activated by IR treatment. Similar to whole thymus extracts, Mdm2 levels also appear decreased in irradiated *Mdm2*$^{A/A}$ thymocytes compared to IR-treated *Mdm2*$^{+/+}$ cells.

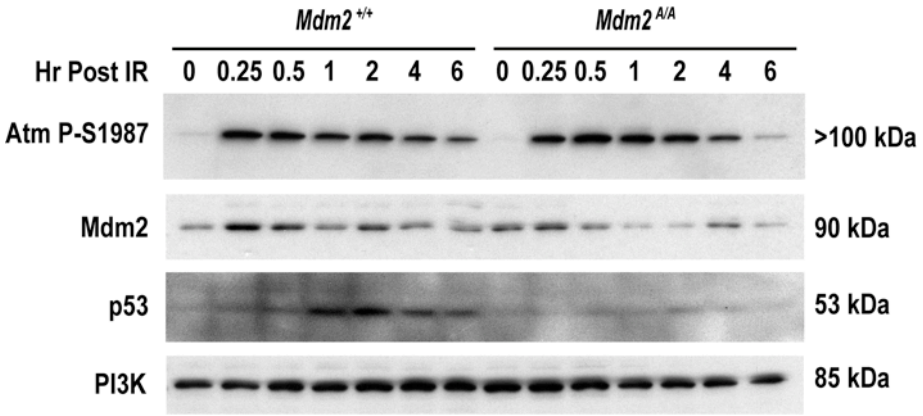

Figure 3.18: Western blot of *Mdm2*$^{+/+}$ and *Mdm2*$^{A/A}$ thymocyte extracts. *Ex vivo* cells were either untreated or irradiated with 2Gy for the indicated times.

The increased levels in wild-type Mdm2 protein may be due to increased p53-induced *Mdm2* transcription, and indeed, like other p53-dependent targets, *Mdm2* transcripts are lower in the irradiated *Mdm2*$^{A/A}$ thymocytes (Figure 3.19). Alternatively, the difference in Mdm2 protein levels after DNA damage may be due to decreased Mdm2 protein stability in *Mdm2*$^{A/A}$ thymocytes compared to *Mdm2*$^{+/+}$ cells. To examine the effects of Mdm2 Ser394 phosphorylation on Mdm2 stability *in vivo*, we incubated untreated and irradiated *Mdm2*$^{+/+}$ and *Mdm2*$^{A/A}$ thymocytes with the protein synthesis

inhibitor cycloheximide (CHX). Although Mdm2 protein is relatively unstable in thymocytes, we found that IR treatment lead to further decreases in Mdm2 stability in both genotypes (Figure 3.20). However, the stability of Mdm2 proteins in untreated and IR-treated *Mdm2*$^{+/+}$ and *Mdm2*$^{A/A}$ thymocytes was comparatively indistinguishable. Therefore, our results indicate that the lower Mdm2 protein levels in *Mdm2*$^{A/A}$ thymocytes after DNA damage reflects less p53 activation of Mdm2 transcription in these cells and not reduced Mdm2-S394A protein stability.

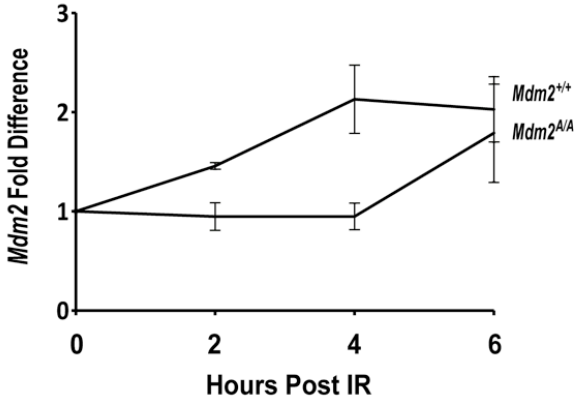

Figure 3.19: Relative expression levels of *Mdm2* in irradiated thymocytes. Cells were either untreated or irradiated with 2Gy for the indicated time points (n=3 per genotype). Data are presented as the ratio of mRNA to *Gapdh* mRNA. Standard deviation indicated by error bars.

The reduced p53 transactivation of *p21* observed in the spleen and thymus of IR-treated *Mdm2*$^{A/A}$ mice (Figures 3.13 and 3.15) suggests that Mdm2 Ser394 phosphorylation may also impact p53 regulation of cell proliferation. To examine this

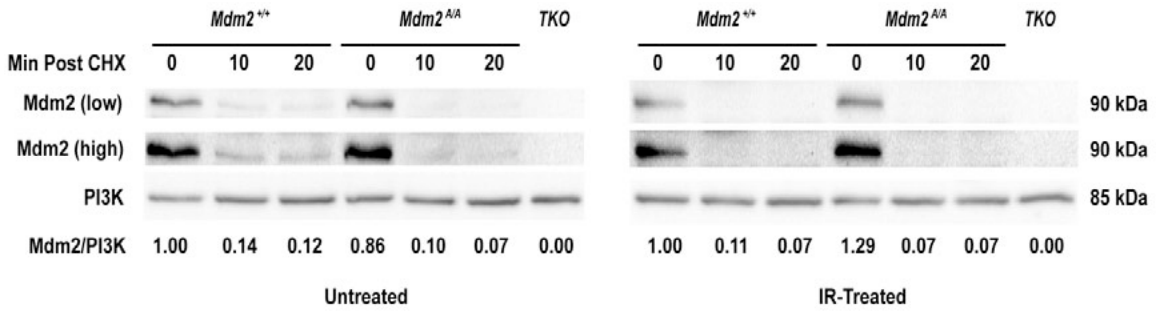

Figure 3.20: Mdm2 protein stability in thymocytes. Western blot of irradiated thymocytes treated with cycloheximide. Cells were incubated with 50 μg/ml of CHX and either left untreated or irradiated with 2Gy for the indicated times. Quantified levels of Mdm2 relative to PI3K were normalized to untreated wild-type.

further, we assayed p53 function in $Mdm2^{+/+}$ and $Mdm2^{A/A}$ MEFs. No difference in the growth rate of $Mdm2^{+/+}$ and $Mdm2^{A/A}$ cells was observed using a standard proliferation assay (Figure 3.21). This result is in keeping with the equivalent low levels of p53 observed in non-damaged $Mdm2^{+/+}$ and $Mdm2^{A/A}$ tissues. However, greater p53 protein stabilization was observed in $Mdm2^{+/+}$ MEFs than in $Mdm2^{A/A}$ MEFs at 6 and 12 hours post-IR (Figure 3.22). Likewise, transactivation of *p21* was greater in $Mdm2^{+/+}$ MEFs than in $Mdm2^{A/A}$ cells, and induction of *Mdm2* transcripts was delayed in $Mdm2^{A/A}$ MEFs (Figure 3.23). FACS analysis of $Mdm2^{+/+}$, $Mdm2^{A/A}$, and $p53^{-/-}$ MEFs at 18 and 45 hours post-IR revealed that $Mdm2^{A/A}$ cells are compromised in their ability undergo growth arrest after DNA damage (Figure 3.24). However, as compared to $p53^{-/-}$ cells, the $Mdm2^{A/A}$ MEFs do retain the ability to undergo a partial growth arrest after IR damage. These data reveal that phosphorylation of Mdm2 Ser394 also governs the ability of Mdm2 to regulate p53-mediated cell growth arrest after IR.

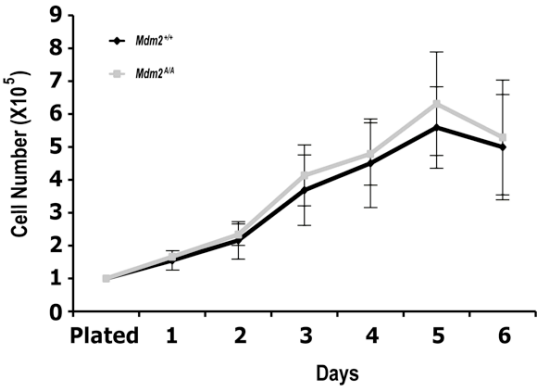

Figure 3.21: Untreated *Mdm2*$^{+/+}$ and *Mdm2*$^{A/A}$ MEF proliferation. Cell numbers were counted each day (n=3 per genotype). Standard deviation indicated by error bars.

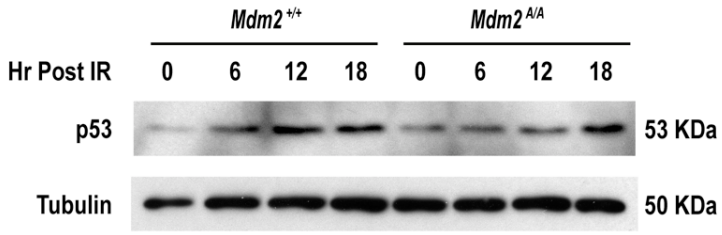

Figure 3.22: Western blot of *Mdm2*$^{+/+}$ and *Mdm2*$^{A/A}$ MEF extracts. Cells were either untreated or irradiated with 4Gy for the indicated times.

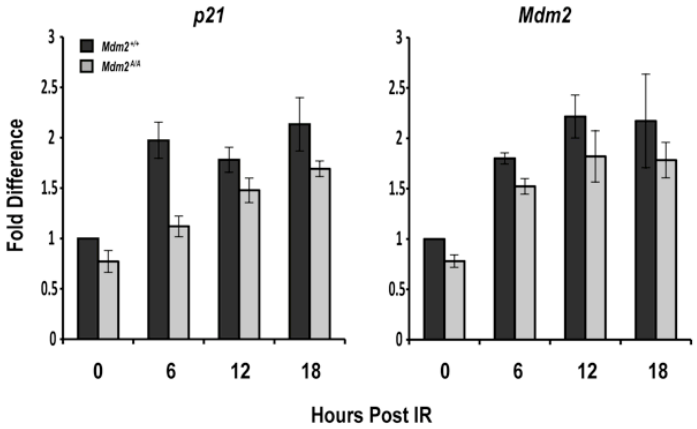

Figure 3.23: Relative expression levels of p53 target genes in irradiated *Mdm2*$^{+/+}$ and *Mdm2*$^{A/A}$ MEFs determined by qRT-PCR. Cells were either untreated or irradiated with 4Gy for the indicated times. (n=3 per genotype). Data are presented as the ratio of mRNA to *Gapdh* mRNA. Standard deviation indicated by error bars

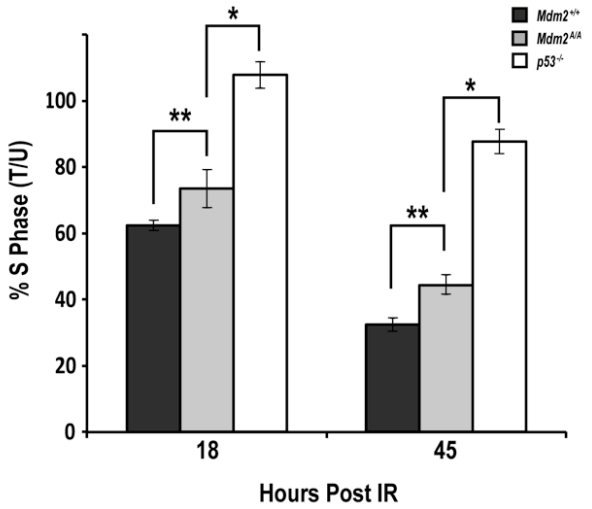

Figure 3.24: Cell cycle arrest in IR treated *Mdm2*$^{+/+}$ and *Mdm2*$^{A/A}$ MEFs. Cells were treated with 4Gy IR for the indicated time points and then incubated with bromodeoxyuridine (BrdU) for 3 hours (n=3 per genotype). Standard deviation indicated by error bars. Asterisks indicate a significant difference: double asterisk 18 hours p=0.0318, 45 hours p=0.0126; single asterisk 18 hours, p=0.0004, 45 hours p=0.0001.

Because ATM phosphorylation of Mdm2 Ser394 is necessary for robust p53 activation after DNA damage, we wanted to test whether this post-translational modification alone was sufficient to induce p53 activity in untreated tissues. To this end, we generated a different mouse model in which Mdm2 Ser394 was mutated to aspartic acid (S394D), thus mimicking a constitutively phosphorylated serine residue (Figure 3.25). We followed the same gene replacement strategy used to generate the S394A model (3.26). We confirmed properly targeted ES cells (Figure 3.27) and the presence of the D394 allele in F_2 generation mice (Figure 3.28). We hypothesized that if phosphorylation of Mdm2 Ser394 is sufficient by itself to disrupt Mdm2 regulation of p53, then substitution of aspartic acid at codon 394 might lead to embryonic lethality in mice bearing functional p53 alleles (as is seen in Mdm2-null mice). However, both heterozygous (*Mdm2*$^{D/+}$) and homozygous (*Mdm2*$^{D/D}$) mice proved to be viable, and both

genotypes were recovered from heterozygous intercrosses at Mendelian ratios (Table 3.3). The viability of this knock-in mutant suggests that baseline levels of p53 protein would be unchanged in this model compared to controls, and subsequent quantitation of p53 and Mdm2 protein levels in untreated thymus protein extracts revealed no significant differences between *Mdm2*$^{+/+}$ and *Mdm2*$^{D/D}$ (Figure 3.29).

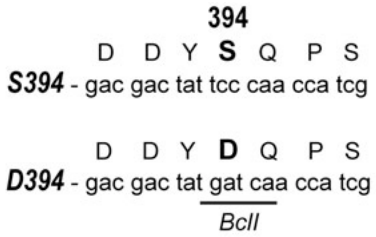

Figure 3.25: Sequence of the S394 and mutant D394 alleles. The mutations in D394 also introduce a *BclI* restriction digest site.

The viability of *Mdm2*$^{D/D}$ mice also suggests that either multiple DNA damage signals are needed to attenuate Mdm2 regulation and activate p53, or that the Mdm2 S394D mutation poorly mimics a phosphoserine residue. The latter possibility would result in *Mdm2*$^{D/D}$ mice presenting with phenotypes similar to our *Mdm2*$^{A/A}$ model, because aspartic acid (like alanine) cannot be phosphorylated. To test this, we treated *Mdm2*$^{+/+}$ and *Mdm2*$^{D/D}$ mice with 4Gy whole-body irradiation and examined p53 stabilization in thymus cells at various early time points after DNA damage. In contrast to what we observed in *Mdm2*$^{A/A}$ cells, p53 protein stabilization by IR damage in *Mdm2*$^{D/D}$ thymus extracts was comparable to *Mdm2*$^{+/+}$ (Figure 3.30). This p53 stabilization was also observed in IR-treated *ex vivo* thymocytes (Figure 3.30).

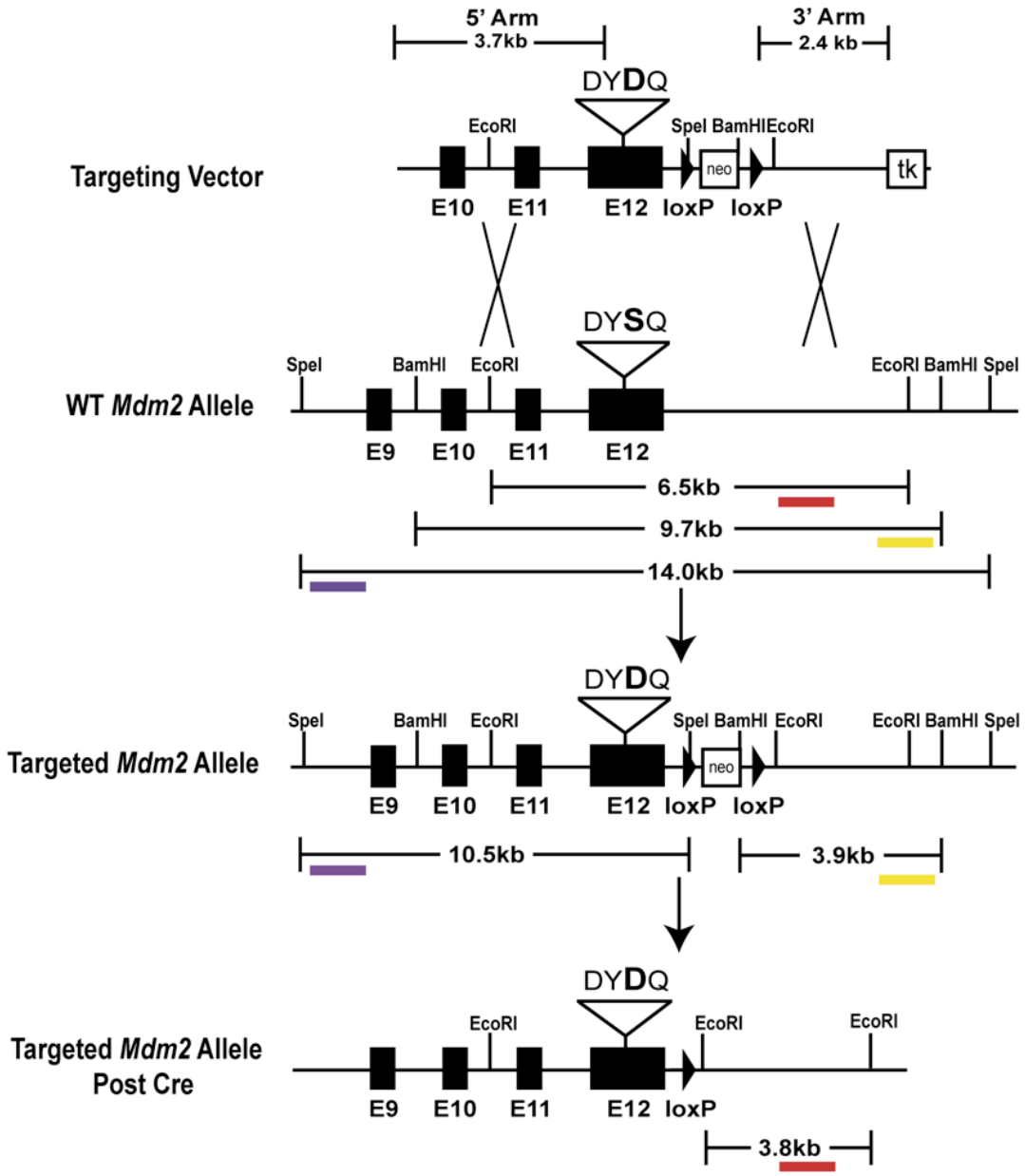

Figure 3.26: Diagram of the targeting strategy used to generate the D394 allele. The targeting vector was linearized and electroporated into PC3 ES cells, and proper homologous recombination was detected by Southern blot. We took advantage of *BamHI* and *SpeI* sites found within the neo cassette to probe on both the 5' (purple bar) and 3' (yellow bar) ends, respectively. PC3 cells have a protamine-cre recombinase transgene that excised the floxed neo cassette in chimeric male germ cells. We utilized a final Southern blot with an *EcoRI* digest and 3' probe (red bar).

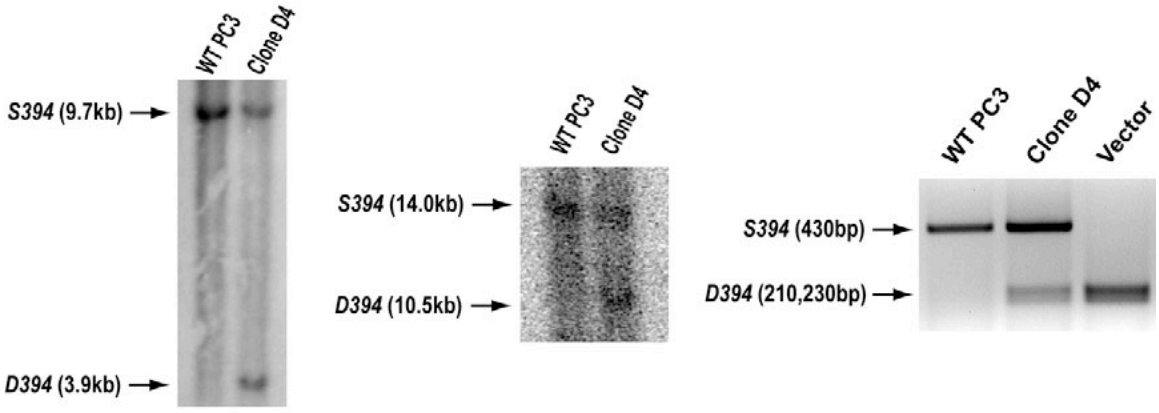

Figure 3.27: Southern blots and genomic PCR in D394 targeted ES cells. Initial Southern blot of ES cells (*left*). DNA samples were digested with *BamHI* and probed with a 3' external probe (yellow bar from Figure 3.26). The neo cassette within the D394 gene replacement vector inserted an exogenous *BamHI* site, resulting in the shorter band (3.9 kb) seen in the targeted ES cell clone in lane 2. Southern blot of ES cells (*center*). DNA samples were digested with *SpeI* and probed with a 5' external probe (purple bar from Figure 3.26). The neo cassette within the D394 gene replacement vector inserted an exogenous *SpeI* site, resulting in the shorter band (10.5 kb) seen in the targeted ES cell clone in lane 2. PCR-*BclI* analysis of targeted ES cells (*right*). Primers flanking Mdm2 codon 394 were used to amplify DNA samples from wild-type PC3 cells (lane 1), the targeted ES cell clone (lane 2), and the D394 gene replacement vector (lane 3), followed by *BclI* digestion.

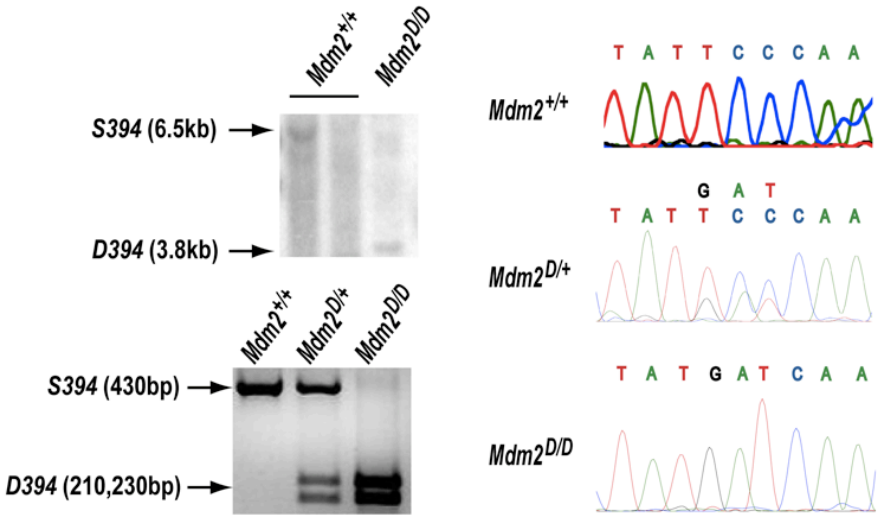

Figure 3.28: Southern blot, genomic PCR, and genotyping in D394 mice. Southern blot of F_2 generation mice (*top left*). DNA samples were digested with *EcoRI* and probed with a 3' internal probe (red bar from Figure 3.2). The D394 allele inserted an exogenous *EcoRI* site resulting in the shorter band (3.8 kb). PCR-*BclI* analysis of F_2 generation mice (*bottom left*). Primers flanking Mdm2 codon 394 were used to amplify DNA samples from $Mdm2^{+/+}$, $Mdm2^{D/+}$, and $Mdm2^{D/D}$ F_2 generation mice, followed by *BclI* digestion. Representative DNA sequencing chromatograms of the Mdm2 394 codon from $Mdm2^{+/+}$, $Mdm2^{D/+}$, and $Mdm2^{D/D}$ F_2 generation mice (*right*).

Genotype	Observed	Expected
$Mdm2^{+/+}$	17	16
$Mdm2^{D/+}$	31	32
$Mdm2^{D/D}$	16	16

Table 3.3: $Mdm2^{D/+}$ and $Mdm2^{D/D}$ viability. Mice either heterozygous or homozygous for the D394 allele are viable and were observed at Mendelian ratios after heterozygous intercrosses (p=0.76).

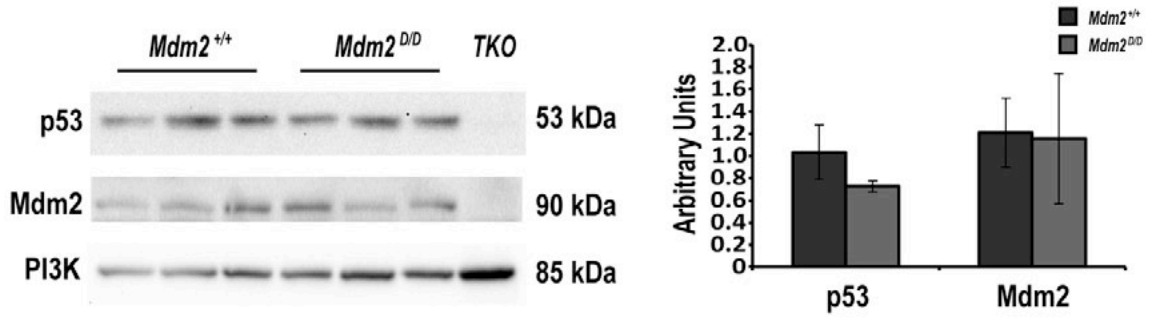

Figure 3.29: Basal levels of p53 and Mdm2 protein in *Mdm2*$^{+/+}$ and *Mdm2*$^{D/D}$ thymus. All mice were untreated (n=3 per genotype). Quantified levels of p53 and Mdm2 relative to PI3K were normalized to wild-type.

Likewise, the pattern of Mdm2 protein destabilization followed by recovery was equivalent between the *Mdm2*$^{+/+}$ and *Mdm2*$^{D/D}$ tissues (Figure 3.30), which reflects the equal induction of *Mdm2* transcript levels seen in DNA damaged thymocytes (Figure 3.31). *Puma* transcript levels were also similarly increased in the IR-treated *Mdm2*$^{+/+}$ and *Mdm2*$^{D/D}$ cell (Figure 3.31), and the levels of DNA damage-induced apoptosis were

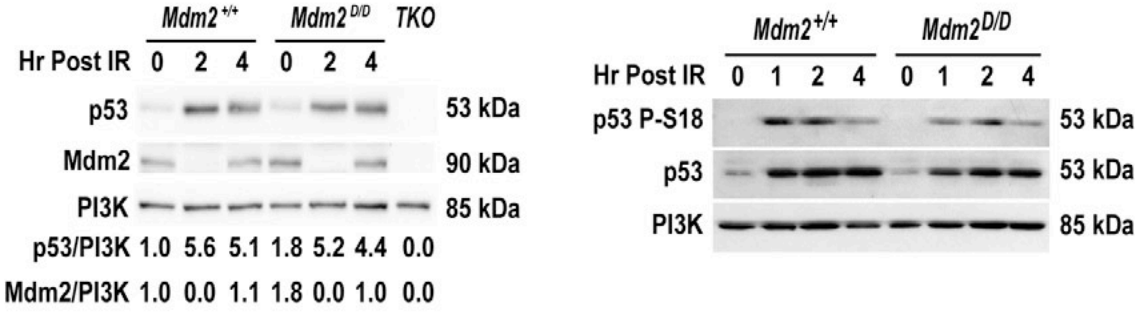

Figure 3.30: Western blots of *Mdm2*$^{+/+}$ and *Mdm2*$^{A/A}$ whole thymus and thymocyte extracts. Western blot of whole thymus extracts (*left*). Mice were either untreated or irradiated with 4Gy for the indicated times. Quantified levels of p53 and Mdm2 relative to PI3K were normalized to untreated wild-type. Western blot of thymocyte extracts (*right*). *Ex vivo* cells were either untreated or irradiated with 2Gy for the indicated times. PI3K was used as a loading control.

the same between *Mdm2*$^{+/+}$ and *Mdm2*$^{D/D}$ thymocytes at 12 hours after IR treatment (Figure 3.32). Similar results were obtained in thymocytes at 24 hours post-IR, as well as in thymocytes isolated 48 hours after whole-body IR in *Mdm2*$^{+/+}$, *Mdm2*$^{D/D}$, and *p53*$^{-/-}$ mice (Figure 3.33). Collectively, these findings demonstrate that Mdm2 S394D mimics the effects of the phosphorylated Mdm2 Ser394 protein in *Mdm2*$^{+/+}$ mice after DNA damage. As baseline levels of p53 protein and apoptosis in non-damaged *Mdm2*$^{+/+}$ and *Mdm2*$^{D/D}$ cells are the same in these assays, the mimicking of Mdm2 Ser394 phosphorylation in *Mdm2*$^{D/D}$ thymocytes is not sufficient in the absence of other DNA damage-induced signals to induce p53 activation. Alternatively, different phosphorylation sites on Mdm2 may be affected by either of the two knock-in mutants and could cause this difference in the DNA damage responses. The effect of MDM2 phosphorylation of Y394 modification has previously been tested, but the effect on other Mdm2 posttranslational modifications remain to be studied (Goldberg et al., 2002).

To confirm the effects of this Mdm2 Ser394 phospho-mimic in cell growth, *Mdm2*$^{+/+}$ and *Mdm2*$^{D/D}$ MEFs were analyzed for cell proliferation (Figure 3.34). As with *Mdm2*$^{A/A}$ MEFs, the *Mdm2*$^{D/D}$ MEFs proliferated at the same rate as *Mdm2*$^{+/+}$ MEFs in culture. However, IR-treatment of *Mdm2*$^{D/D}$ MEFs induced p53 stabilization at levels similar to IR-treated *Mdm2*$^{+/+}$ MEFs (Figure 3.35), and IR damage induced an equivalent p53-mediated reduction in S phase in both *Mdm2*$^{+/+}$ and *Mdm2*$^{D/D}$ cells (Figure 3.36).

Previous *in vitro* work has established that the Wip1 phosphatase can de-phosphorylate multiple ATM targets, including human ATM Ser1981, p53 Ser15, and

MDM2 Ser395 (Shreeram *et al.*, 2006a; Lu *et al.*, 2005; Lu *et al.*, 2007). This de-phosphorylation has been proposed to return DNA damage signaling to basal levels once the DNA damage has been resolved. Since Wip1 cannot de-phosphorylate the Mdm2-S394D residue, we hypothesized that $Mdm2^{D/D}$ and $Mdm2^{+/+}$ mice might have differences in the duration of Mdm2-p53 signaling after IR treatment. Therefore, we analyzed p53 stabilization and activity at later time points in the DNA damage response. Like $Mdm2^{D/D}$ thymocytes (Figure 3.30), $Mdm2^{+/+}$ and $Mdm2^{D/D}$ spleen samples had equal levels of ATM activity and p53 levels at 4 hours post-IR. However, the level of p53 protein remained persistently elevated at 8 hours post-IR in $Mdm2^{D/D}$ extracts, despite the reduction in ATM activity and similar levels of Mdm2 by this later time point (Figure 3.37).

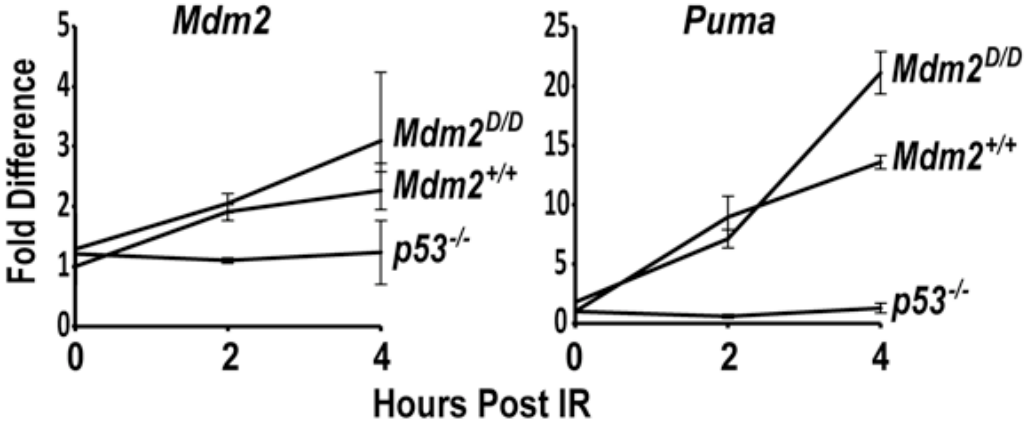

Figure 3.31: Relative expression of p53 target genes in $Mdm2^{+/+}$ and $Mdm2^{D/D}$ thymocytes determined by qRT-PCR. Cells were either untreated or irradiated with 2Gy for 2 or 4 hours (n=3 per genotype). Data are presented as the ratio of mRNA to *Gapdh* mRNA. Standard deviation indicated by error bars.

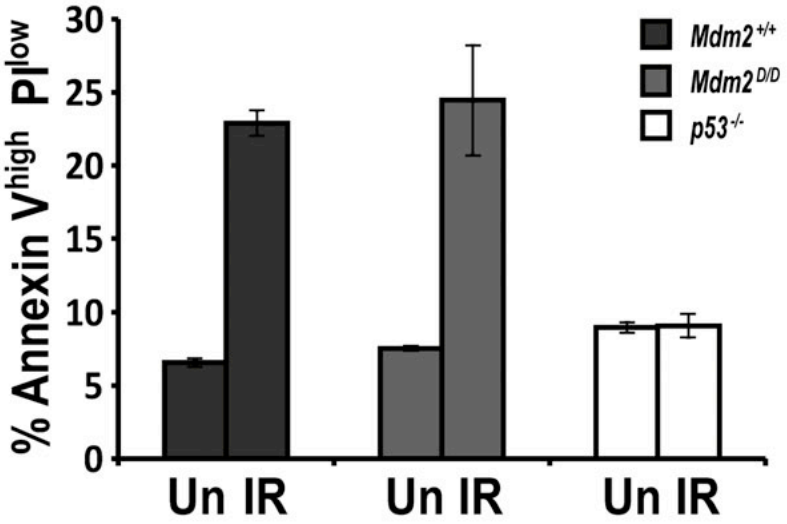

Figure 3.32: Quantification of apoptotic cells in primary *Mdm2*$^{+/+}$ and *Mdm2*$^{D/D}$ thymocytes. *Ex vivo* thymocytes were isolated and were either left untreated or irradiated with 2Gy for 12 hours (n=3 per genotype). Standard deviation indicated by error bars.

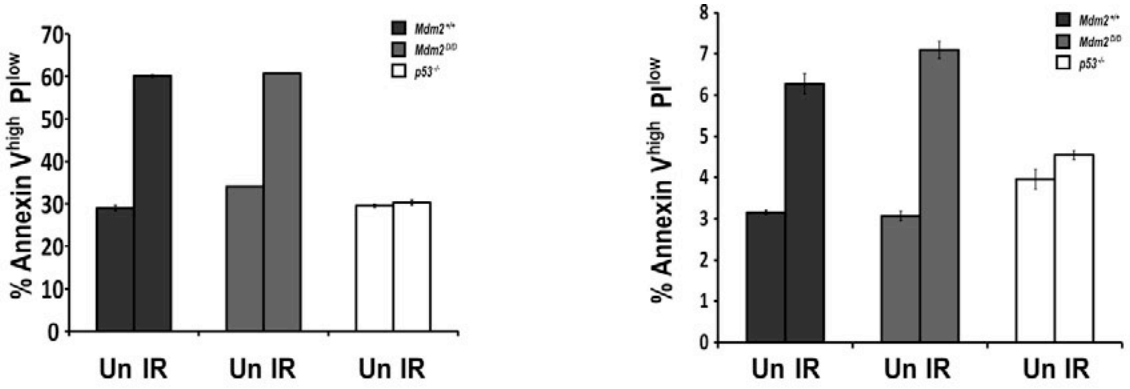

Figure 3.33: Quantification of apoptotic cells in *ex vivo* and whole-body irradiated *Mdm2*$^{+/+}$ and *Mdm2*$^{D/D}$ thymocytes. *Ex vivo* thymocytes were either left untreated, irradiated with 2Gy for 24 hours (*left*), or irradiated with 2Gy for 48 hours (n=3 per genotype). Standard deviation indicated by error bars.

A similar response pattern was seen in primary thymocytes. Although p53 was stabilized to a similar extent in *Mdm2*$^{+/+}$ and *Mdm2*$^{D/D}$ mice at early time points after IR damage (Figure 3.30), p53 levels remain elevated in *Mdm2*$^{D/D}$ thymocytes at 12 hours post-IR, whereas p53 stabilization is less obvious at this later time point in *Mdm2*$^{+/+}$ cells (Figure 3.38). As in spleen, the elongated duration of p53 stabilization in *Mdm2*$^{D/D}$ thymocytes was seen well after resolution of the DNA damage response, as indicated by the absence of phospho-ATM at 12 hours post-IR, and despite the presence of Mdm2.

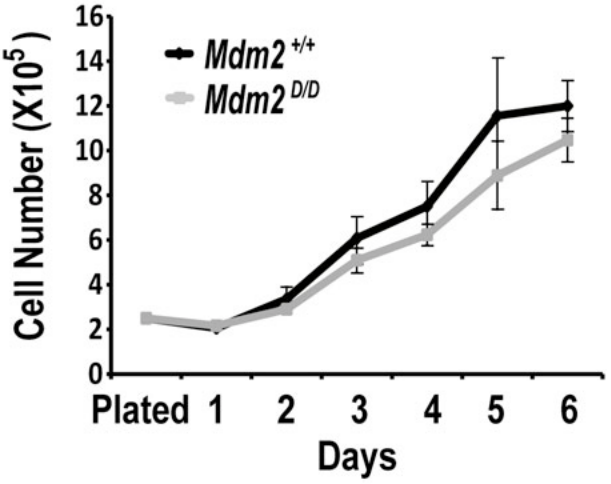

Figure 3.34: Untreated *Mdm2*$^{+/+}$ and *Mdm2*$^{D/D}$ MEF proliferation. Cell numbers were counted each day (n=3 per genotype). Standard deviation indicated by error bars.

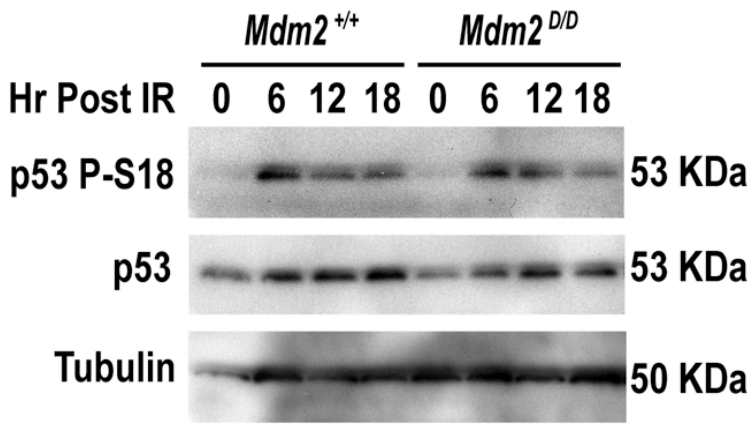

Figure 3.35: Western blot of *Mdm2*$^{+/+}$ and *Mdm2*$^{D/D}$ MEF extracts. Cells were either untreated or irradiated with 4Gy for the indicated times.

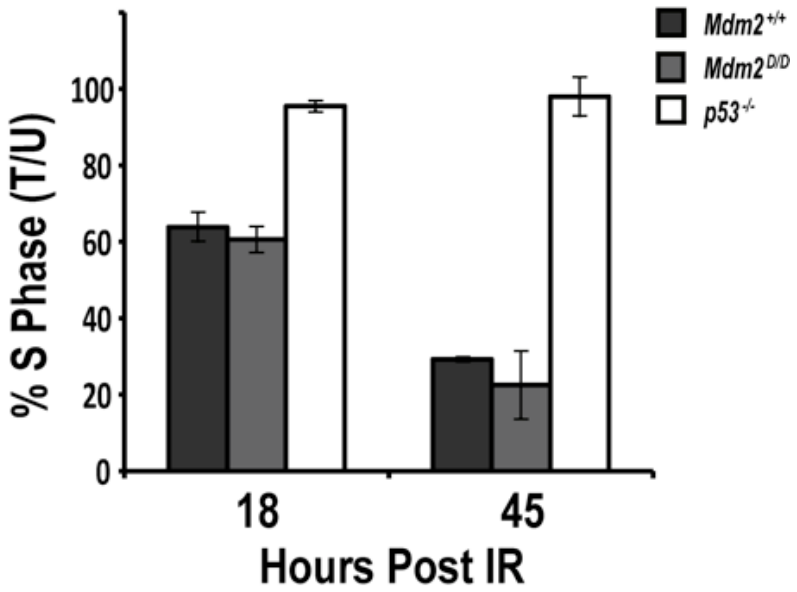

Figure 3.36: Cell cycle arrest in IR treated *Mdm2*$^{+/+}$ and *Mdm2*$^{D/D}$ MEFs. Cells were treated with 4Gy IR for 18 hours or 8Gy IR for 45 hours and incubated with BrdU for 3 hours (n=3 per genotype). Standard deviation indicated by error bars.

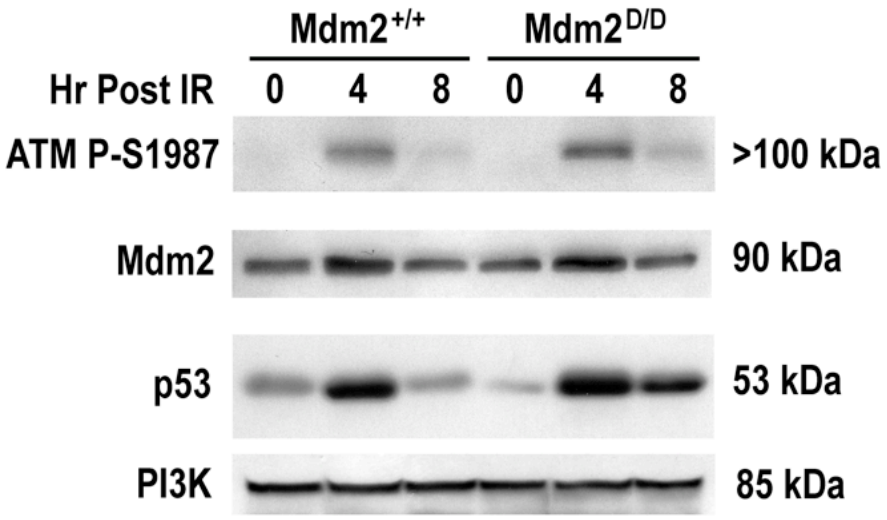

Figure 3.37: Western blot of *Mdm2*$^{+/+}$ and *Mdm2*$^{D/D}$ whole spleen extracts. Mice were either untreated or irradiated with 4Gy and spleens were harvested either 4 or 8 hours later.

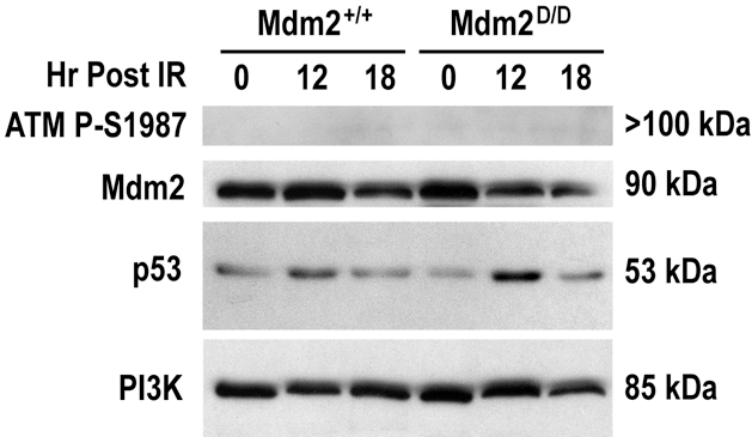

Figure 3.38: Western blot of *Mdm2*$^{+/+}$ and *Mdm2*$^{D/D}$ whole thymocyte extracts. *Ex vivo* cells were either untreated or irradiated with 2Gy for either 12 or 18 hours.

The elongated p53 response in *Mdm2*$^{D/D}$ thymocytes was reflected by increased levels of *Puma*, *p21*, *Mdm2,* and *Wip1* expression found in these cells at 12 and 18 hours

post-IR (Figure 3.39), and p53 signaling pathway PCR array analysis of additional p53 target genes confirmed that p53 activation remained elevated in *Mdm2*$^{D/D}$ thymocytes relative to *Mdm2*$^{+/+}$ levels at 12 hours following IR (Table 3.4).

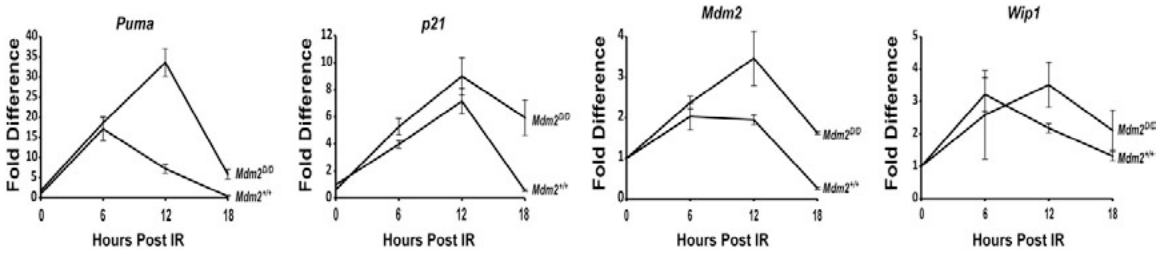

Figure 3.39: Relative expression of p53 target genes in *Mdm2*$^{+/+}$ and *Mdm2*$^{D/D}$ thymocytes determined by qRT-PCR. Cells were either untreated or irradiated with 2Gy for the indicated times (n=3 per genotype). Data are presented as the ratio of mRNA to *Gapdh* mRNA. Standard deviation indicated by error bars.

p53 Target Genes	*Mdm2*$^{+/+}$	*Mdm2*$^{D/D}$	*Mdm2*$^{D/D}$
Bax	3.2	10.6	4.2
Cyclin B2	0.7	5.4	3.7
GADD45	1.3	1.7	3.2
Msh2	1.0	5.8	3.0
Noxa	2.8	9.2	4.2
Wip1	1.5	4.9	2.2
Sesn2	1.7	7.4	1.8

Table 3.4: *Mdm2*$^{+/+}$ and *Mdm2*$^{D/D}$ thymocyte target gene expression by PCR Array. Relative expression levels of p53 target genes in irradiated thymocyte extracts determined by quantitative real time PCR using Qiagen p53 Signaling Pathway PCR Arrays. Cells were either untreated or irradiated with 2Gy and were harvested 12 hours later. Data are presented as the fold increase in individual treated *Mdm2*$^{+/+}$ and *Mdm2*$^{D/D}$ animals normalized to untreated WT levels and as the ratio of mRNA to *Gapdh* mRNA.

Finally, to explore the importance of Mdm2 Ser394 phosphorylation in p53-mediated tumor suppression, we established cohorts of *Mdm2*$^{+/+}$, *Mdm2*$^{A/A}$, and *Mdm2*$^{D/D}$ mice and performed a tumor assay. In 24 months, 20 of 31 (65%) *Mdm2*$^{A/A}$ mice developed spontaneous tumors, whereas only 1 of 24 (4%) *Mdm2*$^{D/D}$ mice presented with a tumor of the salivary gland epithelium (Figure 3.40). None of the *Mdm2*$^{+/+}$ mice presented with a tumor during this interval. Most of the *Mdm2*$^{A/A}$ tumors arose between 18-24 months of age, which closely resembles previous *p53*$^{+/-}$ tumor curves (Harvey *et al.*, 1993; Jacks *et al.*, 1994). Like other mouse models with diminished Atm activity, most of the tumors (13/20; 65%) were found to be T-cell derived lymphomas as staining for the T-cell marker CD3 (Figure 3.41). The remaining *Mdm2*$^{A/A}$ tumors displayed severe splenomegaly and cellular infiltration in the liver and kidneys. One of these

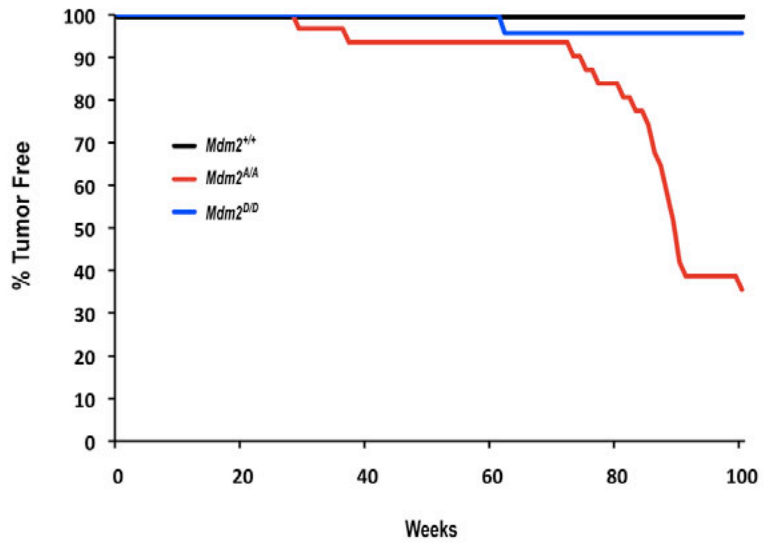

Figure 3.40: Spontaneous tumor cohorts. Spontaneous tumorigenesis in *Mdm2*$^{+/+}$ (n=50), *Mdm2*$^{A/A}$ (n=31), and *Mdm2*$^{D/D}$ (n=24) mice.

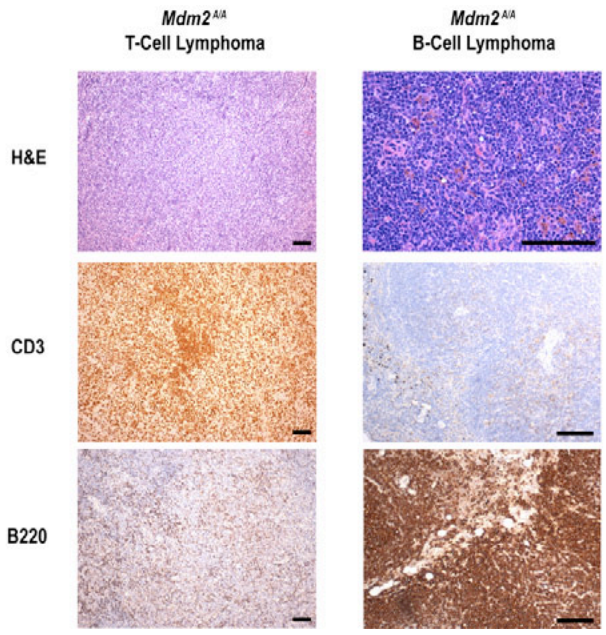

Figure 3.41: Representative CD3 and B220 staining in *Mdm2*$^{A/A}$ lymphomas. Representative tumor sections from an *Mdm2*$^{A/A}$ T-cell lymphoma (mesenteric lymph node, *left*) and an *Mdm2*$^{A/A}$ B-cell lymphoma (spleen, *right*). Tissue sections were stained with hematoxylin and eosin (H&E), anti-CD3, or anti-B220. Scale bars are 100 μm.

tumors stained positive for B220 and displayed expansion of the white pulp in the spleen, indicative of B cell lymphoma (Figure 3.41). Sequencing of p53 transcripts isolated from four randomly selected tumors indicated *Mdm2*$^{+/+}$ p53 expression levels and no p53 mutations in these *Mdm2*$^{A/A}$ samples. These results reveal that post-translational modification of Mdm2 Ser394 impacts p53-mediated tumor suppression as well as the p53 DNA damage response *in vivo*.

Discussion

Activation of the p53 tumor suppressor by DNA damage and a role for DNA damage-induced kinases in p53 activation has been well established. However, *in vivo* analyses have revealed that phosphorylation of p53 by these kinases serves only to fine-

tune the p53 response without having a large effect on p53 stability (Toledo and Wahl, 2006). Mdm2 is also a potential target for post-translational modification by DNA damage- induced kinases such as ATM (Maya *et al.*, 2001), but there has been no direct *in vivo* analysis of the effects of Mdm2 phosphorylation on p53 stability and functions.

In our present study utilizing mouse models of Mdm2 Ser394 phosphorylation, we provide direct evidence that ATM phosphorylation of Mdm2 Ser394 regulates the ability of Mdm2 to destabilize p53 *in vivo*, and that this signaling impacts p53-mediated apoptosis and tumor suppression. $Mdm2^{A/A}$ mice lack p53-dependent physiological responses in radiosensitive organs after IR treatment resulting in phenotypes that nearly match those seen in IR treated $p53^{-/-}$ mice: radioresistance, greatly reduced p53 target gene induction, and greatly reduced apoptosis. Importantly, the differences between $Mdm2^{A/A}$ and $Mdm2^{+/+}$ mice were seen only in irradiated mice and tissues, as baseline levels were similar in all assays. This owes to the conservation of Mdm2 structure and function in the S394A protein, and indicates that the only difference between the wild-type and mutant Mdm2 protein is the phosphorylation status of Ser394 after cellular stress. It is likely that the compromised p53 transactivation and the reduced number of cells undergoing apoptosis and cell cycle arrest are due to the lack of p53 protein accumulation in DNA damaged $Mdm2^{A/A}$ cells. Thus, phosphorylation of Mdm2 Ser394 by the ATM kinase is a major regulator of p53 stability and the subsequent p53-mediated DNA damage response in multiple tissue types.

Although the levels of p53 induction and activation are equivalent at early time points after IR in *Mdm2*$^{+/+}$ and *Mdm2*$^{D/D}$ cells, p53 protein levels and activities remain elevated in *Mdm2*$^{D/D}$ cells at later time points after IR treatment (Figures 3.37-3.40). In contrast, the DNA damage response in *Mdm2*$^{+/+}$ cells begins to wane after 6 hours post-IR, coincident with the induction of *Wip1* expression (Figures 3.38 and 3.39). Since Wip1 is unable to dephosphorylate the Mdm2 S394D residue, elevation of p53 functions in *Mdm2*$^{D/D}$ cells at later time points after IR indicates that Mdm2-S394 phosphorylation also regulates the duration of the p53 response. However, p53 levels and activities eventually return to baseline in the *Mdm2*$^{D/D}$ cells, possibly due to the eventual loss of other secondary modifications to Mdm2 or p53 (which remain to be reliably detected and tested). These findings are in keeping with a proposed role for Wip1 as gatekeeper of the Mdm2-p53 autoregulatory loop (Lu *et al.*, 2007). Collectively, our results indicate that ATM phosphorylation of Mdm2 Ser394 is necessary but not sufficient to induce a robust p53 response to IR.

Interestingly, p53 tumor suppressor function is deficient in untreated S394A mice, as 65% of these mice developed spontaneous lymphomagenesis in the absence of exogenous IR treatment. Since our data indicate that p53 levels and activities are identical between *Mdm2*$^{+/+}$ and *Mdm2*$^{A/A}$ cells in the absence of DNA damage, the stochastic nature of endogenous DNA damage signaling arising from inappropriate oncogene activation or DNA replication errors may account for this rather long latency period. Tumor formation in our *Mdm2*$^{A/A}$ model is in keeping with previous reports of a role for ATM–p53 signaling and p53 activation of the pro-apoptotic gene *Puma* in p53-

mediated suppression of lymphoma formation (Jeffers *et al.*, 2003; Sluss *et al.*, 2010). Likewise, the reduced capacity of p53 to suppress growth after DNA damage in *Mdm2*$^{A/A}$ cells may also contribute to the spontaneous tumorigenic phenotype of *Mdm2*$^{A/A}$ mice. It remains to be seen if phosphorylation of Mdm2 Ser394 by ATM also regulates p53-mediated suppression of tumors induced by sub-lethal doses of radiation or the forced expression of activated oncogenes.

Transfection-based experiments have determined that mutation of six separate ATM phosphorylation sites in the carboxy-terminus of MDM2, including Ser395, alters MDM2 protein oligomerization, E3-ligase activity, and the interaction of MDM2 with p53 (Cheng *et al.*, 2009; Cheng *et al.*, 2011). Because p53 activity is not totally ablated in the *Mdm2*$^{A/A}$ model, these additional ATM targets on Mdm2 may contribute to full p53 activation after DNA damage. Furthermore, a recent study found that ATM phosphorylation of MDM2 Ser395 led to increased p53 mRNA translation, which suggests that MDM2 may be necessary for p53 protein upregulation after DNA damage (Gajjar *et al.*, 2012). Diminished Mdm2 E3 ligase activity and phospho-Mdm2-dependent upregulation of p53 would each explain the seemingly paradoxical results of having decreased p53 levels and activities in the absence of Mdm2 protein in IR-treated *Mdm2*$^{A/A}$ thymus extracts. These mechanisms would also explain the increased p53 activation at later times of the DNA damage response in *Mdm2*$^{D/D}$ cells despite nearly equivalent levels of Mdm2 compared to *Mdm2*$^{+/+}$. Our *in vivo* data are in keeping with both of these proposed models and confirm a significant role for Mdm2 S394 phosphorylation in the p53 DNA damage response.

In conclusion, our study reveals that ATM phosphorylation of Mdm2 at serine residue 394 is a critical regulator of Mdm2-p53 signaling. Phosphorylation of this Mdm2 residue by ATM following DNA damage is necessary for p53 stabilization, thereby upregulating p53 activity and activating p53 downstream functions in primary cells and tissues. Furthermore, the phosphorylation status of Mdm2 Ser394 governs the duration of the p53 response, underscoring the importance of this single phosphorylation target in regulating Mdm2-p53 signaling and p53-mediated tumor suppression. Full understanding of the multiple post-translational modifications that influence p53 signaling will likely assist in developing better molecular diagnostics and therapeutics for human cancer patients.

Materials and Methods

Generation of S394A and S394D mice

The targeting constructs contain a subcloned fragment of the Mdm2 genomic sequence (129Sv strain). Site-directed mutagenesis was performed (Stratagene #200523). The targeting vectors were sequenced to ensure that no unwanted mutations were introduced. PC3 ES cells were electroporated with each targeting vector. Homologous recombination was detected by Southern blot using 5' and 3' external probes after *SpeI* and *BamHI* restriction digests, respectively. Targeted cells were microinjected into E3.5 blastocysts (C57BL/6 strain), and the embryos were surgically implanted into pseudopregnant foster mice by standard procedures. Transmission of the knock-in allele and excision of the neo cassette in F_1 offspring of male chimeric mice was confirmed by digestion with *EcoRI*

followed by Southern analysis using a 3' internal probe described previously (Steinman and Jones, 2002).

Mice

All mice used in this study were on a mixed 129Sv×C57Bl/6 background. Sequencing of DNA samples was performed by Sequegen. All mice and cells were irradiated with a cesium-137 source (Gammacell 40). Animals in the spontaneous tumor cohorts or IR-treated cohorts were killed if tumor burden was apparent or when moribund. Animals were maintained and used in accordance with federal guidelines and those established by the Institutional Animal Care and Use Committee at the University of Massachusetts Medical School.

Mdm2 S394A and Mdm2 S394D Genotyping

Mouse tail DNA was amplified by PCR using the following primers: Forward 5'-AAAGATGCTGGACCCTTCGTGAGA-3' and Reverse 5'-GCACACGTGAAACATGACATGAGG-3'. This produces a 430 base pair (bp) PCR fragment that must then be digested by specific restriction enzymes. For Mdm2 S394A, 1 µl NEB Buffer 3 supplemented with S-adenosylmethionine (SAM) and 1 µl *BcgI* was added directly to the PCR reaction tube and incubated at 37 °C for 1 hour. For Mdm2 S394D, 1 µl *BclI* was added directly to the PCR reaction tube and incubated at 50 °C for 1 hour. These digestions each approximately bisect the DNA fragment so that the WT and mutant alleles can be distinguished by running on a 1% agarose gel.

Histology

Tissues were fixed in 10% formalin. Irradiated tissue sections (5μm) were stained with anti-cleaved caspase-3 antibody (Cell Signaling #9661) or stained for TUNEL using the *In Situ* Cell Death Detection Kit, POD (Roche 11684817910). Tumor samples were stained with anti-CD3 (Abcam ab16044) or anti-CD45R/B220 (BD Pharmingen). All staining was performed by the UMMS Diabetes and Endocrinology Research Center Morphology Core.

Western Blotting and Reagents

Tissues and cells were lysed in NP-40 lysis buffer (50 mM Tris–HCl, pH 7.5; 150 mM NaCl; 0.5% NP-40; 20% Glycerol) supplemented with 1×protease inhibitor cocktail (Roche). Protein extracts were analyzed by standard western blotting with the following antibodies: p53 (1C12), phospho-Atm Ser1987 (10H11.E12), and phospho-p53 Ser18 (#9284) from Cell Signaling; Mdm2 (mix of sc-812 and sc-1022) and lamin A/C (sc-6215) from Santa Cruz; MdmX (MDMX-82) and tubulin (T5168) from Sigma; PI3K (#06-496) from Upstate; actin (ab8229) from Abcam. Nutlin-3a (N6287) and cycloheximide (C4859) were from Sigma. PI3K and tubulin were used as loading controls. KU55933 (118502) was from Calbiochem. The CIP (M0290) and phosphatase treatment protocol were from NEB. Protein levels in Figure 3C were quantified by densitometry using the ImageJ software. All other protein quantification was performed using the Chemidoc XRS+ Molecular Imaging System from BioRad.

Gene Expression Analysis

Total mRNA was isolated according to the Trizol Reagent protocol (Invitrogen) and cDNA was generated using the SuperScript II First Strand Synthesis Kit (Invitrogen). The following primers were used in qRT-PCR:

p21: 5'-TGAGGAGGAGCATGAATGGAGACA-3'

5'-AACAGGTCGGACATCACCAGGATT-3',

Puma: 5'-CCTGGAGGGTCATGTACAATCT-3'

5'-TGCTACATGGTGCAGAAAAAGT-3',

Bax: 5'-CTGAGCTGACCTTGGAGC-3'

5'-GACTCCAGCCACAAAGATG-3',

Noxa: 5'-CCACCTGAGTTCGCAGCTCAA-3'

5'-GTTGAGCACACTCGTCCTTCA-3',

Mdm2: 5'-GCATTCTGGTGATTGCCTGGATCA-3'

5'-AGACTGTGACCCGATAGACCTCAT-3'

Gapdh: 5'-TGGCAAAGTGGAGATTGTTGCC-3'

5'-AAGATGGTGATGGGCTTCCCG-3'.

All data are presented as the ratio of mRNA to *Gapdh* mRNA.

For the Qiagen p53 PCR Array experiments, mRNA was isolated using the RNeasy kit (74104) with DNase (79254) from Qiagen. cDNA was synthesized using the RT2 First Strand Kit (330401) from Qiagen. p53 PCR Arrays (PAMM-027C) were run according to manufacturer's protocol using the RT2 SYBR Green ROX qPCR Mastermix (330520) from Qiagen.

Flow Cytometry

For apoptosis, samples were treated according to the Annexin V-FITC Apoptosis Detection Kit I protocol (BD Pharmingen #556547). Early apoptotic cells (Annexin V^{high} PI^{low}) were quantitated and presented. For cell cycle arrest, treated MEFs were pulse labeled with 60μM bromodeoxyuridine (BrdU) for 3 hours. Cells were then trypsinized, fixed in 70% ethanol overnight, incubated with anti-BrdU antibody (Becton Dickinson #347583) and PI, and analyzed by flow cytometry. Data are presented as the percentage of cells in S phase in the treated samples compared to the untreated samples. Flow cytometry was performed by the UMASS Medical School Flow Cytometry Core Lab.

CHAPTER IV:

UNPUBLISHED AND ONGOING WORK

Foreword

The results presented in Chapter 3 of this dissertation revealed the necessity of Mdm2 Ser394 in the p53-dependent response to IR. However, p53-Mdm2 signaling has a role in many cellular processes, and the role of Mdm2 Ser394 phosphorylation in response to these alternate stressors remains to be tested. Additionally, older *Mdm2*$^{A/A}$ mice displayed greatly increased spontaneous tumorigenesis, revealing a role for this residue in tumor suppression even in the absence of exogenous IR treatment. We have conducted preliminary experiments to further characterize the role of Mdm2 Ser394 in these p53-dependent effects.

Introduction

The positive correlation between the tumorigenic potential of primary cells and the incidence of tumorigenesis in the corresponding animal model is substantiated in *p53*$^{-/-}$ mice and cells. MEFs derived from *p53*$^{-/-}$ embryos have been used to determine the role of p53 in various cell culture assays such as low-density plating stress experiments and immortalization assays. Previous studies have shown that p53 restricts the survival and growth of cells at very low densities, as *p53*$^{-/-}$ MEFs readily grow robust colonies under these conditions (Harvey *et al.*, 1993; Jones *et al.*, 1996). Likewise, p53 limits the immortalization of MEFs that undergo stress and increased mutations caused by serial plating. In these experiments, wild-type MEFs fail to immortalize in culture due to decreased viability and increased senescence, while *p53*$^{-/-}$ MEFs immortalize after only a few passages in culture (Harvey *et al.*, 1993; Jones *et al.*, 1996). These results mirror the increased tumorigenesis seen in *p53*$^{-/-}$ mice, and established the potential link between

p53 responses under cell culture conditions and the ability to inhibit tumor initiation and development at the organismal level (Donehower *et al.*, 1992).

As p53 activity is critical in limiting spontaneous tumorigenesis, it is not surprising that p53 also suppresses tumors that are initiated by cellular stressors such as ionizing radiation and activated oncogene expression. We have previously shown that wild-type mice that are irradiated with 8Gy die in a p53-dependent manner at 2-3 weeks post-IR (see Figure 3.5). However, previous reports have shown that p53 protects against DNA damage-induced tumorigenesis in mice treated with sub-lethal doses of IR (Kemp *et al.*, 1994). In this study, wild-type mice treated with 4Gy survived up to 80 weeks with 100% of the mice being tumor free. Conversely, IR-treated $p53^{+/-}$ mice died by 55 weeks of age and $p53^{-/-}$ mice died by 17 weeks of age due to increased incidences of lymphomas and sarcomas. These tumors arose significantly faster than untreated $p53^{+/-}$ and $p53^{-/-}$ control cohorts, revealing the importance of p53 signaling in protecting against total body IR-induced tumorigenesis in mice (Kemp et al., 1994; Harvey et al., 1993).

A common mouse model that has been used to examine the cellular response to activated oncogenes is the *Eμ-Myc* transgenic model (Adams *et al.*, 1985). These mice bear the *c-myc* oncogene under the control of the immunoglobulin heavy chain enhancer so that *c-myc* is overexpressed in progenitor B cells and, therefore, these mice develop rapid B-cell lymphomagenesis. Multiple members of the p53 regulatory pathway, including ATM and Wip1, have been shown to be important in determining tumor free survival in these mice, as the genetic disruption of p53 function and regulation results in

increased lymphomagenesis rates (Eischen *et al.*, 1999; Schmitt *et al.*, 1999; Maclean *et al.*, 2007; Garrison *et al.*, 2008; Sluss *et al.*, 2010). As Mdm2 Ser394 has been shown to be an important regulatory site for ATM-dependent p53 activation, we expect this site to be crucial for p53 tumor suppression in *Eμ-Myc* mice. Preliminary experiments describing the effects of Mdm2 Ser394 status on the function of p53 in cell culture stress, IR-induced tumorigenesis and survival, and oncogene-induced lymphomagenesis will be presented in this Chapter.

Results

It is clear from our previous results that Mdm2 Ser394 phosphorylation is necessary for p53-dependent cell-cycle arrest in MEFs treated with γ-irradiation. To further characterize the necessity of this Mdm2 residue in response to other DNA damaging agents, we repeated the BrdU incorporation assays using the topoisomerase II inhibitors etoposide and doxorubicin and the topoisomerase I inhibitor camptothecin (Figure 4.1). As expected, $Mdm2^{+/+}$ cells treated with these reagents displayed a large decrease in cells in S phase. Interestingly, $p53^{-/-}$ cell cycle profiles were unaffected by doxorubicin and camptothecin, but did undergo a partial cell cycle arrest in response to etoposide, albeit not to the same extent as $Mdm2^{+/+}$ cells. This likely owes to some p53-independent effects in the cellular response to etoposide. Importantly, the decline in S phase in treated $Mdm2^{A/A}$ cells showed no significant difference compared to $Mdm2^{+/+}$ cells in all three genotoxic treatments. These results suggest that, while Mdm2 Ser394 phosphorylation is important in the response to IR in MEFs, alternate mechanisms must exist to activate p53 in response to these topoisomerase inhibitors.

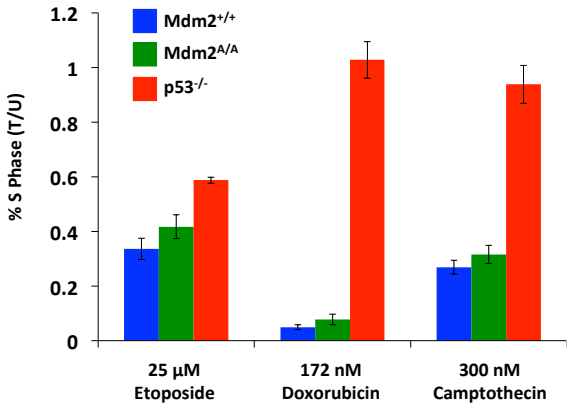

Figure 4.1: Cell cycle arrest in *Mdm2*$^{+/+}$ and *Mdm2*$^{A/A}$ MEFs treated with genotoxic drugs. Cells were treated with 25 µM etoposide, 172 nM doxorubicin, or 300 nM camptothecin for 15 hours and were pulse-labeled with bromodeoxyuridine (BrdU) for 3 hours (n=3 per genotype). Standard deviation indicated by error bars.

Because the *Mdm2*$^{A/A}$ mice exhibited enhanced tumorigenesis in the absence of exogenous stress, we determined that Mdm2 Ser394 phosphorylation may have roles in cellular stressors independent of DNA damage. One known p53-dependent cellular stress that limits proliferation and growth in MEFs is low plating density. We plated *Mdm2*$^{+/+}$, *p53*$^{-/-}$, and *Mdm2*$^{A/A}$ MEFs at 10^4 cells/10cm plate and cell colony formation was observed after 2 weeks in culture (Figure 4.2). We observed significantly more *Mdm2*$^{A/A}$ colonies that were greater than 2mm in diameter compared with *Mdm2*$^{+/+}$. However, the number of *Mdm2*$^{A/A}$ colonies was greatly reduced compared to *p53*$^{-/-}$, suggesting only a modest effect of Mdm2 Ser394 phosphorylation on low plating stress responses.

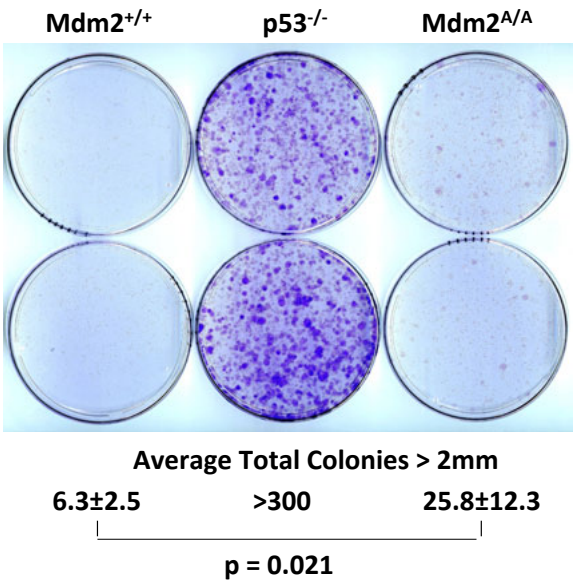

Figure 4.2: Low plating density assay. Representative MEF lines from low plating density assays. *Mdm2*$^{+/+}$, *p53*$^{-/-}$ and *Mdm2*$^{A/A}$ MEFs were plated at 10^4 cells/10 cm plate and grew for 14 days. Cells were then stained with crystal violet and colonies larger than 2 mm in diameter were counted. Average number of colonies and standard deviations are presented (n=3 per genotype).

Another well-studied assay that is dependent on functional p53 activity is the 3T3 immortalization assay. Serial passaging in culture leads to the accumulation of genetic mutations, which triggers p53-dependent cell growth suppression and eventual senescence to prevent immortalization and the potential for transformation in cells (Harvey *et al.*, 1993; Jones *et al.*, 1996). Therefore, disrupted p53 function results in increased immortalization rates following serial passaging. As *p53*$^{-/-}$ cells have no checkpoint, they readily immortalized (Figure 4.3). Expectedly, *Mdm2*$^{+/+}$ and *Mdm2*$^{D/D}$ cells failed to immortalize. Surprisingly, *Mdm2*$^{A/A}$ cells were indistinguishable from the *Mdm2*$^{+/+}$ and *Mdm2*$^{D/D}$ cells, which indicates that Mdm2 Ser394 is dispensable for p53-dependent suppression of immortalization in this assay. The 3T3 experiment was

subsequently repeated and the results in each of the curves were qualitatively comparable, as only the *p53*$^{-/-}$ cell lines spontaneously immortalized.

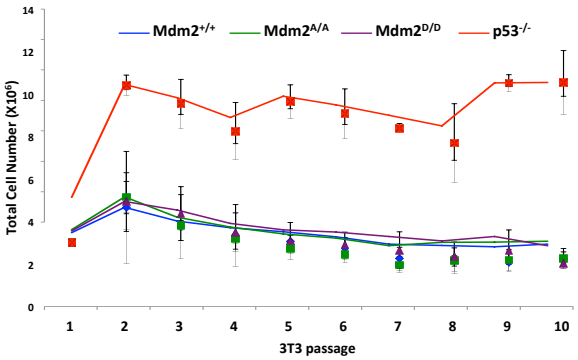

Figure 4.3: 3T3 immortalization assay (n=3 per genotype). Standard deviation indicated by error bars.

Because *Mdm2*$^{A/A}$ mice have increased spontaneous tumorigenesis and a greatly diminished p53 response to IR, we wanted to determine if there is a role for Mdm2 Ser394 phosphorylation in IR-induced tumorigenesis. To test this we treated cohorts of *Mdm2*$^{+/+}$, *Mdm2*$^{A/A}$, and *Mdm2*$^{D/D}$ mice with a low dose of IR (6Gy) and observed their survival (Figure 4.4). All treated mice showed characteristic hair greying, confirming that they had been irradiated. However, none of the irradiated mice died before 200 days post-IR, which differs from the rapid lethality seen in mice treated with 8Gy (Figure 3.5). The survival of the irradiated mice was negatively affected in each genotype when compared to the respective spontaneous survival curves (see Figure 3.40); however, no obvious tumors developed in any of the irradiated mice regardless of genotype. Interestingly, while the *Mdm2*$^{+/+}$ and *Mdm2*$^{A/A}$ survival rates nearly overlap, the *Mdm2*$^{D/D}$ mice were more protected from the low dose IR-induced death.

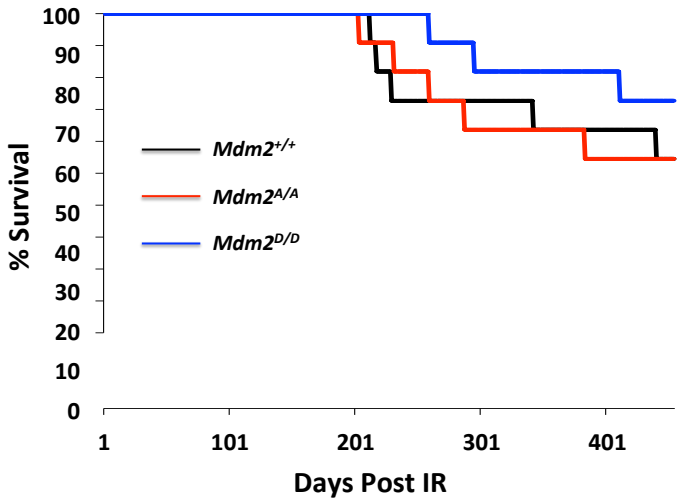

Figure 4.4: Survival in mouse cohorts irradiated with 6Gy. Cohorts of *Mdm2*$^{+/+}$ (n=11), *Mdm2*$^{A/A}$ (n=11), and *Mdm2*$^{D/D}$ (n=9) mice were irradiated with 6Gy and survival was observed over 450 days.

The DNA damage-p53 signaling axis has been shown to be an important suppressor of oncogene-induced B-cell lymphomagenesis that develops in the *Eμ-Myc* transgenic mouse model (Eischen *et al.*, 1999; Schmitt *et al.*, 1999; Shreeram *et al.*, 2006b; Maclean *et al.*, 2007; Garrison *et al.*, 2008; Sluss *et al.*, 2010). Since we have shown that Mdm2 S394 phosphorylation is critical for the p53 response to DNA damage, we expect this posttranslational modification to be a critical signaling event in activating p53 in the *Eμ-Myc* mouse model. To test this we crossed inbred C57Bl/6 (generation N8) *Mdm2*$^{A/A}$ mice to mice expressing the *Eμ-Myc* transgene and have generated 5 *Mdm2*$^{A/+}$, *Eμ-Myc* mice and 1 *Mdm2*$^{A/A}$, *Eμ-Myc* mouse to date. All of these mice developed enlarged spleens and thymii and did not survive past 115 days. While these cohorts are small, the survival rates are similar to other published *Eμ-Myc* tumor-free curves in mice with diminished ATM-p53 signaling, and further confirm the necessity for the ATM-

Mdm2-p53 signaling axis in tumor suppression in response to the activated *c-myc* oncogene (Eischen *et al.*, 1999; Schmitt *et al.*, 1999; Shreeram *et al.*, 2006b; Maclean *et al.*, 2007; Garrison *et al.*, 2008; Sluss *et al.*, 2010).

Discussion

Our previous work demonstrated a critical role for Mdm2 Ser394 in the activation of the DNA damage response to IR and in suppressing spontaneous tumorigenesis. The studies presented in this chapter were performed to explore the role of this residue in the p53 response to alternate cellular stressors, including different DNA damaging agents. Unexpectedly, Mdm2 S394 phosphorylation was dispensable for the cell cycle arrest after treatment with the cytotoxic drugs etoposide, doxorubicin, and camptothecin. This may be due to additional, ATM-independent mechanisms that are activated by these drugs to inhibit Mdm2 function and allow p53 stability and activity. One variable that could account for these differences is the time of exposure to these DNA damaging agents. The IR doses used in our previous studies require minutes in the irradiator, where the ATM pathway may be the sole or predominant signaling mechanism. The cytotoxic agents are present in the cell culture media for the total length of the assay, which could potentially activate auxiliary pathways that do not rely on the posttranslational status of Mdm2 Ser394.

We also sought to characterize the immortalization potential of *Mdm2*$^{A/A}$ MEFs via the 3T3 assay. We have shown that most *Mdm2*$^{A/A}$ mice develop lymphomas relatively late in life (Figure 3.40). Because these tumors arose even in the absence of

exogenous IR, we hypothesized that the differences may be due to a failure in p53 signaling in response to accumulated mutations. The serial passaging of MEFs in the 3T3 assay could be argued to parallel the accumulated stress that occurs with age at the organismal level. However, none of the *Mdm2*$^{A/A}$ MEF lines showed any spontaneous immortalization, suggesting that the response to accumulated mutations in the mice is similarly unaltered. The tumors that develop in the *Mdm2*$^{A/A}$ model most likely arise from a variety of complicated processes that still need to be elucidated, such as the sensitivity to DNA double strand breaks. This could be further tested using known, infrequent DNA restriction digest enzymes such as SecI or SalI to induced double strand breaks in the DNA. This would isolate the response to the DNA damage rather than any other independent effects exhibited by ionizing radiation or genotoxic drugs.

The results of the IR-induced tumorigenesis experiments were surprising. Since the *Mdm2*$^{A/A}$ mice have severely impaired IR responses and develop lymphomas even in the absence of exogenous stress, we anticipated a greatly increased tumorigenesis rate in the *Mdm2*$^{A/A}$ mice compared to wild-type. However, no tumors arose in the irradiated *Mdm2*$^{A/A}$ mice and the survival rates between *Mdm2*$^{+/+}$ and *Mdm2*$^{A/A}$ mice were indistinguishable. Conversely, we expected the *Mdm2*$^{D/D}$ mice to be protected from IR-induced tumorigenesis since this model displayed slightly overactive p53 activity following irradiation. This potential tumor protection in the *Mdm2*$^{D/D}$ model was unable to be tested, as no tumors were seen in any genotype; however, the *Mdm2*$^{D/D}$ mice did show an overall increase in survival. While no obvious explanation of the deaths of the treated mice arose, bone marrow failure and an overall decrease in hematopoiesis are

likely candidates. A possible explanation of the tumorigenesis results might be that the phenotypic effects of Mdm2 Ser394 in the response to IR are separate from its effects on p53 tumor suppression. Very recent work utilizing p53 mutant mouse models has revealed that the tumor suppressive function of p53 may rely on the ability of p53 to regulate glucose metabolism rather than cell cycle arrest and apoptosis (Li *et al.*, 2012). As altered metabolism plays an important role in facilitating tumor growth (Cairns *et al.*, 2011), the capability of Mdm2 Ser394 phosphorylation to regulate spontaneous tumorigenesis may be distinct from its role in regulating the DNA damage response. Further work on the ability of Mdm2 Ser394 to regulate p53-dependent expression of glycolytic genes such as TP53-induced glycolysis and apoptosis regulator (TIGAR) may unveil the Mdm2 Ser394-dependent mechanism(s) that regulate tumor suppression (Bensaad *et al.*, 2006).

Materials and Methods

Mice

Mice used in the IR-treated cohorts were on a mixed 129Sv×C57Bl/6 background, and mice used in the *Eμ-Myc* cohorts were on an inbred C57Bl/6 (generation N8) background. All mice and cells were irradiated with a cesium-137 source (Gammacell 40). Animals in the spontaneous tumor cohorts or IR-treated cohorts were killed if tumor burden was apparent or when moribund. Animals were maintained and used in accordance with federal guidelines and those established by the Institutional Animal Care and Use Committee at the University of Massachusetts Medical School.

Cell Cycle Arrest

MEFs were either untreated or treated with 25 μM etoposide (Sigma E1385), 172 nM doxorubicin (Sigma D1515), or 300 nM camptothecin (Sigma C9911) and then pulsed labeled with 60 μM bromodeoxyuridine (BrdU) for 3 hours. Cells were then trypsinized, fixed in 70% ethanol overnight, incubated with anti-BrdU antibody (Becton Dickinson #347583) and PI, and analyzed by flow cytometry. Data are presented as the percentage of cells in S phase in the treated samples compared to the untreated samples. Flow cytometry was performed by the UMASS Medical School Flow Cytometry Core Lab.

Low Plating Assay

MEFs were plated at 10^4 cells/10cm plate and allowed to grow in culture for 14 days. Cells were then briefly fixed in methanol and stained with 0.1% crystal violet for 30 minutes. The plates were then washed in PBS and colonies larger than 2mm in diameter were counted for each genotype.

3T3 Immortalization Assay

Triplicate cultures of three independent cell lines of each genotype were plated at a density of 5.5 X 10^4 MEFs/cm^2 on 10cm plates. These independent cell lines were harvested every third day, pooled, counted, and replated under the same conditions. As cell numbers decreased, the plates used were adjusted to maintain the original cell density.

CHAPTER V:

GENERAL DISCUSSION

Foreword

The p53-Mdm2 signaling pathway has been extensively studied over the years, and genetically engineered mouse models have played important roles in determining the validity and significance of results produced *in vitro*. The novel work presented throughout this dissertation has revealed new roles for Mdm2-p53 signaling in maintaining tissue homeostasis and stem cell function, and has demonstrated the importance of a single Mdm2 amino acid residue in controlling the cellular response to DNA damage and limiting IR-induced survival and spontaneous tumorigenesis. While the studies presented in the preceding Chapters have contributed to the Mdm2-p53 field, additional experiments are still needed in order to fully uncover the physiological roles of the Mdm2-p53 signaling axis.

What We Have Learned from *K5-Cre* X *Mdm2*$^{c/c}$ Mice

Chapter 2 describes the genetic ablation of *Mdm2* in the epidermis of our *Mdm2*$^{\Delta/\Delta}$ mouse model. The data obtained from these mice reinforce the results of previous tissue-specific *Mdm2* knockout mice while contributing novel insights to the Mdm2-p53 signaling axis in tissue homeostasis. Deletion of *Mdm2* in the epidermis resulted in dramatic phenotypes in aged *Mdm2*$^{\Delta/\Delta}$ mice. While the timing and specificity of the p53 responses differ between the conditional *Mdm2* knockout studies (see Table 1.1), our results corroborate the important role of Mdm2-dependent regulation of p53, but not p63, to ensure proper cellular function regardless of the tissue type that was analyzed.

It was previously known that genetic deletion of *Mdm2* results in the activation of tissue-specific p53 responses. For example, *Mdm2* ablation in bone led to osteoblast cell cycle arrest, whereas, deletion of *Mdm2* in the heart resulted in cardiomyocyte apoptosis (Lengner *et al.*, 2006; Grier *et al.*, 2006). Notably, the cellular senescence observed in aged $Mdm2^{\Delta/\Delta}$ epidermal stem cells had not been previously observed as the primary response to *Mdm2* deletion in any other tissue. The explanations for why certain p53 target genes and functions are activated in *Mdm2* ablated tissues remain unresolved. It is likely that the numerous epigenetic changes that have been shown in epidermal stem cells may affect the specific target genes or signaling pathways that are activated in response to stress (Mulder *et al.*, 2012). In tumors harboring wild-type *p53*, these tissue-specific responses may prove to be critical factors when considering therapies that activate p53 in various affected tissues.

The epidermis proved to be a unique tissue to study the roles of Mdm2 and p53 in stem cell function and premature aging in mice. A key feature of our $Mdm2^{\Delta/\Delta}$ mouse model is that the lifespan of these mice is relatively unchanged compared to controls. To date, *Mdm2* deletion in the small intestine has been the only other such model to display long-term survival (see Table 1.1). However, the survival in the intestinal model is most likely due to the negative selection of cells that ablated *Mdm2* via apoptosis, thus eliminating the cells of interest (Valentin-Vega *et al.*, 2008). The rare premature deaths that were seen in the $Mdm2^{\Delta/\Delta}$ cohort were due to persistently open wounds likely

resulting from conventional grooming, which allowed the majority of the mice to be studied and observed throughout their lifespan.

Another advantage of the epidermis is the ease with which one can noninvasively assess stem cell function. The results of wound healing and hair regrowth experiments accurately reflect the function of epidermal stem cells while causing minimal pain to the animals (Figures 2.17 and 2.18). The survival of the $Mdm2^{\Delta/\Delta}$ mice allowed epidermal stem cell function in the absence of *Mdm2* to be properly assessed and enabled the proposed role of Mdm2 regulation of p53 in preventing premature aging phenotypes to be substantiated. The characteristics of this tissue may allow future genetic manipulations in the epidermis and potential drug treatments in the skin to be effectively studied while avoiding the lethality and severe atrophy seen in other tissues.

Further studies using the $Mdm2^{\Delta/\Delta}$ mouse model can be done to address some unanswered questions. While p53 protein levels and senescence-specific p53 target genes were upregulated in the skin of older $Mdm2^{\Delta/\Delta}$ mice, it is still unknown if the aging phenotypes are truly p53-dependent. Unfortunately, crossing the $Mdm2^{\Delta/\Delta}$ model onto a $p53^{-/-}$ background would result in death before the premature aging phenotypes would arise due to tumorigenesis, and crossing the $Mdm2^{\Delta/\Delta}$ model onto a $p53^{+/-}$ background would not determine if the effects were solely p53-dependent. Alternatively, the $Mdm2^{\Delta/\Delta}$ model could be crossed to a conditional p53 knockout mouse model so that p53

could be specifically ablated in older mice. However, the timing of p53 deletion to ensure stem cell function and avoid potential spontaneous tumor formation would be difficult to determine.

We proposed that the phenotypes arising in the older *Mdm2*$^{\Delta/\Delta}$ mice were due to the inability of stem cells to self-renew and replenish progenitor cells in hair follicles and the interfollicular epidermis. The delayed timing of the phenotypes that we observed in *Mdm2*$^{\Delta/\Delta}$ mice fits this "premature stem cell exhaustion" hypothesis because normal epidermal stem cell turnover is between 12-14 months. If this was the case, then forcing the epidermal stem cells to renew earlier than normal should result in even earlier premature aging phenotypes compared to untreated *Mdm2*$^{\Delta/\Delta}$ mice. Continual hair shaving of young mice would drive the hair cycle and could determine whether the ability of epidermal stem cells to self-renew is truly affected in *Mdm2*$^{\Delta/\Delta}$ mice.

Mdm2 regulation has been suggested to regulate overactive p53-induced organismal aging, however, less is known of the role of MdmX in this process. As the tissue specific knockout of *MdmX* generally results in a less severe phenotype compared to the *Mdm2* knockout in each respective tissue, it would be interesting to observe whether the same phenotypes occur in mice with epidermal *MdmX* deletion. Similarly, concurrent ablation of *Mdm2* and *MdmX* in the epidermis could determine whether one regulator was more important than the other in limiting p53 activity or whether they act synergistically to regulate p53 in the skin. Since most tissue specific deletions of *Mdm2*

result in lethality, codeletion of *Mdm2* and *MdmX* has only been tested in cells of the central nervous system (Xiong *et al.*, 2006). The lack of lethality in the $Mdm2^{\Delta/\Delta}$ model combined with the unique functional characteristics of the epidermis may provide a viable model to study Mdm2-MdmX-p53 dynamics in tissue homeostasis.

Finally, it will be important to test the various Mdm2 and MdmX conditional deletion alleles in both previously tested and novel tissue types. Because there are significant differences in the p53-dependent responses between the two described Mdm2 conditional models (deletion of exons 5-6 versus exons 11-12 described in Table 1.1), the direct comparison of the phenotypes of these models in the same cell type are needed. Each of these models can also be used in parallel to test the dependence of Mdm2 in new cell types and functions such as regeneration of the liver. Another approach would be to delete these regulators of p53 at different times during embryonic development and throughout the lifespan of the mice using different cre drivers. These preliminary studies are just a few that can be asked using these conditional deletion mouse models and should lead to a greater overall understanding of the physiological regulation of p53 over time.

What We Have Learned from Mdm2 S394 Knock-In Mice

Chapters 3 and 4 describe the physiological role of Mdm2 Ser394 in a variety of p53-depedent responses. We have shown that this residue is specifically critical in upregulating p53 stability and activity after DNA damage via γ-irradiation in multiple tissues of the $Mdm2^{A/A}$ and $Mdm2^{D/D}$ models. As the p53 response to IR was also shown

to be dependent on the activity of the ATM kinase (Figure 3.11), our data support ATM-dependent Mdm2 Ser394 phosphorylation as a critical upstream regulatory modification that allows p53 to be stabilized so that downstream pathways such as apoptosis and cell cycle arrest can be activated.

While the response to IR was profoundly affected in our *Mdm2*$^{A/A}$ and *Mdm2*$^{D/D}$ cells and tissues, the posttranslational status of Mdm2 Ser394 was unnecessary for the response to other DNA damaging agents. The cytotoxic drugs etoposide, doxorubicin, and camptothecin inhibit topoisomerase enzymes resulting in increased DNA torsional strain and breaks (Wang, 1996). However, the many differences that exist between these drugs and IR treatment may account for the functional differences that we observed in MEFs (Figures 3.24 and 4.1). Firstly, the irradiation of cells lasts minutes, whereas the cytotoxic drugs were present in the media throughout the 18 hours of the assay. This longer incubation time could result in more severe DNA damage and would not allow the cells to recover. Likewise, the cytotoxic drugs are likely activating multiple signaling pathways that are able to activate p53 in a manner that is independent of ATM and, thus, independent on Mdm2 Ser394. Further characterization of the response to varying times of exposure and doses of these drugs may uncover whether Mdm2 Ser394 phosphorylation is truly dispensable for cell cycle arrest in MEFs. The apoptotic response to these cytotoxic agents could also be tested in primary *Mdm2*$^{+/+}$, *Mdm2*$^{A/A}$, and *Mdm2*$^{D/D}$ thymocytes, but these cells are very sensitive to DNA damage and ATM-independent effects may mask the role of Mdm2 Ser394. As cytotoxic drugs and IR are

used in cancer therapies, it will be useful to know the exact pathways that are activated by each in order to predict the response of individual patients.

Loss of Mdm2 Ser394 phosphorylation greatly reduced p53-mediated apoptosis in lymphocytes and growth arrest in MEFs but it did not completely abrogate these responses (as seen in $p53^{-/-}$ mice). As anticipated by the literature, other modifications to Mdm2, MdmX, and p53 must also assist in regulating p53 functions after DNA damage (Chao *et al.*, 2003; Sluss *et al.*, 2004; Chao *et al.*, 2006; Wang *et al.*, 2009). In agreement with this hypothesis, it is interesting to note the lack of p53 stabilization or p53 target gene activation in $Mdm2^{D/D}$ mice and cells in the absence of IR treatment (Figures 3.29-3.31). Although the absence of a p53 response in undamaged $Mdm2^{D/D}$ cells may reflect the inability of the substituted aspartate residue to perfectly mimic a phosphorylated serine residue (due to differences in the size and overall negative charge of these residues), equivalent levels of p53-mediated apoptosis and growth arrest are seen in $Mdm2^{+/+}$ and $Mdm2^{D/D}$ cells after DNA damage. Therefore, other DNA-damage induced signals in addition to Mdm2-S394 phosphorylation are required to fully activate the DNA damage response. This interpretation also accounts for the viability of the $Mdm2^{D/D}$ mice, along with the similar growth characteristics and tumorigenic potential of undamaged $Mdm2^{+/+}$, $Mdm2^{A/A}$, and $Mdm2^{D/D}$ MEFs. Due to the relatively modest effect seen in the $Mdm2^{D/D}$ model, the value of future attempts to mimic phosphorylated protein residues must be carefully considered. Studies of serine-to-alanine knock-in mutations in mice have revealed clear roles for these phosphorylation sites *in vivo*, and the roles of successive sites should be investigated accordingly.

While the *Mdm2*$^{A/A}$ and *Mdm2*$^{D/D}$ models have confirmed a significant role for Mdm2 Ser394 in the p53 response to IR, further questions about the role of this residue in p53-dependent responses still remain. Crossing these models onto a p53-null background would determine whether these effects are truly p53-dependent and would reveal whether the modification of Ser394 has an effect on p53-independent cellular processes. Likewise, these models could be bred to both *Atm*$^{-/-}$ and *Wip1*$^{-/-}$ mouse models. Serine phosphorylation is a dynamic process, and the absence of a specific kinase or phosphatase shifts the balance to hypophosphorylated and hyperphosphorylated at each target site, respectively. A recent study showed that codeletion of Wip1 and ATM partially rescued the phenotypes seen in *Atm*$^{-/-}$ mice, presumably due in part to the restoration of the balance of phosphorylated target sites (Darlington *et al.*, 2012). *Mdm2*$^{A/A}$, *Wip1*$^{-/-}$ and *Mdm2*$^{D/D}$, *Atm*$^{-/-}$ mice would uncover whether the absence or constitutive presence of Mdm2 Ser394 phosphorylation could rescue some of the deleterious phenotypes in *Wip1*$^{-/-}$ and *Atm*$^{-/-}$ mice, and would reveal the relative importance of the Mdm2 Ser394 site in ATM-Wip1 signaling.

Further analysis is also needed to determine ATM-Mdm2-p53 signaling in IR-induced tumorigenesis. The experiment presented in Figure 4.4 will need to be repeated with a range of IR doses. As previous studies have shown that 4Gy IR can induce tumors in p53 deficient mice, it will be important to include irradiated *p53*$^{-/-}$ and *p53*$^{+/-}$ cohorts as a positive control for tumor development (Kemp *et al.*, 1994). It will be critical to control the irradiation conditions in all of the genotypes tested to eliminate the variability

that is inherent in the irradiation process. Additionally, it has been shown that genetic background is a key determinant in the responses of mice to whole-body IR, and the newly generated inbred C57Bl/6 strains of the *Mdm2*$^{A/A}$ and *Mdm2*$^{D/D}$ knock-in mutants should be used to test these differences (Roderick *et al.*, 1963; Lindsay *et al.*, 2007). It would be interesting to study the role of Mdm2 Ser394 in the organismal response to sub-lethal IR doses and determine whether the increased survival observed in the *Mdm2*$^{D/D}$ mice is reproducible at multiple IR doses (Figure 4.4).

The exact mechanism of action that accounts for how Mdm2 Ser394 phosphorylation affects Mdm2 function also needs to be elucidated. We used careful biochemistry experiments to determine whether this phosphorylation site affected Mdm2-p53 protein interaction and Mdm2 E3 ligase activity after IR treatment in primary cells. However, the lack of results even in the positive controls in these assays indicated that the endogenous protein levels were too low and/or the reagents were not robust enough to generate a sufficient signal. These limitations may preclude these assays from being performed in our *in vivo* setting, and co-overexpression of Mdm2 Ser394 mutated constructs and wild-type p53 in cell lines may be needed to further determine this mechanism.

Additional experiments should be performed to ascertain the role of Mdm2 Ser394 phosphorylation in cellular processes that are independent of exogenous IR treatments. These include, but are certainly not limited to, the p53-dependent responses to ribosomal stress and oncogene activation. Recent evidence has shown that the Mdm2

Zn finger is needed to activate the p53 response to ribosomal stressors such as actinomycin D and mycophenolic acid, but not to DNA damaging agents such as IR and doxorubicin (Macias *et al.*, 2010). As Mdm2 Ser394 is important in the DNA damage response, it would be important to determine whether there were overlapping mechanisms of p53 activation between ribosomal and DNA damage-induced stress responses. If these stressors activate p53 in non-redundant ways, it could allow multiple strategies for anti-Mdm2 therapies in order to activate wild-type p53 in certain tumor cell populations.

Finally, activated oncogenes are a known inducer of p53 activity and tumor suppressive function, and the essential role for p53 has been demonstrated in the *Eμ-Myc* transgenic mouse model (Eischen *et al.*, 1999; Schmitt *et al.*, 1999; Maclean *et al.*, 2007; Garrison *et al.*, 2008; Sluss *et al.*, 2010). Preliminary analysis of $Mdm2^{A/+}$, *Eμ-Myc* and $Mdm2^{A/A}$, *Eμ-Myc* mice suggest that the ability of Mdm2 Ser394 to be phosphorylated will be a critical determinant of lymphomagenesis development. Previous work has also shown that absence of Wip1 in the *Eμ-Myc* model prolongs survival, presumably because ATM target sites are hyperphosphorylated due to the lack of this specific phosphatase (Shreeram *et al.*, 2006b). It will be interesting to generate $Mdm2^{D/+}$, *Eμ-Myc* and $Mdm2^{D/D}$, *Eμ-Myc* mouse cohorts to investigate the potential protective role of constitutive phosphorylation of the Mdm2 Ser394 residue against oncogene activation.

The Future of the Mdm2-p53 Field

Much has been learned regarding the *in vivo* role of MDM-p53 signaling in development, in tissue homeostasis, and in tumorigenesis. Work in mice has clearly demonstrated the importance of Mdm2 and MdmX in regulating p53 activity in normal cells and how perturbation of this pathway can readily lead to cancer. Addressing stress-induced modifications of Mdm2 and MdmX on MDM-p53 signaling in mice is a relatively new area of scientific exploration in the MDM field. However, based upon the rather large phenotypic impact in mice of the few MDM modifications modeled to date, it would appear that the MDM-p53 signaling axis truly serves as a critical node for the conversion of stress signals into changes in p53 function, and further *in vivo* explorations of the effects of post-translational modifications to Mdm2 and MdmX are warranted. A complete understanding of the upstream modifications that induce p53 activity would allow the response to specific therapies in tumors harboring wild-type p53 to be anticipated.

Conclusions

In conclusion, the mouse models presented in this dissertation have described novel roles of Mdm2 in a number of physiological contexts. The $Mdm2^{\Delta/\Delta}$ mouse model linked premature aging phenotypes to disrupted Mdm2-p53 signaling, and *Mdm2* deletion in the epidermis led to an increase in senescence and the loss of adult tissue stem cell function. The $Mdm2^{A/A}$ and $Mdm2^{D/D}$ models demonstrated a key role for this posttranslational modification in the activation and duration of the p53 DNA damage response, and these mice will be used to further determine the role of Mdm2 Ser394 in

many p53-dependent and -independent cellular functions. As our knowledge of the p53 pathway and other diverse cell signaling pathways widens and deepens, the development and implementation of the proper combination of targeted therapies will be developed and utilized to treat different diseases not just limited to cancer.

REFERENCES

Adams, J. M., Harris, A. W., Pinkert, C. A., Corcoran, L. M., Alexander, W. S., Cory, S., Palmiter, R. D., and Brinster, R. L. (1985). The c-myc oncogene driven by immunoglobulin enhancers induces lymphoid malignancy in transgenic mice. Nature 318, 533-538.

Armstrong, J. F., Kaufman, M. H., Harrison, D. J., and Clarke, A. R. (1995). High-frequency developmental abnormalities in p53-deficient mice. Curr Biol 5, 931-936.

Badciong, J. C., and Haas, A. L. (2002). MdmX is a RING finger ubiquitin ligase capable of synergistically enhancing Mdm2 ubiquitination. J Biol Chem 277, 49668-49675.

Baker, S. J., Markowitz, S., Fearon, E. R., Willson, J. K., and Vogelstein, B. (1990). Suppression of human colorectal carcinoma cell growth by wild-type p53. Science 249, 912-915.

Balasubramanian, S., Ahmad, N., Jeedigunta, S., and Mukhtar, H. (1998). Alterations in cell cycle regulation in mouse skin tumors. Biochem Biophys Res Commun 243, 744-748.

Barlow, C., Hirotsune, S., Paylor, R., Liyanage, M., Eckhaus, M., Collins, F., Shiloh, Y., Crawley, J. N., Ried, T., Tagle, D., and Wynshaw-Boris, A. (1996). Atm-deficient mice: a paradigm of ataxia telangiectasia. Cell 86, 159-171.

Bartel, F., Schulz, J., Bohnke, A., Blumke, K., Kappler, M., Bache, M., Schmidt, H., Wurl, P., Taubert, H., and Hauptmann, S. (2005). Significance of HDMX-S (or MDM4) mRNA splice variant overexpression and HDMX gene amplification on primary soft tissue sarcoma prognosis. Int J Cancer 117, 469-475.

Bates, S., Phillips, A. C., Clark, P. A., Stott, F., Peters, G., Ludwig, R. L., and Vousden, K. H. (1998). p14ARF links the tumour suppressors RB and p53. Nature 395, 124-125.

Bensaad, K., Tsuruta, A., Selak, M. A., Vidal, M. N., Nakano, K., Bartrons, R., Gottlieb, E., and Vousden, K. H. (2006). TIGAR, a p53-inducible regulator of glycolysis and apoptosis. Cell *126*, 107-120.

Bischoff, J. R., Friedman, P. N., Marshak, D. R., Prives, C., and Beach, D. (1990). Human p53 is phosphorylated by p60-cdc2 and cyclin B-cdc2. Proc Natl Acad Sci U S A 87, 4766-4770.

Boesten, L. S., Zadelaar, S. M., De Clercq, S., Francoz, S., van Nieuwkoop, A., Biessen, E. A., Hofmann, F., Feil, S., Feil, R., Jochemsen, A. G., et al. (2006). Mdm2, but not

Mdm4, protects terminally differentiated smooth muscle cells from p53-mediated caspase-3-independent cell death. Cell Death Differ 13, 2089-2098.

Bossy-Wetzel, E., and Green, D. R. (1999). Caspases induce cytochrome c release from mitochondria by activating cytosolic factors. J Biol Chem 274, 17484-17490.

Brown, D. R., Thomas, C. A., and Deb, S. P. (1998). The human oncoprotein MDM2 arrests the cell cycle: elimination of its cell-cycle-inhibitory function induces tumorigenesis. EMBO J 17, 2513-2525.

Brugarolas, J., Chandrasekaran, C., Gordon, J. I., Beach, D., Jacks, T., and Hannon, G. J. (1995). Radiation-induced cell cycle arrest compromised by p21 deficiency. Nature 377, 552-557.

Cairns, R. A., Harris, I. S., and Mak, T. W. (2011). Regulation of cancer cell metabolism. Nat Rev Cancer *11*, 85-95.

Campisi, J. (2005). Senescent cells, tumor suppression, and organismal aging: good citizens, bad neighbors. Cell 120, 513-522.

Chang, B. D., Broude, E. V., Fang, J., Kalinichenko, T. V., Abdryashitov, R., Poole, J. C., and Roninson, I. B. (2000). p21Waf1/Cip1/Sdi1-induced growth arrest is associated

with depletion of mitosis-control proteins and leads to abnormal mitosis and endoreduplication in recovering cells. Oncogene 19, 2165-2170.

Chang, C., Simmons, D. T., Martin, M. A., and Mora, P. T. (1979). Identification and partial characterization of new antigens from simian virus 40-transformed mouse cells. J Virol 31, 463-471.

Chao, C., Hergenhahn, M., Kaeser, M. D., Wu, Z., Saito, S., Iggo, R., Hollstein, M., Appella, E., and Xu, Y. (2003). Cell type- and promoter-specific roles of Ser18 phosphorylation in regulating p53 responses. J Biol Chem 278, 41028-41033.

Chao, C., Herr, D., Chun, J., and Xu, Y. (2006). Ser18 and 23 phosphorylation is required for p53-dependent apoptosis and tumor suppression. EMBO J 25, 2615-2622.

Chao, C., Saito, S., Anderson, C. W., Appella, E., and Xu, Y. (2000). Phosphorylation of murine p53 at ser-18 regulates the p53 responses to DNA damage. Proc Natl Acad Sci U S A 97, 11936-11941.

Chavez-Reyes, A., Parant, J. M., Amelse, L. L., de Oca Luna, R. M., Korsmeyer, S. J., and Lozano, G. (2003). Switching mechanisms of cell death in mdm2- and mdm4-null mice by deletion of p53 downstream targets. Cancer Res 63, 8664-8669.

Chen, J., Lin, J., and Levine, A. J. (1995). Regulation of transcription functions of the p53 tumor suppressor by the mdm-2 oncogene. Mol Med 1, 142-152.

Cheng, Q., Chen, L., Li, Z., Lane, W. S., and Chen, J. (2009). ATM activates p53 by regulating MDM2 oligomerization and E3 processivity. EMBO J 28, 3857-3867.

Cheng, Q., Cross, B., Li, B., Chen, L., Li, Z., and Chen, J. (2011). Regulation of MDM2 E3 Ligase Activity by Phosphorylation after DNA Damage. Mol Cell Biol 31, 4951-4963.

Darlington, Y., Nguyen, T. A., Moon, S. H., Herron, A., Rao, P., Zhu, C., Lu, X., and Donehower, L. A. (2012). Absence of Wip1 partially rescues Atm deficiency phenotypes in mice. Oncogene 31, 1155-1165.

De Clercq, S., Gembarska, A., Denecker, G., Maetens, M., Naessens, M., Haigh, K., Haigh, J. J., and Marine, J. C. (2010). Widespread overexpression of epitope-tagged Mdm4 does not accelerate tumor formation in vivo. Mol Cell Biol 30, 5394-5405.

Diller, L., Kassel, J., Nelson, C. E., Gryka, M. A., Litwak, G., Gebhardt, M., Bressac, B., Ozturk, M., Baker, S. J., Vogelstein, B., and et al. (1990). p53 functions as a cell cycle control protein in osteosarcomas. Mol Cell Biol 10, 5772-5781.

Donehower, L. A. (2009). Using mice to examine p53 functions in cancer, aging, and longevity. Cold Spring Harb Perspect Biol 1, a001081.

Donehower, L. A., Harvey, M., Slagle, B. L., McArthur, M. J., Montgomery, C. A., Jr., Butel, J. S., and Bradley, A. (1992). Mice deficient for p53 are developmentally normal but susceptible to spontaneous tumours. Nature 356, 215-221.

Donehower, L. A., and Lozano, G. (2009). 20 years studying p53 functions in genetically engineered mice. Nat Rev Cancer 9, 831-841.

Eischen, C. M., Weber, J. D., Roussel, M. F., Sherr, C. J., and Cleveland, J. L. (1999). Disruption of the ARF-Mdm2-p53 tumor suppressor pathway in Myc-induced lymphomagenesis. Genes Dev 13, 2658-2669.

el-Deiry, W. S., Kern, S. E., Pietenpol, J. A., Kinzler, K. W., and Vogelstein, B. (1992). Definition of a consensus binding site for p53. Nat Genet 1, 45-49.

el-Deiry, W. S., Tokino, T., Velculescu, V. E., Levy, D. B., Parsons, R., Trent, J. M., Lin, D., Mercer, W. E., Kinzler, K. W., and Vogelstein, B. (1993). WAF1, a potential mediator of p53 tumor suppression. Cell 75, 817-825.

Eliyahu, D., Michalovitz, D., Eliyahu, S., Pinhasi-Kimhi, O., and Oren, M. (1989). Wild-type p53 can inhibit oncogene-mediated focus formation. Proc Natl Acad Sci U S A 86, 8763-8767.

Eliyahu, D., Raz, A., Gruss, P., Givol, D., and Oren, M. (1984). Participation of p53 cellular tumour antigen in transformation of normal embryonic cells. Nature 312, 646-649.

Elson, A., Wang, Y., Daugherty, C. J., Morton, C. C., Zhou, F., Campos-Torres, J., and Leder, P. (1996). Pleiotropic defects in ataxia-telangiectasia protein-deficient mice. Proc Natl Acad Sci U S A 93, 13084-13089.

Fakharzadeh, S. S., Rosenblum-Vos, L., Murphy, M., Hoffman, E. K., and George, D. L. (1993). Structure and organization of amplified DNA on double minutes containing the mdm2 oncogene. Genomics 15, 283-290.

Fang, L., Igarashi, M., Leung, J., Sugrue, M. M., Lee, S. W., and Aaronson, S. A. (1999). p21Waf1/Cip1/Sdi1 induces permanent growth arrest with markers of replicative senescence in human tumor cells lacking functional p53. Oncogene 18, 2789-2797.

Fang, S., Jensen, J. P., Ludwig, R. L., Vousden, K. H., and Weissman, A. M. (2000). Mdm2 is a RING finger-dependent ubiquitin protein ligase for itself and p53. J Biol Chem 275, 8945-8951.

Finch, R. A., Donoviel, D. B., Potter, D., Shi, M., Fan, A., Freed, D. D., Wang, C. Y., Zambrowicz, B. P., Ramirez-Solis, R., Sands, A. T., and Zhang, N. (2002). mdmx is a negative regulator of p53 activity in vivo. Cancer Res 62, 3221-3225.

Finlay, C. A., Hinds, P. W., and Levine, A. J. (1989). The p53 proto-oncogene can act as a suppressor of transformation. Cell 57, 1083-1093.

Flores, I., and Blasco, M. A. (2009). A p53-dependent response limits epidermal stem cell functionality and organismal size in mice with short telomeres. PLoS One 4, e4934.

Freedman, D. A., and Levine, A. J. (1998). Nuclear export is required for degradation of endogenous p53 by MDM2 and human papillomavirus E6. Mol Cell Biol 18, 7288-7293.

Funk, W. D., Pak, D. T., Karas, R. H., Wright, W. E., and Shay, J. W. (1992). A transcriptionally active DNA-binding site for human p53 protein complexes. Mol Cell Biol 12, 2866-2871.

Gajjar, M., Candeias, M. M., Malbert-Colas, L., Mazars, A., Fujita, J., Olivares-Illana, V., and Fahraeus, R. (2012). The p53 mRNA-Mdm2 Interaction Controls Mdm2 Nuclear Trafficking and Is Required for p53 Activation following DNA Damage. Cancer Cell 21, 25-35.

Garcia-Cao, I., Garcia-Cao, M., Martin-Caballero, J., Criado, L. M., Klatt, P., Flores, J. M., Weill, J. C., Blasco, M. A., and Serrano, M. (2002). "Super p53" mice exhibit enhanced DNA damage response, are tumor resistant and age normally. EMBO J 21, 6225-6235.

Garrison, S. P., Jeffers, J. R., Yang, C., Nilsson, J. A., Hall, M. A., Rehg, J. E., Yue, W., Yu, J., Zhang, L., Onciu, M., et al. (2008). Selection against PUMA gene expression in Myc-driven B-cell lymphomagenesis. Mol Cell Biol 28, 5391-5402.

Gentry, A., and Venkatachalam, S. (2005). Complicating the role of p53 in aging. Aging Cell 4, 157-160.

Geyer, R. K., Yu, Z. K., and Maki, C. G. (2000). The MDM2 RING-finger domain is required to promote p53 nuclear export. Nat Cell Biol 2, 569-573.

Goldberg, Z., Vogt Sionov, R., Berger, M., Zwang, Y., Perets, R., Van Etten, R. A., Oren, M., Taya, Y., and Haupt, Y. (2002). Tyrosine phosphorylation of Mdm2 by c-Abl: implications for p53 regulation. EMBO J *21*, 3715-3727.

Grier, J. D., Xiong, S., Elizondo-Fraire, A. C., Parant, J. M., and Lozano, G. (2006). Tissue-specific differences of p53 inhibition by Mdm2 and Mdm4. Mol Cell Biol 26, 192-198.

Grier, J. D., Yan, W., and Lozano, G. (2002). Conditional allele of mdm2 which encodes a p53 inhibitor. Genesis 32, 145-147.

Gudkov, A. V., and Komarova, E. A. (2003). The role of p53 in determining sensitivity to radiotherapy. Nat Rev Cancer 3, 117-129.

Guo, X., Keyes, W. M., Papazoglu, C., Zuber, J., Li, W., Lowe, S. W., Vogel, H., and Mills, A. A. (2009). TAp63 induces senescence and suppresses tumorigenesis in vivo. Nat Cell Biol 11, 1451-1457.

Gurley, K. E., and Kemp, C. J. (2007). Ataxia-telangiectasia mutated is not required for p53 induction and apoptosis in irradiated epithelial tissues. Mol Cancer Res 5, 1312-1318.

Harvey, D. M., and Levine, A. J. (1991). p53 alteration is a common event in the spontaneous immortalization of primary BALB/c murine embryo fibroblasts. Genes Dev 5, 2375-2385.

Harvey, M., McArthur, M. J., Montgomery, C. A., Jr., Butel, J. S., Bradley, A., and Donehower, L. A. (1993). Spontaneous and carcinogen-induced tumorigenesis in p53-deficient mice. Nat Genet 5, 225-229.

Harvey, M., Sands, A. T., Weiss, R. S., Hegi, M. E., Wiseman, R. W., Pantazis, P., Giovanella, B. C., Tainsky, M. A., Bradley, A., and Donehower, L. A. (1993). In vitro growth characteristics of embryo fibroblasts isolated from p53-deficient mice. Oncogene 8, 2457-2467.

Haupt, Y., Maya, R., Kazaz, A., and Oren, M. (1997). Mdm2 promotes the rapid degradation of p53. Nature 387, 296-299.

Herzog, K. H., Chong, M. J., Kapsetaki, M., Morgan, J. I., and McKinnon, P. J. (1998). Requirement for Atm in ionizing radiation-induced cell death in the developing central nervous system. Science 280, 1089-1091.

Hickson, I., Zhao, Y., Richardson, C. J., Green, S. J., Martin, N. M., Orr, A. I., Reaper, P. M., Jackson, S. P., Curtin, N. J., and Smith, G. C. (2004). Identification and characterization of a novel and specific inhibitor of the ataxia-telangiectasia mutated kinase ATM. Cancer Res 64, 9152-9159.

Hollstein, M., Sidransky, D., Vogelstein, B., and Harris, C. C. (1991). p53 mutations in human cancers. Science 253, 49-53.

Honda, R., Tanaka, H., and Yasuda, H. (1997). Oncoprotein MDM2 is a ubiquitin ligase E3 for tumor suppressor p53. FEBS Lett 420, 25-27.

Honda, R., and Yasuda, H. (1999). Association of p19(ARF) with Mdm2 inhibits ubiquitin ligase activity of Mdm2 for tumor suppressor p53. EMBO J 18, 22-27.

Huang, L., Yan, Z., Liao, X., Li, Y., Yang, J., Wang, Z. G., Zuo, Y., Kawai, H., Shadfan, M., Ganapathy, S., and Yuan, Z. M. (2011). The p53 inhibitors MDM2/MDMX complex is required for control of p53 activity in vivo. Proc Natl Acad Sci U S A 108, 12001-12006.

Itahana, K., Mao, H., Jin, A., Itahana, Y., Clegg, H. V., Lindstrom, M. S., Bhat, K. P., Godfrey, V. L., Evan, G. I., and Zhang, Y. (2007). Targeted inactivation of Mdm2 RING finger E3 ubiquitin ligase activity in the mouse reveals mechanistic insights into p53 regulation. Cancer Cell 12, 355-366.

Ito, A., Lai, C. H., Zhao, X., Saito, S., Hamilton, M. H., Appella, E., and Yao, T. P. (2001). p300/CBP-mediated p53 acetylation is commonly induced by p53-activating agents and inhibited by MDM2. EMBO J 20, 1331-1340.

Jack, M. T., Woo, R. A., Hirao, A., Cheung, A., Mak, T. W., and Lee, P. W. (2002). Chk2 is dispensable for p53-mediated G1 arrest but is required for a latent p53-mediated apoptotic response. Proc Natl Acad Sci U S A 99, 9825-9829.

Jacks, T., Remington, L., Williams, B. O., Schmitt, E. M., Halachmi, S., Bronson, R. T., and Weinberg, R. A. (1994). Tumor spectrum analysis in p53-mutant mice. Curr Biol 4, 1-7.

Jackson, M. W., and Berberich, S. J. (2000). MdmX protects p53 from Mdm2-mediated degradation. Mol Cell Biol 20, 1001-1007.

Jeffers, J. R., Parganas, E., Lee, Y., Yang, C., Wang, J., Brennan, J., MacLean, K. H., Han, J., Chittenden, T., Ihle, J. N., et al. (2003). Puma is an essential mediator of p53-dependent and -independent apoptotic pathways. Cancer Cell 4, 321-328.

Jenkins, G. (2002). Molecular mechanisms of skin ageing. Mech Ageing Dev 123, 801-810.

Jones, S. N., Hancock, A. R., Vogel, H., Donehower, L. A., and Bradley, A. (1998). Overexpression of Mdm2 in mice reveals a p53-independent role for Mdm2 in tumorigenesis. Proc Natl Acad Sci U S A 95, 15608-15612.

Jones, S. N., Roe, A. E., Donehower, L. A., and Bradley, A. (1995). Rescue of embryonic lethality in Mdm2-deficient mice by absence of p53. Nature 378, 206-208.

Jones, S. N., Sands, A. T., Hancock, A. R., Vogel, H., Donehower, L. A., Linke, S. P., Wahl, G. M., and Bradley, A. (1996). The tumorigenic potential and cell growth

characteristics of p53-deficient cells are equivalent in the presence or absence of Mdm2. Proc Natl Acad Sci U S A 93, 14106-14111.

Juven, T., Barak, Y., Zauberman, A., George, D. L., and Oren, M. (1993). Wild type p53 can mediate sequence-specific transactivation of an internal promoter within the mdm2 gene. Oncogene 8, 3411-3416.

Kamijo, T., Weber, J. D., Zambetti, G., Zindy, F., Roussel, M. F., and Sherr, C. J. (1998). Functional and physical interactions of the ARF tumor suppressor with p53 and Mdm2. Proc Natl Acad Sci U S A 95, 8292-8297.

Kemp, C. J., Wheldon, T., and Balmain, A. (1994). p53-deficient mice are extremely susceptible to radiation-induced tumorigenesis. Nat Genet 8, 66-69.

Kern, S. E., Kinzler, K. W., Bruskin, A., Jarosz, D., Friedman, P., Prives, C., and Vogelstein, B. (1991). Identification of p53 as a sequence-specific DNA-binding protein. Science 252, 1708-1711.

Khosravi, R., Maya, R., Gottlieb, T., Oren, M., Shiloh, Y., and Shkedy, D. (1999). Rapid ATM-dependent phosphorylation of MDM2 precedes p53 accumulation in response to DNA damage. Proc Natl Acad Sci U S A 96, 14973-14977.

Komarova, E. A., Kondratov, R. V., Wang, K., Christov, K., Golovkina, T. V., Goldblum, J. R., and Gudkov, A. V. (2004). Dual effect of p53 on radiation sensitivity in vivo: p53 promotes hematopoietic injury, but protects from gastro-intestinal syndrome in mice. Oncogene 23, 3265-3271.

Kress, M., May, E., Cassingena, R., and May, P. (1979). Simian virus 40-transformed cells express new species of proteins precipitable by anti-simian virus 40 tumor serum. J Virol 31, 472-483.

Kubbutat, M. H., Jones, S. N., and Vousden, K. H. (1997). Regulation of p53 stability by Mdm2. Nature 387, 299-303.

Lane, D. P. (1992). Cancer. p53, guardian of the genome. Nature 358, 15-16.

Lane, D. P., and Crawford, L. V. (1979). T antigen is bound to a host protein in SV40-transformed cells. Nature 278, 261-263.

Laurie, N. A., Donovan, S. L., Shih, C. S., Zhang, J., Mills, N., Fuller, C., Teunisse, A., Lam, S., Ramos, Y., Mohan, A., et al. (2006). Inactivation of the p53 pathway in retinoblastoma. Nature 444, 61-66.

Lengner, C. J., Steinman, H. A., Gagnon, J., Smith, T. W., Henderson, J. E., Kream, B. E., Stein, G. S., Lian, J. B., and Jones, S. N. (2006). Osteoblast differentiation and skeletal development are regulated by Mdm2-p53 signaling. J Cell Biol 172, 909-921.

Levine, A. J. (1997). p53, the cellular gatekeeper for growth and division. Cell 88, 323-331.

Levine, A. J., Tomasini, R., McKeon, F. D., Mak, T. W., and Melino, G. (2011). The p53 family: guardians of maternal reproduction. Nat Rev Mol Cell Biol 12, 259-265.

Li, M., Brooks, C. L., Wu-Baer, F., Chen, D., Baer, R., and Gu, W. (2003). Mono- versus polyubiquitination: differential control of p53 fate by Mdm2. Science 302, 1972-1975.

Li, T., Kon, N., Jiang, L., Tan, M., Ludwig, T., Zhao, Y., Baer, R., and Gu, W. (2012). Tumor Suppression in the Absence of p53-Mediated Cell-Cycle Arrest, Apoptosis, and Senescence. Cell 149, 1269-1283.

Linares, L. K., Hengstermann, A., Ciechanover, A., Muller, S., and Scheffner, M. (2003). HdmX stimulates Hdm2-mediated ubiquitination and degradation of p53. Proc Natl Acad Sci U S A 100, 12009-12014.

Lindsay, K. J., Coates, P. J., Lorimore, S. A., and Wright, E. G. (2007). The genetic basis of tissue responses to ionizing radiation. Br J Radiol 80 Spec No 1, S2-6.

Linzer, D. I., and Levine, A. J. (1979). Characterization of a 54K dalton cellular SV40 tumor antigen present in SV40-transformed cells and uninfected embryonal carcinoma cells. Cell 17, 43-52.

Little, N. A., and Jochemsen, A. G. (2001). Hdmx and Mdm2 can repress transcription activation by p53 but not by p63. Oncogene 20, 4576-4580.

Liu, Y., Lyle, S., Yang, Z., and Cotsarelis, G. (2003). Keratin 15 promoter targets putative epithelial stem cells in the hair follicle bulge. J Invest Dermatol 121, 963-968.

Lowe, S. W., Schmitt, E. M., Smith, S. W., Osborne, B. A., and Jacks, T. (1993). p53 is required for radiation-induced apoptosis in mouse thymocytes. Nature 362, 847-849.

Lozano, G. (2009). Mouse models of p53 functions. Cold Spring Harb Perspect Biol 2, a001115.

Lu, X., Ma, O., Nguyen, T. A., Jones, S. N., Oren, M., and Donehower, L. A. (2007). The Wip1 Phosphatase acts as a gatekeeper in the p53-Mdm2 autoregulatory loop. Cancer Cell 12, 342-354.

Lu, X., Nannenga, B., and Donehower, L. A. (2005). PPM1D dephosphorylates Chk1 and p53 and abrogates cell cycle checkpoints. Genes Dev 19, 1162-1174.

Lu, X., Nguyen, T. A., Moon, S. H., Darlington, Y., Sommer, M., and Donehower, L. A. (2008). The type 2C phosphatase Wip1: an oncogenic regulator of tumor suppressor and DNA damage response pathways. Cancer Metastasis Rev 27, 123-135.

Macias, E., Jin, A., Deisenroth, C., Bhat, K., Mao, H., Lindstrom, M. S., and Zhang, Y. (2010). An ARF-independent c-MYC-activated tumor suppression pathway mediated by ribosomal protein-Mdm2 Interaction. Cancer Cell 18, 231-243.

MacPherson, D., Kim, J., Kim, T., Rhee, B. K., Van Oostrom, C. T., DiTullio, R. A., Venere, M., Halazonetis, T. D., Bronson, R., De Vries, A., et al. (2004). Defective apoptosis and B-cell lymphomas in mice with p53 point mutation at Ser 23. EMBO J 23, 3689-3699.

Maetens, M., Doumont, G., Clercq, S. D., Francoz, S., Froment, P., Bellefroid, E., Klingmuller, U., Lozano, G., and Marine, J. C. (2007). Distinct roles of Mdm2 and Mdm4 in red cell production. Blood 109, 2630-2633.

Maier, B., Gluba, W., Bernier, B., Turner, T., Mohammad, K., Guise, T., Sutherland, A., Thorner, M., and Scrable, H. (2004). Modulation of mammalian life span by the short isoform of p53. Genes Dev 18, 306-319.

Martins, C. P., Brown-Swigart, L., and Evan, G. I. (2006). Modeling the therapeutic efficacy of p53 restoration in tumors. Cell 127, 1323-1334.

Maya, R., Balass, M., Kim, S. T., Shkedy, D., Leal, J. F., Shifman, O., Moas, M., Buschmann, T., Ronai, Z., Shiloh, Y., et al. (2001). ATM-dependent phosphorylation of Mdm2 on serine 395: role in p53 activation by DNA damage. Genes Dev 15, 1067-1077.

Melero, J. A., Stitt, D. T., Mangel, W. F., and Carroll, R. B. (1979). Identification of new polypeptide species (48-55K) immunoprecipitable by antiserum to purified large T antigen and present in SV40-infected and -transformed cells. Virology 93, 466-480.

Mendrysa, S. M., McElwee, M. K., Michalowski, J., O'Leary, K. A., Young, K. M., and Perry, M. E. (2003). mdm2 Is critical for inhibition of p53 during lymphopoiesis and the response to ionizing irradiation. Mol Cell Biol 23, 462-472.

Mendrysa, S. M., O'Leary, K. A., McElwee, M. K., Michalowski, J., Eisenman, R. N., Powell, D. A., and Perry, M. E. (2006). Tumor suppression and normal aging in mice with constitutively high p53 activity. Genes Dev 20, 16-21.

Midgley, C. A., Desterro, J. M., Saville, M. K., Howard, S., Sparks, A., Hay, R. T., and Lane, D. P. (2000). An N-terminal p14ARF peptide blocks Mdm2-dependent ubiquitination in vitro and can activate p53 in vivo. Oncogene 19, 2312-2323.

Migliorini, D., Lazzerini Denchi, E., Danovi, D., Jochemsen, A., Capillo, M., Gobbi, A., Helin, K., Pelicci, P. G., and Marine, J. C. (2002). Mdm4 (Mdmx) regulates p53-induced

growth arrest and neuronal cell death during early embryonic mouse development. Mol Cell Biol 22, 5527-5538.

Miyashita, T., and Reed, J. C. (1995). Tumor suppressor p53 is a direct transcriptional activator of the human bax gene. Cell 80, 293-299.

Momand, J., Jung, D., Wilczynski, S., and Niland, J. (1998). The MDM2 gene amplification database. Nucleic Acids Res 26, 3453-3459.

Momand, J., Zambetti, G. P., Olson, D. C., George, D., and Levine, A. J. (1992). The mdm-2 oncogene product forms a complex with the p53 protein and inhibits p53-mediated transactivation. Cell 69, 1237-1245.

Montes de Oca Luna, R., Wagner, D. S., and Lozano, G. (1995). Rescue of early embryonic lethality in mdm2-deficient mice by deletion of p53. Nature 378, 203-206.

Morris, R. J., and Potten, C. S. (1999). Highly persistent label-retaining cells in the hair follicles of mice and their fate following induction of anagen. J Invest Dermatol 112, 470-475.

Mowat, M., Cheng, A., Kimura, N., Bernstein, A., and Benchimol, S. (1985). Rearrangements of the cellular p53 gene in erythroleukaemic cells transformed by Friend virus. Nature 314, 633-636.

Mulder, K. W., Wang, X., Escriu, C., Ito, Y., Schwarz, R. F., Gillis, J., Sirokmany, G., Donati, G., Uribe-Lewis, S., Pavlidis, P., Murrell, A. Markowetz, F. Watt, F. M. (2012). Diverse epigenetic strategies interact to control epidermal differentiation. Nat Cell Biol *14*, 753-763.

Munroe, D. G., Rovinski, B., Bernstein, A., and Benchimol, S. (1988). Loss of a highly conserved domain on p53 as a result of gene deletion during Friend virus-induced erythroleukemia. Oncogene 2, 621-624.

Nakano, K., and Vousden, K. H. (2001). PUMA, a novel proapoptotic gene, is induced by p53. Mol Cell 7, 683-694.

Nowak, J. A., and Fuchs, E. (2009). Isolation and culture of epithelial stem cells. Methods Mol Biol 482, 215-232.

O'Gorman, S., Dagenais, N. A., Qian, M., and Marchuk, Y. (1997). Protamine-Cre recombinase transgenes efficiently recombine target sequences in the male germ line of mice, but not in embryonic stem cells. Proc Natl Acad Sci U S A 94, 14602-14607.

Oda, E., Ohki, R., Murasawa, H., Nemoto, J., Shibue, T., Yamashita, T., Tokino, T., Taniguchi, T., and Tanaka, N. (2000). Noxa, a BH3-only member of the Bcl-2 family and candidate mediator of p53-induced apoptosis. Science 288, 1053-1058.

Oliner, J. D., Kinzler, K. W., Meltzer, P. S., George, D. L., and Vogelstein, B. (1992). Amplification of a gene encoding a p53-associated protein in human sarcomas. Nature 358, 80-83.

Oliner, J. D., Pietenpol, J. A., Thiagalingam, S., Gyuris, J., Kinzler, K. W., and Vogelstein, B. (1993). Oncoprotein MDM2 conceals the activation domain of tumour suppressor p53. Nature 362, 857-860.

Pant, V., Xiong, S., Iwakuma, T., Quintas-Cardama, A., and Lozano, G. (2011). Heterodimerization of Mdm2 and Mdm4 is critical for regulating p53 activity during embryogenesis but dispensable for p53 and Mdm2 stability. Proc Natl Acad Sci U S A 108, 11995-12000.

Parada, L. F., Land, H., Weinberg, R. A., Wolf, D., and Rotter, V. (1984). Cooperation between gene encoding p53 tumour antigen and ras in cellular transformation. Nature 312, 649-651.

Parant, J., Chavez-Reyes, A., Little, N. A., Yan, W., Reinke, V., Jochemsen, A. G., and Lozano, G. (2001). Rescue of embryonic lethality in Mdm4-null mice by loss of Trp53 suggests a nonoverlapping pathway with MDM2 to regulate p53. Nat Genet 29, 92-95.

Pellegrini, M., Celeste, A., Difilippantonio, S., Guo, R., Wang, W., Feigenbaum, L., and Nussenzweig, A. (2006). Autophosphorylation at serine 1987 is dispensable for murine Atm activation in vivo. Nature 443, 222-225.

Poyurovsky, M. V., and Prives, C. (2006). Unleashing the power of p53: lessons from mice and men. Genes Dev 20, 125-131.

Ressler, S., Bartkova, J., Niederegger, H., Bartek, J., Scharffetter-Kochanek, K., Jansen-Durr, P., and Wlaschek, M. (2006). p16INK4A is a robust in vivo biomarker of cellular aging in human skin. Aging Cell 5, 379-389.

Rhee, H., Polak, L., and Fuchs, E. (2006). Lhx2 maintains stem cell character in hair follicles. Science 312, 1946-1949.

Riemenschneider, M. J., Buschges, R., Wolter, M., Reifenberger, J., Bostrom, J., Kraus, J. A., Schlegel, U., and Reifenberger, G. (1999). Amplification and overexpression of the MDM4 (MDMX) gene from 1q32 in a subset of malignant gliomas without TP53 mutation or MDM2 amplification. Cancer Res 59, 6091-6096.

Riemenschneider, M. J., Knobbe, C. B., and Reifenberger, G. (2003). Refined mapping of 1q32 amplicons in malignant gliomas confirms MDM4 as the main amplification target. Int J Cancer 104, 752-757.

Roderick, T. H. (1963). The Response of Twenty-Seven Inbred Strains of Mice to Daily Doses of Whole-Body X-Irradiation. Radiat Res 20, 631-639.

Rodier, F., Campisi, J., and Bhaumik, D. (2007). Two faces of p53: aging and tumor suppression. Nucleic Acids Res 35, 7475-7484.

Schmitt, C. A., McCurrach, M. E., de Stanchina, E., Wallace-Brodeur, R. R., and Lowe, S. W. (1999). INK4a/ARF mutations accelerate lymphomagenesis and promote chemoresistance by disabling p53. Genes Dev 13, 2670-2677.

Sengupta, S., and Harris, C. C. (2005). p53: traffic cop at the crossroads of DNA repair and recombination. Nat Rev Mol Cell Biol 6, 44-55.

Sherr, C. J., and Weber, J. D. (2000). The ARF/p53 pathway. Curr Opin Genet Dev 10, 94-99.

Shieh, S. Y., Ikeda, M., Taya, Y., and Prives, C. (1997). DNA damage-induced phosphorylation of p53 alleviates inhibition by MDM2. Cell 91, 325-334.

Shreeram, S., Demidov, O. N., Hee, W. K., Yamaguchi, H., Onishi, N., Kek, C., Timofeev, O. N., Dudgeon, C., Fornace, A. J., Anderson, C. W., et al. (2006). Wip1 phosphatase modulates ATM-dependent signaling pathways. Mol Cell 23, 757-764.

Shreeram, S., Hee, W. K., Demidov, O. N., Kek, C., Yamaguchi, H., Fornace, A. J., Jr., Anderson, C. W., Appella, E., and Bulavin, D. V. (2006). Regulation of ATM/p53-dependent suppression of myc-induced lymphomas by Wip1 phosphatase. J Exp Med 203, 2793-2799.

Shvarts, A., Steegenga, W. T., Riteco, N., van Laar, T., Dekker, P., Bazuine, M., van Ham, R. C., van der Houven van Oordt, W., Hateboer, G., van der Eb, A. J., and Jochemsen, A. G. (1996). MDMX: a novel p53-binding protein with some functional properties of MDM2. EMBO J 15, 5349-5357.

Sluss, H. K., Armata, H., Gallant, J., and Jones, S. N. (2004). Phosphorylation of serine 18 regulates distinct p53 functions in mice. Mol Cell Biol 24, 976-984.

Sluss, H. K., Gannon, H., Coles, A. H., Shen, Q., Eischen, C. M., and Jones, S. N. (2010). Phosphorylation of p53 serine 18 upregulates apoptosis to suppress Myc-induced tumorigenesis. Mol Cancer Res 8, 216-222.

Soussi, T., and Beroud, C. (2001). Assessing TP53 status in human tumours to evaluate clinical outcome. Nat Rev Cancer 1, 233-240.

Stad, R., Ramos, Y. F., Little, N., Grivell, S., Attema, J., van Der Eb, A. J., and Jochemsen, A. G. (2000). Hdmx stabilizes Mdm2 and p53. J Biol Chem 275, 28039-28044.

Steinman, H. A., Hoover, K. M., Keeler, M. L., Sands, A. T., and Jones, S. N. (2005). Rescue of Mdm4-deficient mice by Mdm2 reveals functional overlap of Mdm2 and Mdm4 in development. Oncogene 24, 7935-7940.

Steinman, H. A., Hoover, K. M., Keeler, M. L., Sands, A. T., and Jones, S. N. (2005). Rescue of Mdm4-deficient mice by Mdm2 reveals functional overlap of Mdm2 and Mdm4 in development. Oncogene 24, 7935-7940.

Steinman, H. A., and Jones, S. N. (2002). Generation of an Mdm2 conditional allele in mice. Genesis 32, 142-144.

Steinman, H. A., Sluss, H. K., Sands, A. T., Pihan, G., and Jones, S. N. (2004). Absence of p21 partially rescues Mdm4 loss and uncovers an antiproliferative effect of Mdm4 on cell growth. Oncogene 23, 303-306.

Stenn, K. S., and Paus, R. (2001). Controls of hair follicle cycling. Physiol Rev 81, 449-494.

Stommel, J. M., and Wahl, G. M. (2004). Accelerated MDM2 auto-degradation induced by DNA-damage kinases is required for p53 activation. EMBO J 23, 1547-1556.

Stott, F. J., Bates, S., James, M. C., McConnell, B. B., Starborg, M., Brookes, S., Palmero, I., Ryan, K., Hara, E., Vousden, K. H., and Peters, G. (1998). The alternative product from the human CDKN2A locus, p14(ARF), participates in a regulatory feedback loop with p53 and MDM2. EMBO J 17, 5001-5014.

Taylor, G., Lehrer, M. S., Jensen, P. J., Sun, T. T., and Lavker, R. M. (2000). Involvement of follicular stem cells in forming not only the follicle but also the epidermis. Cell 102, 451-461.

Toledo, F., and Wahl, G. M. (2006). Regulating the p53 pathway: in vitro hypotheses, in vivo veritas. Nat Rev Cancer 6, 909-923.

Tumbar, T., Guasch, G., Greco, V., Blanpain, C., Lowry, W. E., Rendl, M., and Fuchs, E. (2004). Defining the epithelial stem cell niche in skin. Science 303, 359-363.

Tyner, S. D., Venkatachalam, S., Choi, J., Jones, S., Ghebranious, N., Igelmann, H., Lu, X., Soron, G., Cooper, B., Brayton, C., et al. (2002). p53 mutant mice that display early ageing-associated phenotypes. Nature 415, 45-53.

Valentin-Vega, Y. A., Okano, H., and Lozano, G. (2008). The intestinal epithelium compensates for p53-mediated cell death and guarantees organismal survival. Cell Death Differ 15, 1772-1781.

Vassilev, L. T., Vu, B. T., Graves, B., Carvajal, D., Podlaski, F., Filipovic, Z., Kong, N., Kammlott, U., Lukacs, C., Klein, C., et al. (2004). In vivo activation of the p53 pathway by small-molecule antagonists of MDM2. Science 303, 844-848.

Venkatachalam, S., Shi, Y. P., Jones, S. N., Vogel, H., Bradley, A., Pinkel, D., and Donehower, L. A. (1998). Retention of wild-type p53 in tumors from p53 heterozygous mice: reduction of p53 dosage can promote cancer formation. EMBO J 17, 4657-4667.

Vijg, J., and Hasty, P. (2005). Aging and p53: getting it straight. A commentary on a recent paper by Gentry and Venkatachalam. Aging Cell 4, 331-333.

Vousden, K. H., and Lu, X. (2002). Live or let die: the cell's response to p53. Nat Rev Cancer 2, 594-604.

Vousden, K. H., and Ryan, K. M. (2009). p53 and metabolism. Nat Rev Cancer 9, 691-700.

Wang, J. C. (1996). DNA topoisomerases. Annu Rev Biochem 65, 635-692.

Wang, X., Arooz, T., Siu, W. Y., Chiu, C. H., Lau, A., Yamashita, K., and Poon, R. Y. (2001). MDM2 and MDMX can interact differently with ARF and members of the p53 family. FEBS Lett 490, 202-208.

Wang, Y., Blandino, G., and Givol, D. (1999). Induced p21waf expression in H1299 cell line promotes cell senescence and protects against cytotoxic effect of radiation and doxorubicin. Oncogene 18, 2643-2649.

Wang, Y. V., Leblanc, M., Wade, M., Jochemsen, A. G., and Wahl, G. M. (2009). Increased radioresistance and accelerated B cell lymphomas in mice with Mdmx mutations that prevent modifications by DNA-damage-activated kinases. Cancer Cell 16, 33-43.

Weber, J. D., Taylor, L. J., Roussel, M. F., Sherr, C. J., and Bar-Sagi, D. (1999). Nucleolar Arf sequesters Mdm2 and activates p53. Nat Cell Biol 1, 20-26.

Wu, X., Bayle, J. H., Olson, D., and Levine, A. J. (1993). The p53-mdm-2 autoregulatory feedback loop. Genes Dev 7, 1126-1132.

Wu, Z., Earle, J., Saito, S., Anderson, C. W., Appella, E., and Xu, Y. (2002). Mutation of mouse p53 Ser23 and the response to DNA damage. Mol Cell Biol 22, 2441-2449.

Xiong, S., Pant, V., Suh, Y. A., Van Pelt, C. S., Wang, Y., Valentin-Vega, Y. A., Post, S. M., and Lozano, G. (2010). Spontaneous tumorigenesis in mice overexpressing the p53-negative regulator Mdm4. Cancer Res 70, 7148-7154.

Xiong, S., Van Pelt, C. S., Elizondo-Fraire, A. C., Liu, G., and Lozano, G. (2006). Synergistic roles of Mdm2 and Mdm4 for p53 inhibition in central nervous system development. Proc Natl Acad Sci U S A 103, 3226-3231.

Xu, Y., and Baltimore, D. (1996). Dual roles of ATM in the cellular response to radiation and in cell growth control. Genes Dev 10, 2401-2410.

Yu, J., Zhang, L., Hwang, P. M., Kinzler, K. W., and Vogelstein, B. (2001). PUMA induces the rapid apoptosis of colorectal cancer cells. Mol Cell 7, 673-682.

Zhang, Y., Xiong, Y., and Yarbrough, W. G. (1998). ARF promotes MDM2 degradation and stabilizes p53: ARF-INK4a locus deletion impairs both the Rb and p53 tumor suppression pathways. Cell 92, 725-734.

Zhou, Z., Wang, D., Wang, X. J., and Roop, D. R. (2002). In utero activation of K5.CrePR1 induces gene deletion. Genesis 32, 191-192.